RESEARCH ON

DIGITAL TRANSDUCER PRINCIPLES

Final Report Vol. II

LOW TEMPERATURE RECOMBINATION AND TRAPPING ANALYSIS IN HIGH PURITY GALLIUM ARSENIDE BY MICROWAVE PHOTODIELECTRIC TECHNIQUES

by

Moiz B. Khambaty

William H. Hartwig

September 30, 1972

for the

NATIONAL AERONAUTICS AND SPACE ADMINISTRATION

GRANT NGL-44-012-043

Department of Electrical Engineering

THE UNIVERSITY OF TEXAS AT AUSTIN

Austin, Texas 78712

Page Intentionally Left Blank

PREFACE

Digital transducers based upon the photodielectric effect have been demonstrated by various techniques in this laboratory for several years (Ref. 21-25, 45). The basic principle of transduction is the conversion of an input optical signal into a change in resonant frequency of a microwave cavity loaded with an illuminated semiconductor crystal. During the final months of the grant, this was the only phase of the research which was supported. The project reported in this volume represents a detailed examination of material properties.

The photodielectric (PD) effect has matured as a very useful adjunct to conventional photoelectronic techniques for recombination and trapping analyses. The PD effect is a change in both the real and imaginary part of the dielectric constant of a semiconductor when it is illuminated. When non-linear effects are ignored, the free carrier contribution to the dielectric constant is of a sign opposite to the lattice contribution, and it decreases the overall dielectric constant monotonically as an increasing number of photo carriers are generated. In the limit, the overall dielectric constant becomes a very high negative number, in agreement with the metallic model. This description differs from that of earlier work. The modulation of the permittivity can be several hundred per cent with practical light intensities. When the energy-dependance of the transport relaxation time is taken into account, the behavior is modified and can result in a free carrier contribution of the same sign as the lattice contribution. Trapped carriers increase the overall permittivity.

High purity epitaxial GaAs, unavailable till recently, has been studied by photodielectric as well as photoconductivity, Hall effect, and related methods. Irradiation by He-Ne laser light at liquid helium temperatures generates hot electrons in GaAs. The temperature of excited electrons is

determined by an interplay of optical power input, and losses by optical mode scattering as well as carrier-carrier scattering. Electron temperatures as high as $35^{\circ}K$ can result at a sample temperature of $6^{\circ}K$. The relationship between induced photoconductivity and light intensity is highly sublinear, exhibiting a 1/3 power-law dependance. This is explained by a model of quadratic recombination and diffusion away from the excited surface.

A non-contact PD version of the well known thermally stimulated technique is introduced, by which shallow donor-traps were located at 0.005 eV below the conduction band, in agreement with least-squares-fit to Hall effect data.

A combination of the techniques is used to identify two major centers active at low temperatures: shallow residual donors 0.005 eV from the conduction band acting as traps and becoming recombination centers on cooling to the helium range, and deeper residual acceptors approximately 0.03 eV from the valence band, acting as potent hole traps. The great disparity between PC lifetime and response time is due to trapping. The PC lifetime decreases more than 3 orders when GaAs is cooled from liquid nitrogen to liquid helium temperatures; the mechanism is explained by a Shockley Read model involving the shallow donor. Silicon on Arsenic sites is the probable residual acceptor and Silicon on Gallium sites the probable donor.

Use of the photodielectric technique gives a great measure of confidence in the interpretation of data and establishes it as a very sensitive and convenient adjunct to normal techniques.

TABLE OF CONTENTS

LIST OF FIGURES

LIST OF TABLES

Page Intentionally Left Blank

CHAPTER I

INTRODUCTION

PURPOSE OF PRESENT RESEARCH

In recent years the compound semiconductor Gallium Arsenide has achieved great technological importance and has been the subject of extensive theoretical and experimental research. These efforts have been stimulated by the need to exploit some of the unique properties of Gallium Arsenide. Thus, the direct energy-band structure of GaAs has been used to fabricate injection lasers and light-emitting diodes. The high electron mobility in GaAs has been used in microwave field-effect transistors and tunnel diodes. Gunn-effect diodes and related microwave devices exploit the multi-valley band structure and the resulting negative differential mobilities possible in GaAs. The high electro-optic coefficients of this partly-ionic material have found in use in electro-optic modulators. Very recently, high purity epitaxially grown GaAs has been used for very sensitive far-infrared detection[1], at several hundred micron wavelengths. This latter application is based on exciting extrinsic photoconductivity utilizing the shallow residual donors in the pure material. The list of technological applications of Gallium Arsenide is diverse and is rapidly expanding.

The applications of GaAs have steadily expanded as material of higher purity has become available, and this in turn has stimulated

both materials technology and efforts to understand the fundamental physics of the material and to characterize its basic properties. Until late 1968, most of the material available was melt-grown either by the Horizontal Bridgman Method or by the Czochralski method. Such material was highly impure, being heavily contaminated and dislocated. Even so, extensive studies were made on such material.[2-5] Those properties of the material which are impurity sensitive, such as carrier concentration, resistivity, mobility, excess-carrier lifetime, response time as a photoconductor, etc., were strongly indicative of the then state of the art and not very representative of intrinsic GaAs. Thus many samples studied by Naseldov[5] et. al. had room-temperature carrier concentrations of 10^{16} cm^{-3} or more for "undoped" material; such material could not be "frozen-out" i.e., the carrier concentration did not decrease much on cooling, and became constant at 20°K or more. Subsequently, this was correctly interpreted as the effect of impurity-band conduction: at impurity concentrations above about 10^{15} cm^{-3} the impurity-wavefunctions overlap and form an independent band. The small effective mass of electrons ($0.065\ m_o$) in GaAs especially favors this by increasing the size of the Bohr orbit of the electrons. None of Naseldov's samples exhibited a monotonic increase in Hall coefficient as they were cooled. In the same quality of materials numerous photo-electronic investigations were

carried out. Thus, Shirafuji[6] cited the presence of at least six residual acceptors between 0.33 eV and 0.02 eV from the valence band in n-GaAs, and attributed these to various structural or chemical origins. Bube[7], Kalashnikov[8] and other found some different acceptor levels. Kolchanova[9] et. al. studied n-type undoped material and a series of donor-like traps as well as acceptor-like traps. The donor-like traps, at 0.05, 0.065 and 0.105 eV from the conduction band were found to be multiply-charged, and hence to control the minority carrier behavior as a function of temperature that they observed. Additionally, they also found hole traps located near the valance band. Hilsum and Holeman[10] studied the lifetime of non-equilibrium carriers and found some four orders of magnitude spread, depending on the sample. This was indicative of gross differences in the impurity content of the samples. Several articles and the review volumes by Willardson and Beer summarize extensive work on the subject.

In order to prepare material of higher resistivity, needed for Gunn-effect diodes, etc., compensating species were deliberately introduced commercially.[13] The electrical properties of such material were very difficult to analyze, as the material rapidly became insulating when cooled below -30°C in an effort to enhance device performance.

Such attempts at preparing device-quality GaAs were supplanted from 1968 by the development of epitaxial GaAs, grown on melt-

grown GaAs substrates by vapor-phase epitaxy.[14] This technique yielded material of much lower total impurity content and dislocation count than previous GaAs, and became the subject of many investigations.[15]

The material investigated in this research is high-purity n-type epitaxial GaAs grown from the vapor-phase at Fairchild Semiconductor Research Labs. The electron concentration at 300°K is approximately 6×10^{13} cm^{-3}, and the liquid nitrogen mobility, an index of material quality, is in excess of 120,000 cm^2/volt-second. This was the purest state-of-the art material available when this investigation was started. More recently, both vapor-phase and liquid-phase epitaxial GaAs of about twice this purity has been prepared.

The motivation for the present research is two-fold. First, is the need to determine the properties of as nearly pure material as possible, so as to improve on the data reported in earlier work, cited above. Secondly, it is known that when GaAs is used in injection luminescent diodes (LED's) and similar applications, the overall quantum efficiency of the resulting devices is limited by the presence of shallow states, near the conduction band. Such states constitute centers via which competing non-radiative transitions take place. There has been a great deal of work, mostly using low-temperature photoluminescence[15-18] to identify these residual shallow states (and

other defects, as well) so that the recombination transitions may be better understood, as well as to reduce the density of such centers if possible. Additionally, the speed of response of light-emitting diodes is influenced, even at 300°K by trapping in various states of the material. The present study of recombination and trapping in GaAs is therefore motivated by these needs.

Methods of Analyses

A wide variety of techniques exists for studying defect levels in semiconductors.[19] Steady-state and transient photoconductivity (PC) measurements are powerful tools. Rose[20] has pointed out that PC is "an incisive tool for probing a low density of background states even in the presence of high concentrations of states at a few well-defined levels." Thermally stimulated conductivity[19] is another useful tool, especially suited for the study of deep traps in relatively insulating materials. It's use on materials with high dark conductivity (such as pure GaAs) is difficult because the current due to thermally released charge is swamped by the dark current. Spectral response of PC and PC as a function of light intensity and temperature are other basic techniques. All these have been used in this work.

Photodielectric Techniques

The use of all of the above techniques implies that good ohmic contacts must be made to the sample. This is no minor limitation.

In the first place, ohmic contacts are difficult to make on a large number of materials, especially compound materials wherein the volatile component is lost during the heating phase necessary. Even if applied, such contacts are not linear, especially at low temperatures. Secondly, the basic idea behind the making of an ohmic contact is to alloy a suitable dopant in, to render the local region degenerate. This dopant will inevitably diffuse away during the heating cycle and necessarily contaminate the pure sample. A non-contact technique is therefore highly desirable. The application of the photodielectric effect provides such a method. When a semiconductor is illuminated, the free as well as trapped carriers change the dielectric constant characteristically, by a very significant amount. This effect has been used by Hartwig[22-25] and his students in a series of researches to evolve a mature instrumentation technique that is convenient to use.

There are other important advantages to the use of this non-contact method. PC methods indicate only the presence of free carriers directly; electrons or holes excited from one bound level to another do not influence PC measurements; they do alter the dielectric constant, however. Furthermore, the assignment of traps can be ambiguous when only simple PC methods are used--only the energetic difference between the trap and the nearest band is known, but the identity of the band is unknown.[26] With PD data augmenting, this ambiguity is

resolved. Also, when investigating PC growth and decay transients one major source of concern is "contact effects". Thus, due to sizable thermoelectric emf's developed at contacts as well as rectification effects on the illuminated contacts, misleading data is often obtained. Rapid, two-step transients such as are measured in this work are sometimes ascribed to contact effects and carrier-sweepout. PD data therefore also serve to confirm the validity of standard measurements.

The present work, therefore, takes advantage of the merits of the standard as well as PD techniques to evolve an understanding of recombination and trapping. Chapter II discusses photodielectric theory in detail. The basic properties of GaAs such as its crystal structure, energy-band structure and defect levels commonly found are well documented and the reader is referred to review articles.[11,12]

CHAPTER II

THEORY OF THE PHOTODIELECTRIC EFFECT

The photodielectric effect in semiconductors has been the subject of extensive study, since 1965. Hartwig, Arndt, and Stone[22] developed the relations between the excess photo-induced carrier concentration in a semiconductor and the resultant change in its dielectric constant. They showed that the frequency shift of a superconducting cavity containing the sample, due to the photodielectric effect, constitutes a very sensitive tool for studying some of the properties of the material. Baker[33] calculated the geometric "filling factor" of the cavity containing the samples. Albanese[24] provided several interesting equivalent-circuit viewpoints of the sample-cavity system. Hinds[25] extended the usefulness of the technique by recognizing that in addition to free carriers, trapped carriers also perturb the dielectric constant of the sample, and studied the photo-electronic properties of Cds:Al and similar materials by the trapped-carrier photodielectric effect.

The theory of the photodielectric effect is based on the classical free-electron theory of dielectric susceptibility originated by Drude and Lorenz.[27] In its present form, photodielectric theory embodies the effects of depolarization of free carriers on the dielectric constant of a material. It is proposed to show that the effects of plasma

depolarization are incorrectly included in previous work; the equations have a very restricted range of validity and predict behavior, under limiting conditions, that does not occur physically. This will be discussed more fully in the next section. It is necessary to examine carefully the classical theory of dielectric susceptibility of solids in order to develop the equations pertinent to photodielectric applications. The influence of depolarization effects emerges from that discussion.

CLASSICAL THEORY OF ELECTRIC SUSCEPTIBILITY

Although the determination of electric susceptibility is a quantum mechanical problem, purely classical approaches have been highly successful in explaining observed phenomena, and such an approach[27] is outlined here.

An external electric field acting on a solid induces a dipole moment per unit volume, or polarization $\bar{P}$. given by

$$\bar{P} = \epsilon_o \chi_e \bar{E}_{eff} \tag{2.1}$$

where $\bar{E}_{eff}$ is the effective macroscopic average internal field, χ_e the electric susceptibility and ϵ_o the permittivity of free space.

The relative dielectric constant, ϵ_r, of a material is given by

$$\epsilon_r = 1 + \chi_e \tag{2.2}$$

The polarization $\overline{P}$ is

$$\overline{P} = \sum_{n} q_i \; r_i \qquad (2.3)$$

Where q_i is a charge and r_i is its displacement from equilibrium. The sum is over the total number of dipoles in the unit volume.

To arrive at the displacement r_i in case of a free electron gas, we consider the equation of motion of the electron, executing harmonic motion under the stimulus of an internal harmonic field

$$m^* \frac{d^2 r}{dt^2} + \frac{m^*}{\tau} \frac{dr}{dt} = q E_{loc} e^{j\omega t} \qquad (2.4)$$

where m^* is the effective mass of the electron in the solid, and τ its momentum relaxation time. The second term represents the "frictional" or dissipative force due to collision of electron with the lattice, radiation damping and other loss mechanisms. τ is a function of energy in a real solid, and it is an idealization to treat it as a constant, as has been done above. The energy-dependence of τ can result in greatly modified behavior, as discussed later. E_{loc} is the local effective field acting on the charges.

EFFECTIVE INTERNAL FIELD

Before proceeding with the solution of (2.4) the question of the effective local internal electric field vis-a-vis the external driving field

E_{ext} must be considered in some detail.[27] This is an issue that strongly affects the determination of the dielectric properties of the solid, especially its frequency behavior. The main source of difficulty is the distinction between the external, or applied, electric field E_{ext}, the effective average field E_{eff} in the material, and the local electric field E_{loc} actually polarizing the electrons. The latter two fields need to be distinguished, in principle because the local field in the vicinity of an ion core can be considerably higher than the macroscopic average or "smeared out" electric field E_{eff}. In the definition of susceptibility (2.1) or in Maxwells Equation, E_{eff} only matters whereas the agency causing the displacement of charge is the microscopic, or local field. Lorenz first showed the distinction and indicated an approach to the determination of the local field. The Lorenz correction has been shown in standard texts[27] to add a term $\frac{P_b}{3\epsilon_o}$ to the average field, i.e.

$$\bar{E}_{loc} = \bar{E}_{eff} + \frac{\bar{P}}{3\epsilon_o} \qquad (2.5)$$

where $\bar{P}$ is the volume polarization of the material. The question of the need to include or exclude the local field or Lorenz Correction has been discussed since the 1920's, both in connection with the optical properties of metals (i.e. modified Drude theory) and in ionospheric

research. Data to support either viewpoint has been available, and the correction has alternately been included and excluded in the literature. Ratcliffe[28] and Slater[29] review the theoretical and experimental implications. In the modern viewpoint the Lorenz correction must not be included: Slater has shown that inclusion of this factor modifies the solution of (2.4) by giving rise to a number of discrete resonances, corresponding to a system of coupled oscillators, rather than a single resonance of a bound electron-ion system. He emphasizes that the nature of the result is not altered, only the resonances are shifted and many-valued. Nozieres and Pines,[30] on the other hand, show that on quantum mechanical grounds, the local field corrections are negligible for highly polarizable media such as metals or semiconductors. Wilson[31] points out that the Lorenz correction is inconsistent with the single-electron approximation used in deriving the electron theory of metals. It is therefore justifiable to disregard the distinction between E_{eff} and E_{loc}.

There still remains the more important problem of distinction between the external field and E_{eff}. Several different viewpoints can be brought to bear on this issue; they are ultimately equivalent. The concept of a "dielectric constant" of an insulator is generally introduced in terms of a parallel-plate capacitor model in which the applied field E, in absence of the dielectric, is reduced to $\frac{E}{\epsilon_r}$ due to the

counteracting "depolarization field" set up by surface-induced charges in the dielectric. While this approach is sound, and emphasizes the connection between the dielectric susceptibility and the depolarization field, it can complicate matters unnecessarily and, in some cases, introduce error. Thus, Dresselhaus[32] et. al. in their work on cyclotron resonance in InSb established the coupling between the applied field and E_{eff} using the depolarization effect, viz.

$$E_{eff} = E_{ext} - LP = E - L\,(\chi_1 E_{eff} + Nqr) \quad (2.6)$$

where L is the geometry dependent "depolarization factor" χ_1 the electric susceptibility in absence of the free carriers, N the density of free electrons. The second term denotes the polarization due to free charges. This formulation is conceptually incorrect as it attempts to specify the polarization of a charge in terms of its own coordinates. For such an approach to be valid, a more involved self-consistent argument must be applied.

The result of Dresselhaus et. al.'s approach is to modify (2.4) to

$$m^* \left[\frac{d^2r}{dt^2} + \frac{1}{\tau}\frac{dr}{dt} + L_i \frac{Nq^2}{m^*} r\right] = e E_i e^{j\omega t} \quad (2.7)$$

where the magnetic field has been set equal to zero for clarity, $L_i \equiv$

$L/(1+L)$ and $E_i \equiv \dfrac{L\ E_{ext}}{(1+x_1\ L)}$

Equation (2.7) so obtained differs from (2.4) in that it includes a harmonic restoring force of force-constant $L_i Ne^2$. Eq. (2.7) can be written

$$(-\omega^2 + \omega_p^{\ 2} + \frac{i\omega}{\tau})\ r = \frac{q}{m^*} E_i \qquad (2.8)$$

where ω_p is the plasma frequency, i.e.

$$\omega_p = \left(\frac{L_i Ne^2}{m^*}\right)^{1/2} \qquad (2.9)$$

The coupling between E_{ext} and E_{eff} as given in (2.6) has thus apparently altered the dynamical system by introducing an effective spring-constant to the system--one that is orientation-dependent. If (2.8) is now directly solved and used in conjunction with (2.3) to determine the dielectric constant, the results obtained are incorrect. The error so introduced will be discussed later.

The emergence of a geometry-dependent force-constant in the equations of Dresselhaus et. al. is not also appealing. The dielectric polarization can be determined simply working entirely with an assumed E_{eff} Subsequently, Maxwell's Equations can be used to match the boundary conditions at the surface of the specimen.

The latter approach can be developed simply as follows. Having identified E_{loc} with E_{eff} earlier in the discussion, it is now necessary to determine what effective electric field is seen by the free charges. Since the wave functions of the free charges are in fact smeared out over the entire crystal, it is logical to deduce that they will also experience the same macroscopic average field $\overline{E}_{eff}$ seen by the more localized tightly bound electrons.

Equation (2.4) can now be solved, substituting $\overline{E}_{eff}$ for $\overline{E}_{loc}$ on the right hand side. The solution is

$$r = \frac{q}{m^*} \overline{E}_{eff} e^{j\omega t} \left[\frac{-\omega^2 - j\omega/\tau}{\omega^4 + (\omega/\tau)^2} \right] \tag{2.10}$$

The above result can be combined with (2.1) through (2.3) to yield the real and imaginary parts of the dielectric susceptibility $\chi'_{\downarrow}(\omega)$ and $\chi''_{\downarrow}(\omega)$ respectively:

$$\chi'_{\downarrow}(\omega) = -\frac{Nq^2}{m^* \epsilon_o} \left[\frac{\tau^2}{1 + \omega^2 \tau^2} \right] \tag{2.11}$$

and

$$\chi''_{\downarrow}(\omega) = \frac{Nq^2}{\omega m^* \epsilon_o} \left[\frac{\tau}{1 + \omega^2 \tau^2} \right] \tag{2.12}$$

The imaginary part, $\chi_\psi''(\omega)$ represents the loss component of the dielectric constant. The dielectric constant can alternatively be derived as the imaginary component of the electrical conductivity, starting with the same equation of motion. In fact, in such derivations, the field applied to the semiconductor (by ohmic contacts, for instance) is tacitly taken as the relevant field driving the free electrons, in agreement with the discussion above.

Thus far, attention has been focussed on the polarization due to free electrons. Free holes contribute additional terms such as given by (2.11) and (2.12), with the appropriate effective hole mass used in these equations. The contribution to electric susceptibility of the tightly bound "core" electrons can be determined by writing an equation of motion[27] similar to (2.4) except that a restoring-force term, $\omega_o^2 x$ to the left hand side:

$$m^* \frac{d^2 r}{dt^2} + \frac{m^*}{\tau} \frac{dr}{dt} + m^* \omega_o^2 r = e E_{eff} e^{j\omega t} \quad (2.13)$$

where ω_o^2, the force constant, represents the (natural frequency)^2 of the system, and is given by[25]

$$\omega_o^2 = \frac{2}{m^*} \frac{(4\pi \epsilon_o)^2}{e^4} E_b^3 \quad (2.14)$$

E_b represents the energy binding the electron to the atom. The

corresponding expressions for the dielectric constant contribution of bound electrons can be derived as:

$$(\chi_r)'_{bound} = \frac{Ne^2}{m^* \epsilon_o} \left[\frac{\omega_o^2 - \omega^2}{(\omega_o^2 - \omega^2)^2 + (\frac{\omega}{\tau})^2} \right] \qquad (2.15)$$

and

$$(\chi_r)''_{bound} = \frac{Ne}{m^* \epsilon_o \omega} \left[\frac{\frac{\omega}{\tau}^2}{(\omega_o^2 - \omega^2)^2 + (\frac{\omega}{\tau})^2} \right] \qquad (2.16)$$

Hinds[25] has discussed the behavior of the bound (or trapped) carrier dielectric constant and shown that loosely bound electrons increase the dielectric constant, whereas free electrons, in accordance with (2.11) decrease it.

The overall dielectric susceptibility of a semiconductor containing tightly bound "core" electrons as well as free charges is additive, so that when ω is small compared to frequencies ω_o that characterize the bound electrons, the contribution of the latter to the susceptibility becomes frequency independent. Assuming that ionic resonances do not occur in the frequency range of interest, the dielectric constant contribution of core electrons from far infrared (overlooking possible ionic resonances) frequencies down to dc can be represented by ϵ_∞, the high-frequency "lattice" dielectric constant.[33] From (2.15) ϵ_∞ is given by

$$\epsilon_\infty = \frac{N e^2}{m^* \epsilon_o \omega_o^2} \tag{2.18}$$

where N is the density of atoms in the crystal, and ω_o is in the infrared.

$$\epsilon_r(\omega)_{\text{total}} = 1 + \chi_{\text{free}} + \chi_{\text{bound}} \tag{2.19}$$

The subscript r denotes relative dielectric constant.

Combining (2.18) with (2.12) and (2.13) the overall dielectric constant for the general case can be written as succintly as

$$\epsilon_r(\omega) = \epsilon_\infty - \epsilon' - i\epsilon''$$

or,

$$\epsilon_r(\omega) = \epsilon_\infty \left\{ 1 - \left[\sum_j \frac{\omega_{pj}^2 \tau^2}{(\omega^2\tau^2 + 1)} \right] + \frac{i}{\omega} \left[\sum_j \frac{\omega_{pj}^2 \tau}{(1 + \omega^2\tau^2)} \right] \right\} \tag{2.20}$$

The summations in the above equation are over the various groups of free carriers, and ω_{pj}, given by

$$\omega_{pj} = \left[\frac{N_j q^2}{m^*_j \epsilon_o \epsilon_\infty} \right]^{1/2} \tag{2.21}$$

is a "modified plasma frequency" of the j^{th} group of free carriers; the lattice dielectric constant ϵ_∞ is absorbed in the expression. The plasma frequency is defined in this context as the frequency for which the real part of the overall dielectric constant vanishes in a loss-free system. Both minority and majority carriers must clearly be considered in determination of the plasma frequency of the system, viz

$$\omega_p^2 = \sum_j \omega_{pj}^2 \tag{2.21}$$

for a low-loss system.

Equation (2.19) does not include any contributions due to inter-band or intra-band transitions or due to "restrahlen" (ionic-resonance) effects. The latter are important in ionic semiconductors such as GaAs and must be considered at infrared frequencies. This effect can be neglected at microwave frequencies.

The physical implications of (2.19) can now be discussed, and compared with the implications of using Dresselhaus et. al's equations directly. Starting with a nearly insulating semiconductor, as the free carrier concentration is increased, e.g., optically, keeping the test frequency ω fixed, the free carrier dielectric constant, denoted ϵ_ψ, increases monotonically. This results in a monotonic decrease of the overall dielectric constant, until it is rendered zero--at the plasma frequency--and becomes increasingly negative. This is as expected:

the model is based on the Drude-Lorenz theory for metals, and the semiconductor behavior should smoothly give way to metallic behavior as the free carrier density is increased. In the metallic limit, the overall dielectric constant becomes minus infinity, as for a perfect conductor. For a low-loss semiconductor, when $\omega > \omega_p$, the dielectric constant is positive, and an electromagnetic wave can propagate through the material. For $\omega < \omega_p$, the refractive index and propagation constant are both imaginary and the wave is attenuated. These are well established experimental observations, for instance, in the optical properties of metals or in wave propagation through plasma.

The derivations of $\epsilon_r'(\omega)$ and $\epsilon_r''(\omega)$ based on the direct use of Dresselhaus et. al's equations yield the following expression[23]:

$$\epsilon_r'(\omega) = \epsilon_L \left[1 - \frac{\omega_p^2 (1 - \frac{\omega_p^2}{\omega^2})}{1 + \omega^2 \tau^2 (1 - \frac{\omega_p^2}{\omega^2})^2} \right] \qquad (2.22)$$

As $\omega_p \to \infty$ or $\omega \to 0$ this expression predicts a dielectric constant equal to twice ϵ_L, where ϵ_L is the lattice dielectric constant. This is clearly invalid, physically.

In the remainder of this work, (2.19) will be used. For the greater part, since cavity-frequency changes induced are experimentally more easily observed, the real part of the dielectric constant, $\epsilon_r'(\omega)$

will be of interest. The behavior is shown graphically in Fig. II-1. Damping affects the turn-over point but not the general nature of the photodielectric characteristic.

CAVITY PERTURBATION MEASUREMENTS

The change in $\epsilon_r'(\omega)$ induced optically or thermally, can be measured by placing the sample in the maximum-electric-field position of a microwave resonant cavity and observing the corresponding frequency shift induced on irradiation by light. Slater's Perturbation theory[34] can be used to relate the frequency shift Δf obtained on insertion of a sample of volume V_s into a cavity of initial frequency f_1:

$$\frac{\Delta f}{f_1} = \frac{(\epsilon_o - \epsilon_1)\int_{V_s} E_o E_1 \, dV + (\mu_1 - \mu_o)\int_{V_s} H_o H_1 \, dV}{\int_{V_c} (\epsilon_o E_o^2 + \mu_o H_o^2) \, dV} \qquad (2.23)$$

where V_c is the cavity volume, E and H the electric and magnetic fields respectively. The initial values are denoted by suffix o and perturbed values by 1. The range of validity of the above equations has been discussed by Slagsvold[35] et. al. For the experimental conditions encountered $\Delta f/f_1$ is less than 10^{-4} and (2.23) is valid. The right hand side of (2.2) denotes the fraction of the total electromagnetic energy in the cavity stored in the sample; it is denoted by G, the "filling factor" of the cavity and is readily determined experimentally, using the relation

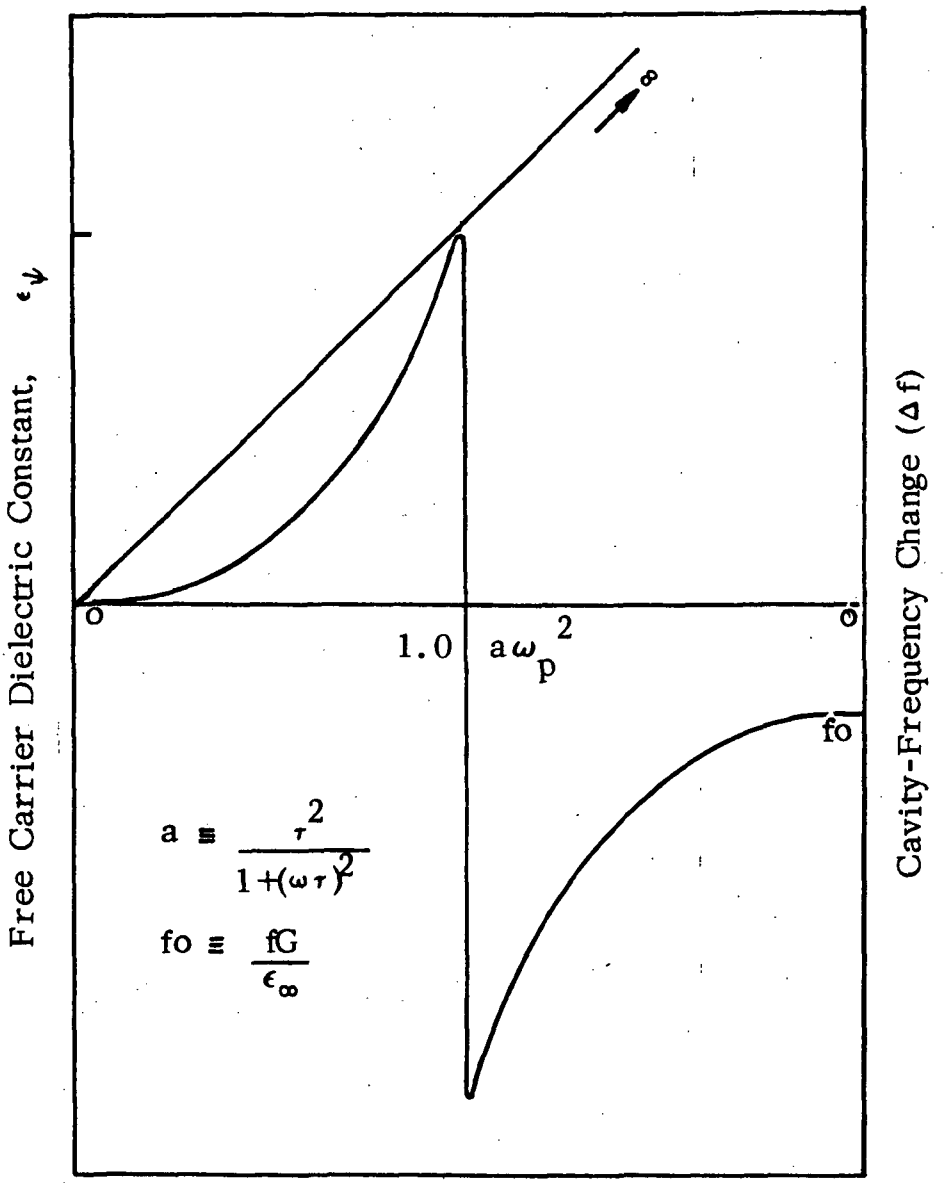

FIG. II-1 Free Carrier Contribution to Dielectric Constant and Resulting Change in Cavity Frequency as a Function of $\left[a\,\omega_p^2\right]$. a is Defined Above and ω_p is the Plasma Frequency. The Discontinuities at $a\omega_p^2 = 1$ will be Rounded Off in Practice Due to Losses and Non-linearities.

$$\frac{\Delta f}{f_1} = \frac{\epsilon_o - \epsilon_1}{\epsilon_1} G \qquad (2.24)$$

Using (2.23) and (2.24) it is a straightforward procedure to show that when $\epsilon_r'(\omega)$ is changed from $\epsilon_1'(\omega)$ to $\epsilon_2'(\omega)$ by illumination, for instance, the cavity frequency f_1 shifts to f_2, given by[36]

$$\frac{f_2 - f_1}{f_2} = \epsilon_o G \left[\frac{1}{\epsilon_2'} - \frac{1}{\epsilon_1'}\right] \qquad (2.25)$$

The above expression is strictly valid when $\epsilon' > \epsilon''$, but it is accurate enough for the situations encountered experimentally.

Fig. II-1 shows the theoretical frequency changes expected when the electron density is increased in a simple system described by (2.19). The sharp transition at $a\omega_p^2 = 1$ will in actual practice be broadened out due to inevitable dissipative mechanisms.

HOT-CARRIER PHOTODIELECTRIC EFFECT

In many practical situations, it is not valid to suppose that τ is energy-independent. Thus, in a cavity with high electric field or in a photodiode, where the depletion region fields are normally several Kilovolts/cm, this approximation is quite invalid. Under these conditions, the susceptibility contribution by free carriers is modified and may be considerably different than that predicted by (2.11).

the free carrier, can in fact then contribute a susceptibility of the same sign as the lattice, as has been observed by Gibson et. al. in Germanium at 77^{o}K. The theory of this effect is outlined in Appendix II.

CHAPTER III

PHOTOEXCITATION AND RECOMBINATION KINETICS

INTRODUCTION

Changes in the dielectric constant and conductivity produced by incident photon flux are ultimately caused by a redistribution of electrons and holes among the available states in the energy band structure of the semiconductor. Recombination of photoexcited carriers, including trapping, is the process by which the equilibrium is restored when a semiconductor sample is illuminated. The kinetics of excitation and restoration are, in general, very complex because of the simultaneous interaction of several active centers in the solid. In addition, the excited carriers often acquire energies far above kT, where T is the temperature of the material. Under these circumstances, general analyses are impossible or unwieldy. It is usual to assume highly simplified energy level schemes and kinetic models. Such theories of recombination and trapping are readily accessible in the literature.[19] In this chapter, some simple models, germane to this research, are summarized. The theory of hot photoexcited electrons will, however, be presented in detail.

MECHANISM OF PHOTO-EXCITATION

In most of the experiments performed in this work, He-Ne laser light was used to excite the semiconductor. It is important for

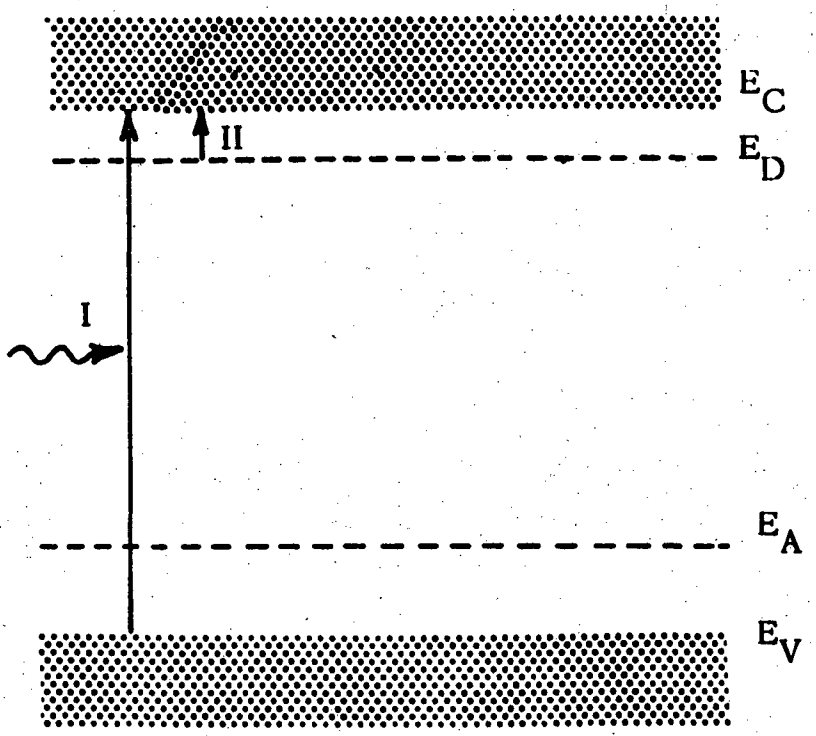

FIG. III-1 Illustrating the Transitions Involved in Intrinsic (I) and Extrinsic (II) Photoconductivity.

the analyses to follow to determine the type of photo-conductivity it gives rise to, viz., fundamental band-to-band, or impurity ionization. These two transitions are labeled I and II respectively in Fig. III-1. Consider transition II as a possibility. The theory of photoelectric absorption of x-rays developed by Hall[37], using a quantum-mechanical treatment, has been applied by Fan[38] to study infrared absorption in semiconductors. Fan has derived the following expression for the cross-section of photon absorption by localized states:

$$\frac{\alpha}{N} = \frac{1}{n} \; 2^{10} \; \frac{\pi^2}{3} \; \frac{\hbar e^2}{m^* E_i} \; \left(\frac{\nu_i}{\nu}\right)^4 \; f\left(\frac{\nu - \nu_i}{\nu}\right) \quad (3.1)$$

where α is the absorption coefficient, N is the concentration of impurity atoms, n the refractive index of the crystal, E_i the ionization energy of the impurity state and ν_i the corresponding frequency. ν corresponds to the photon frequency. f is a function defined by

$$f(x) = \exp(-4x \tan^{-1} x) \; / \; [1 - \exp(-2\pi x)] \quad (3.2)$$

Eq. (3.1) is based on the fact that the matrix element connecting the initial (bound) state to the continuum also decreases very rapidly with photon energy in excess of the minimum ionization energy.

For photon energies much greater than impurity ionization energies, as is the case for GaAs excited by He-Ne light, (3.1) re-

duces to

$$\frac{\alpha}{N} = \frac{5.26 \times 10^{-17}}{n} \frac{m}{m^*} \left(\frac{E_H}{E_i}\right) \left(\frac{\upsilon_i}{\upsilon}\right)^{3.5} \qquad (3.3)$$

Substitution of the appropriate values reveals that for impurity ionization energies 0.25 eV the absorption cross-section per atom is 1.5×10^{-19} cm^2. The intrinsic absorption coefficient for He-Ne light at liquid He temperatures[39] is 3.8×10^4 cm^{-1}, or approximately 4×10^{-22} cm^{-1} per lattice atom. Thus, impurity photoconductivity is small compared to the intrinsic (band-to-band) process. For the shallow donor energies of a few meV impurity ionization is completely negligible. Hence, we may treat the excitations produced by 6328Å light as being band-to-band, resulting in formation of an electron-hole pair for each absorbed photon.

In n-type GaAs, free hole lifetime is several orders smaller than electron lifetime at room temperature, due to rapid capture of holes by electron-occupied traps. As shown by Nasledov[5] et. al., the hole lifetime for the drops vary rapidly as temperature is lowered. This results in strongly asymetric electric conduction by the two charge carriers, and the contribution of holes may be neglected at low temperatures. In the analyses to follow, excitation by He-Ne light will, therefore, be taken as causing unipolar (electron) carrier generation by process I in Fig. III-1.

HOT-ELECTRON TEMPERATURE

In most analyses of photoconductivity the tacit assumption is generally made that the photo-excited free carriers are in equilibrium with the lattice and have the same temperature as the lattice. While this is incorrect, the errors introduced at room temperature are small. It is not at all obvious that this will be the case at low temperatures. The following analysis discusses the temperature of photo-excited electrons at low sample temperatures.

Helium neon light generates photocarriers with instantaneous energies given by

$$E_{inst} = h\nu - E_g \qquad (3.4)$$

where $h\nu$ is the photon energy (1.96 eV) and E_g the band-gap (1.52 eV). Fig. III-2 indicates that the carriers are monoenergetic, due to the momentum-conservation constraint. The 0.34 eV energy corresponds to carrier temperature of 3940^{o}K. These (hot) electrons and holes rapidly dissipate their excess energy and equilibrate with thermal electrons, to establish their equilibrium effective temperature under steady photoexcitation. The electron mobility and momentum relaxation time τ_{mom} entering in photodielectric equations are both dependent on the carrier effective-temperature. To arrive at the steady-state carrier temperatures it is necessary to examine in some detail the rate

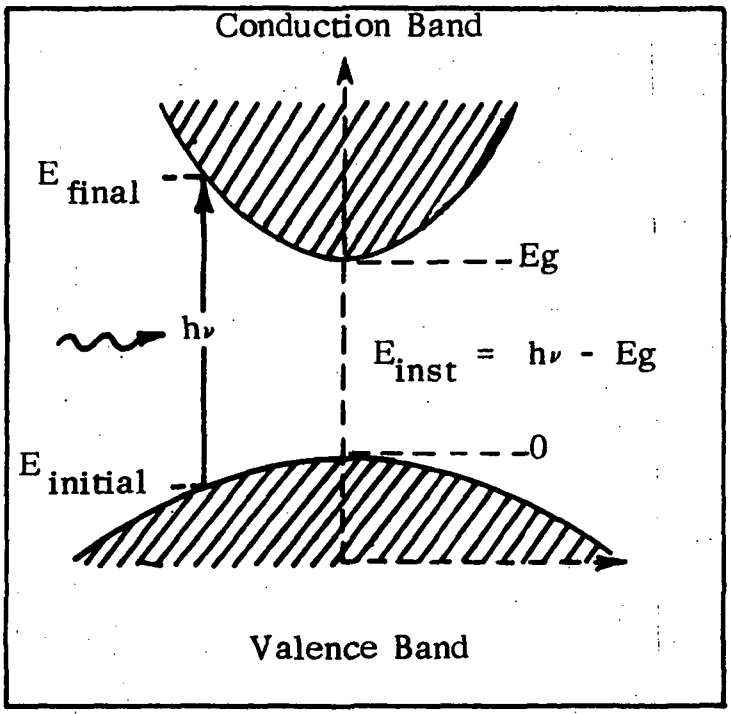

FIG. III-2 Energy Band Scheme of GaAs, Showing Relations Involved in Photo-excited Pair Production.

processes involved. The mechanisms of power transfer and scattering in polar crystals have been discussed in an early work by Stratton[40], and the present analysis is based on it. Fig. III-3 illustrates the processes schematically.

Power from the laser results in an ensemble of excited electrons. These energetic electrons dissipate their energy by two principal modes: energy loss to the lattice by lattice-scattering and energy loss to other electrons by carrier-carrier scattering process. The latter mechanism results in thermalization of the electrons amongst themselves, with a "characteristic electron temperature." An exactly similar process applies for hot holes. The effective carrier temperatures depend on the balance between optical power input and rate of energy loss to the lattice.

The dominant lattice scattering mode involved is optical-mode scattering in case of GaAs. [41] This process is negligible at low temperatures for ordinary thermal electrons since it requires electron energies in excess of the optical-mode phonons (e.g. 36 meV for longitudinal-optical phonon in GaAs) to excite such modes. Thermal electrons, having energies of the order of kT cannot excite optical vibrations. Hot electrons, having initial energies of several tenths of an electron volt preferentially excite these higher-energy modes.

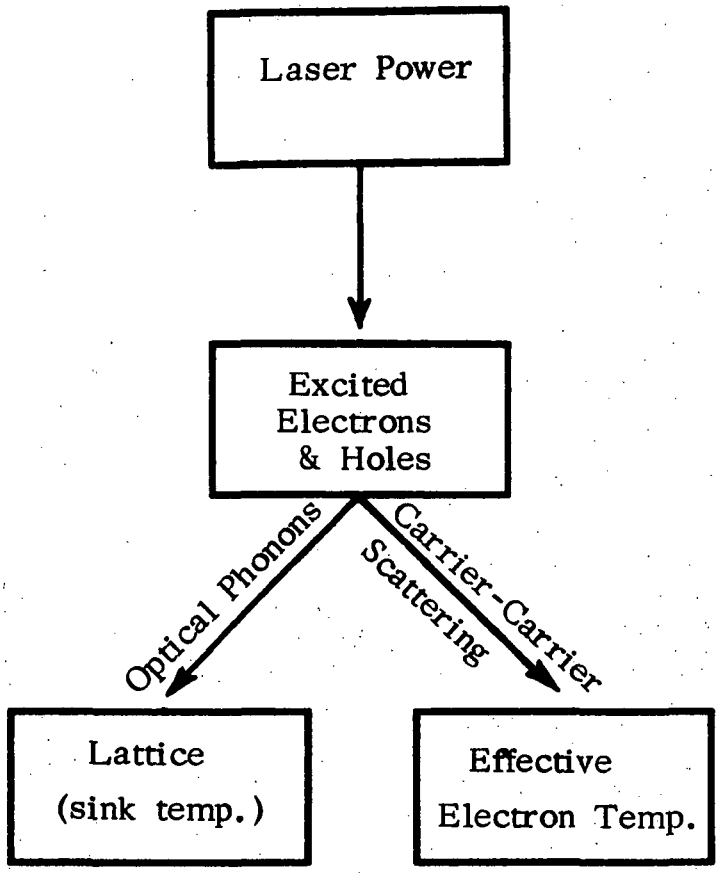

FIG. III-3 Rate Processes Involved In Determination of Temperature of Hot Photo-Excited Electrons.

In equilibrium, under optical excitation, $P(T_e)$ the power per electron rejected to the lattice must equal P_{opt}, the average optical power received by each electron. T_e denotes the effective temperature of the electron:

$$P_{opt} = \frac{P_L (h\nu - E_g) f}{V h \nu n} \tag{3.5}$$

where P_L is the laser power, absorbed by the active volume V of the semiconductor, n is the electron concentration, $h\nu$ is the photon energy, and E_g the energy gap. The factor f is the fraction of P_L that is absorbed by the electron system, viz.:

$$f = \frac{n}{n + n_c^*} \tag{3.6}$$

n_c^* is the density of electrons at which photo-excited high energy electrons lose equal amounts of power to the lattice by optical-phonon emission and to the other carriers by scattering. Frohlich and Paranjape[42] estimated the rate of loss of power to other electrons by considering the stopping power of a metal for fast electrons. Their analysis yields the approximate relation

$$\left(\frac{dp}{dt}\right)_{\text{elec-elec}} \simeq \frac{4\pi n e^{*4}}{(2 m^* \epsilon)^{1/2}} \tag{3.7}$$

where e^* is an effective electronic charge that takes into account the dielectric polarization of the medium. e^* has been approximated by $(e^*/q)^2 = (\epsilon_{lattice})^{-1}$. Stratton has extended the analysis further and shown that when optical polar-mode scattering is dominant, for mono-energetic electrons of energy $E >> k\theta$ where θ is the Debye temperature, n_c^* is given by

$$n_c^* = \frac{8\pi}{e^{*4}} \left|q\right| E_o k\theta \ln \left[2 \left(\frac{E}{k\theta}\right)^{1/2}\right] \qquad (3.8)$$

E_o is an effective electric field given by

$$E_o = m^* q k\theta h^{-2} \left[\frac{1}{\epsilon_\infty} - \frac{1}{\epsilon}\right]$$

ϵ_∞ and ϵ being the high frequency and static dielectric constants, respectively. In the case of GaAs, $\theta = 400$, $\epsilon_\infty = 10.62$, $\epsilon = 12.6$, and E is 0.34 eV when He-Ne light is used. Substituting these values in the above equations, yields the result $n_c^* \simeq 5 \times 10^{17}\ cm^{-3}$. The density of electrons in these experiments is at least two orders of magnitude lower than n_c^* and Eq. (3.5) can be reduced to

$$P_{opt} = \frac{P_L \times 0.34}{V \times 1.96 \times n_c^*} \qquad (3.9)$$

The active volume of the material is difficult to judge precisely; the depth can be taken as the Debye length; the laser spot on the sample is approximately 0.15 cm. It is apparent that as the

sample temperature is raised, the background thermal electron concentration rises, the Debye length decreases, and the active volume shrinks. The increased electron temperatures that this would entail are, however, partially offset by the larger number of electrons sharing the laser power.

The power rejected by each electron by polar optical-mode scattering has been shown by Conwell[43] to be given by

$$P(T_e) = \left(\frac{2k\theta}{\pi m^*_e}\right)^{1/2} |q| E_o \exp\left(\frac{-\theta}{T_e}\right) \left[\left(\frac{\theta}{T_e}\right)^{1/2} K_o\left(\frac{\theta}{2T_e}\right) \exp\frac{\theta}{2T_e}\right] \quad (3.10)$$

where K_o is the modified Bessel function of order zero. This relation expresses the expected fact that optical-mode scattering depends strongly on electron temperature. Eq. (3.10) can be simplified to

$$P(T_e) \simeq 8.7 \times 10^{-8} \exp\left(\frac{-\theta}{T_e}\right) \quad (3.11)$$

Equating P_{opt} in Eq. (3.9) and $P(T_e)$ from Eq. (3.11) yields the equilibrium electron temperature. Fig. III-4 shows the calculated values of electron temperature as a function of incident light power for various sample temperatures. The latter affects the Debye length, and hence the volume V.

It is apparent from Fig. III-4 that under actual experimental conditions the electron temperature is considerably higher than the lattice temperature at very low temperatures. Ultimately at higher

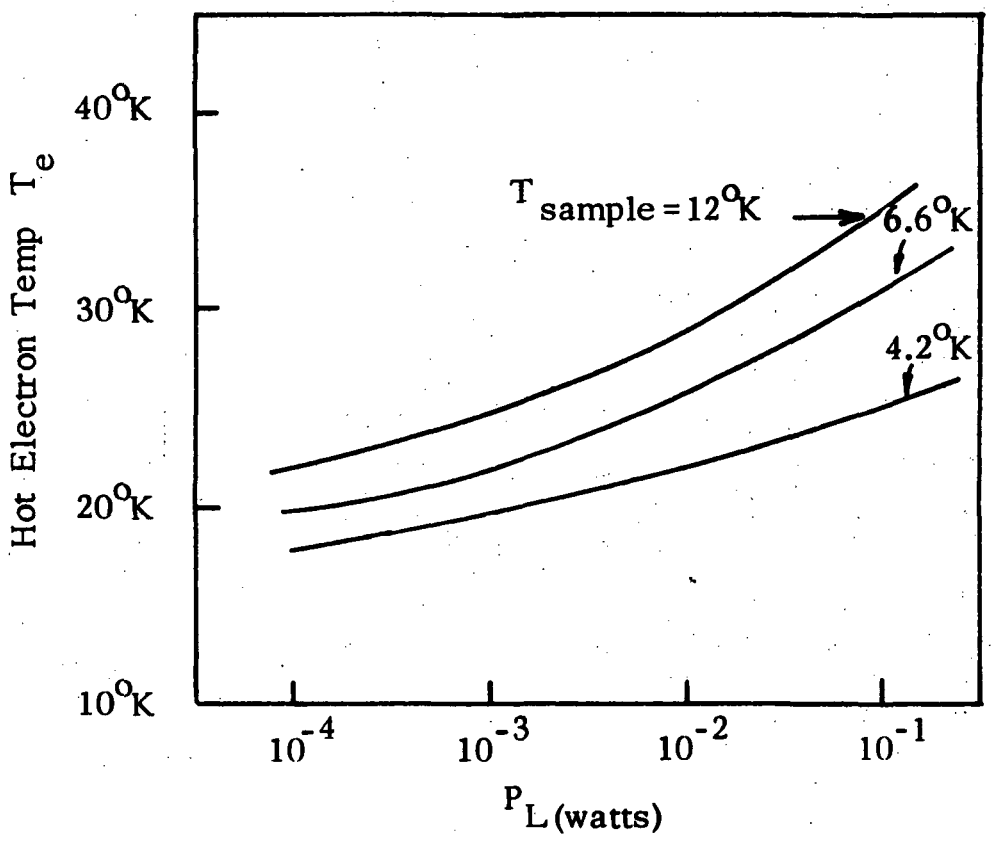

FIG. III-4 Theoretical Electron Temperatures T_e As a Function of Incident Optical Power, for Various Lattice (sample) Temperatures

temperatures the electron temperature equals the lattice temperature. Because of the logarithmic dependence of $P(T_e)$ on T_e the above curve is not affected much by parameters such as active volume, etc.

Before utilizing the values of T_e derived above to determine the appropriate momentum relaxation times, it must be verified if the concept of electron temperature, as used above, is valid. The concept of effective electron temperature is valid only if the energy distribution is Maxwellian. Conwell[43] has shown that when the principal energy-loss mechanism is polar optical-mode scattering, a Maxwellian distribution exists if the carrier density exceeds a critical value n_{min} given by

$$n_{min} = |q| E_o k\theta \left(\frac{T}{\theta}\right)^{1/2} (2\pi e^*)^{-1} \exp\left(\frac{-\theta}{T}\right) \quad (3.12)$$

where $(e^*/q)^2 = 1/\bar{\epsilon}$, $\bar{\epsilon}$ being the mean dielectric constant. Other parameters have already been defined. Taking T to be the maximum electron temperature of interest, n_{min} is 10^{13} cm^{-3}. This density is exceed by photoelectrons at 100μ W level at 4.2°K and at lower power levels as temperature is raised and electron lifetime increases. Hence the calculations of electron temperature are valid.

Although hot holes are generated by light, their lifetime is much shorter than that of the majority carriers; therefore, the hot-hole population can be neglected. The equations presented in the foregoing

can be used to compute hole temperature if the appropriate effective mass of holes, m_h^*, is substituted for m_e^*.

The momentum relaxation time, τ_{mom} corresponding to T_e can be derived theoretically; it is, however, physically correct to obtain τ_{mom} for a given electron temperature simply by referring to the curve for mobility-vs-temperature (Fig. V-1) the same sample (i.e. lattice) temperature. In this case the roles of lattice temperature and carrier temperature are interchanged, but the same scattering mechanism holds. Hence for photoconductivity calculations the values of electron mobility so derived are used; for photo-dielectric computations the corresponding are given by $\tau_{mom} = q\mu/m^*$.

RECOMBINATION AND TRAPPING

A simple model of recombination and trapping, germane to the discussion in Chapter V, is singled out for analysis here. Bube[19], Ryvkin[20] and Rose[44] have discussed the general photoelectronic theory on which these models are based. Fig. III-5 shows the energy band diagram of a semiconductor with two dominant levels, viz. a shallow donor-like trap located at an energy E_{t1}, below the conduction band and a deeper, acceptor-like trap at energy E_{t2} above the valence band. The word "trap" is used in its most general sense; the same level can also act as a recombination center, depending on the position of the

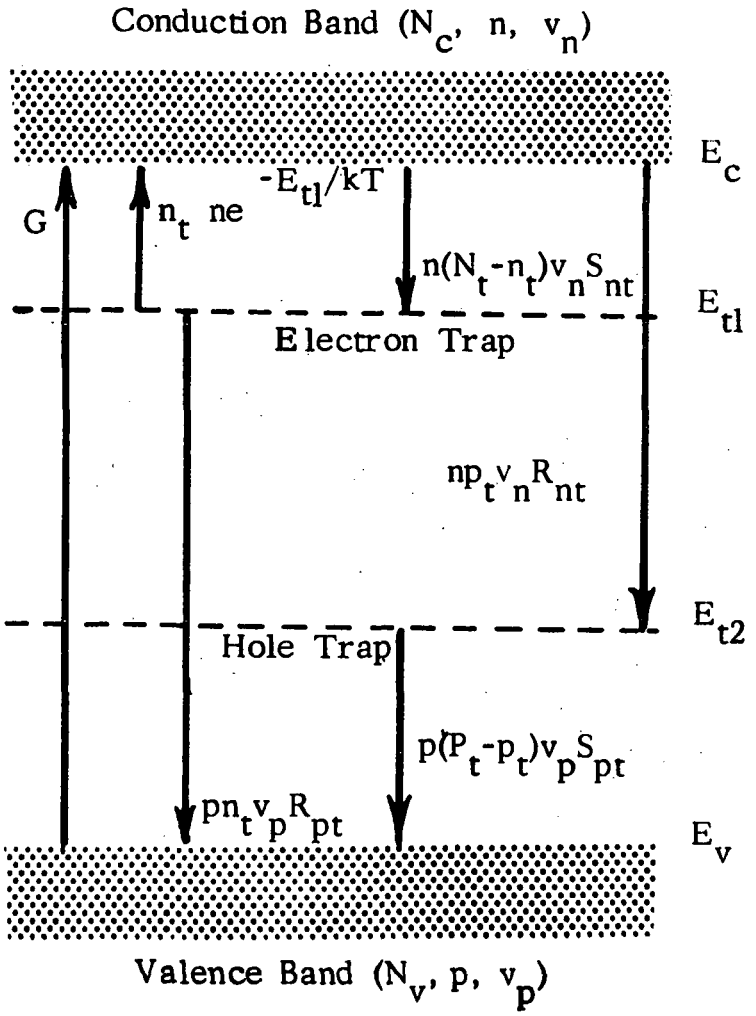

FIG. III-5 Shown is the Energy Level Model for Use When Both Hole and Electron Traps Exist. Direct Band-to-Band Recombination, Thermal Emission from the Hole Trap, and Sub-bandgap Optical Excitation are Neglected.

Fermi level and excitation intensity. In Fig. III-5 it is assumed that the Fermi level lies below the level E_{t1}. In this case it is assumed that the probability of re-emission of an electron captured by this level to the conduction band is much higher than that of capture of a hole at that center i.e., the center is not assuming the role of a recombination center.

Upon irradiation with light, carrier-pairs are generated at the rate G. Assume that the capture cross-section for holes by centers at E_{t2} is very high so that there is virtually instantaneous trapping of these minority carriers, with negligible recombination at electron traps. This situation is very similar to that which obtains in good luminescent phosphors such as CdS. Electrons proceed to both the conduction band and also to shallow electron traps, E_{t1}. When the Fermi level is below E_{t1} there is good "thermal contact" between centers E_{t1} and the conduction band, and electrons circulate back and forth. The rate equations for the system in the steady-state can be written down as follows:

$$\frac{dn}{dt} = 0 = G + n_t \nu_n e^{-E_{t1}/kT} - n(N_t - n_t) v_n S_{nt} - n_{pt} v_n R_{nt} \qquad (3.13)$$

$$\frac{dn_t}{dt} = 0 = n(N_t - n_t) v_n S_{nt} - n_t \nu_n e^{-E_{t1}/kT} - pn_t v_p R_{pt} \qquad (3.14)$$

$$\frac{dp}{dt} = G - pn_t v_p R_{pt} - p(P_t - p_t) v_p S_{pt} \qquad (3.15)$$

$$\frac{dp_t}{dt} = p\,(P_t - p_t)\; v_p\, S_{pt} - n_{pt}\, v_n\, R_{nt} \qquad (3.16)$$

where the terminology is as follows:

G: optical generation rate of carrier pairs

n, p: densities of free electrons and holes respectively

N_t, P_t: density of electron and hole traps, respectively

n_t, p_t: density of electron-occupied and hole-occupied traps, respectively

v_n: thermal (Fermi) velocity of electrons

S_{nt}: capture cross-section of shallow trap for electrons

R_{pt}: recombination cross-section of above center for holes when it is electron-occupied

ν_n: attempt-to-escape frequency for electrons

In equations (3.15) and (3.16) it is assumed that the hole trap is deep enough so that thermal re-emission is not a probable process at the temperatures of interest. If this assumption is removed, additional terms similar to the second term of (3.13) appear in both the above equations.

Rose[20] has shown, using a detailed-balance argument that the attempt-to-escape frequency ν_n is given by

$$\nu_n = N_c v_n S_{nt} \qquad (3.17)$$

where N_c, the effective density of states in the conduction band, is

$$N_c = 2\left(\frac{2\Pi m^* kT}{h^2}\right)^{3/2} \tag{3.18}$$

and

$$v_n = \left(\frac{2kT}{m^*}\right)^{1/2} \tag{3.19}$$

In Fig. III-5 the transition from the conduction band to the hole trap, at the rate $n_{pt} v_n R_{nt}$ represents the radiative recombination process observed in pure GaAs at very low temperatures by several workers.[16,17] It is interesting to note that the competing non-radiative recombination process is the transition from the electron trap to the valence band, whose rate is $pn_t v_p R_{pt}$. This process works essentially by depleting the hole supply. The ratio of the radiative to non-radiative processes, or the "efficiency of luminescence" is thus[27]

$$\eta = \left[1 + \frac{v_p R_{pt}}{v_n R_{nt}} \cdot \frac{v_n S_{nt}}{v_p S_{pt}} \cdot \frac{\nu_n e^{-E_{t1}/kT}}{\nu_{pe}^{-E_{t2}/kT}}\right] \tag{3.20}$$

which simplifies to

$$\eta = \left[1 + \frac{R_{pt} S_{nt} \nu_n}{R_{nt} S_{pt} \nu_p} e^{(E_{t2}-E_{t1})/kT}\right] \tag{3.21}$$

The above equation is important when the material is used in applications such as lasers or in photoluminescence studies.

Returning to the rate equations, a few observations can be made. The deep hole traps fill at a linear rate (after a rapid initial

transient) and until saturation of those traps is achieved, no direct electron-hole recombination is possible.

The transient response of the photoconductivity can be easily determined by noting that

$$\frac{d}{dt}\ (n + n_t) \ = \ G - \frac{n}{\tau_n} \tag{3.22}$$

where τ_n, the electron lifetime in the absence of minority carrier trapping, is given by

$$\tau_n \ = \ \frac{1}{N_t v_n S_{nt}} \tag{3.23}$$

Noting that $\frac{n}{n_t} \ = \ \frac{Ne}{N_t}\ e^{-E_{tl}/kT}$, the solution of (3.22) can be simplified by

$$n \ = \ G \tau_n \ (1 - e^{-t/\tau_r}) \tag{3.24}$$

where the response time τ_r is

$$\tau_r \ = \ \tau_n \left[1 + \frac{N_t}{N_c e^{-E_{tl}/kT}}\right] \tag{3.25}$$

or, approximately $(\tau_r)^{-1} \ \simeq \ N_c v_n S_{nt}\ e^{-E_t/kT}$ (3.26)

and it can exceed τ_n by many orders. This is an important manifestation of minority-carrier trapping. The same τ_r also governs the decay

rate. The decay curve is in general non-exponential because of the non-linear nature of the recombination. However, when $n_t << N_t$ the decay is quite close to being exponential.

A simple extention of the above analyses can be made to yield the steady state photoconductivity in the presence of trapping. When there is a great disparity between electron and hole lifetimes, the desired result can be approximated by using the response time instead of "true" lifetime τ_n in the equation for conductivity, viz.

$$\Delta\sigma = G\,\tau_r\,q\,\mu \tag{3.27}$$

where the hole contribution is neglected. At higher temperatures when the dark Fermi level drops much below E_{tl} the above analyses get complicated by the fact that E_{tl} centers change their role. The analysis of that case is best handled by Shockley-Read statistics and will be discussed in Chapter V.

CHAPTER IV

EXPERIMENTAL TECHNIQUES

The sensitivity of photodielectric measurements is limited primarily by the ability to determine small changes in the frequency and absorbed power of the microwave cavity containing the sample. Since the cavity "Q" determines the frequency resolution of the resonator, there has been considerable effort by Hartwig and coworkers[22-25,45] to exploit the high Q's possible with superconducting cavities, and Q's well above 10^6 have been used by them in sensitive cavity measurements. In addition to high Q, another requirement of a practical photodielectric test system is the ability to track frequency changes automatically, especially for transient measurements. These two considerations, among others, dictate the use of a cavity-controlled stable oscillator. The principal features of the oscillator system are presented in this chapter. In addition, the practical considerations involved in photoconductive and noise measurements are outlined.

X-BAND PHOTODIELECTRIC SYSTEM

The X-Band Cavity-controlled Oscillator is the heart of the instrumentation scheme. Fig. IV-1 shows in schematic form the setup used. The microwave cavity is the main sensing element, and its design features are outlined below.

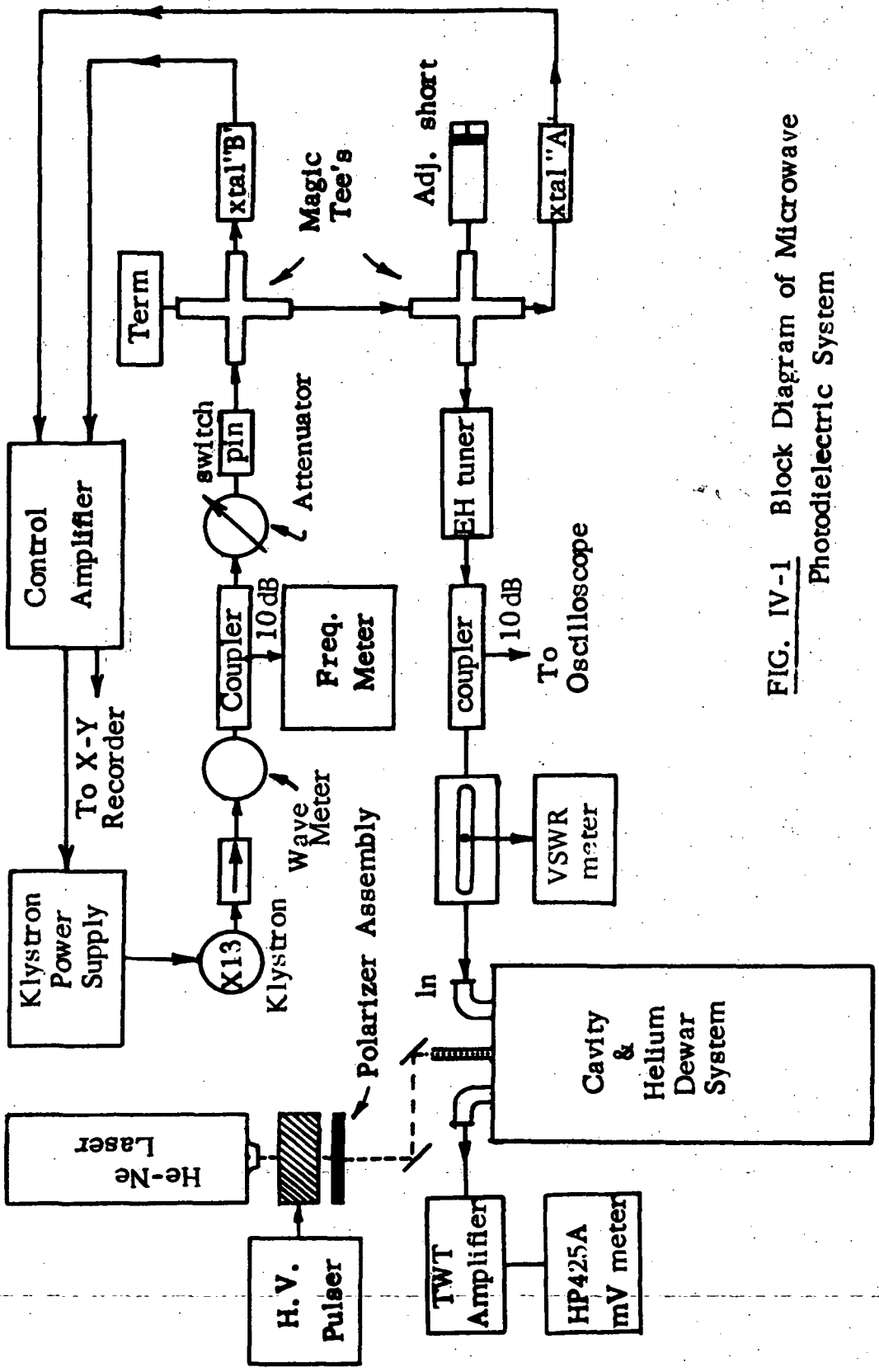

FIG. IV-1 Block Diagram of Microwave Photodielectric System

A. Microwave Cavity

The resonator is a right circular cylinder (Fig. IV-2) machined from solid electrical-grade copper stock. The cavity is designed to operate in the TM_{020} mode. In this mode, the electric field is normal to the cavity floor and its maximum coincides with the axis. This allows for a convenient positioning of the sample (centrally on the bottom) for optimum sensitivity. Light is shone on the sample through a 3/16" diameter aperture in the top cover plate. Since substantial currents flow through the contact between the top plate and cavity lip, the design emphasizes good pressure contact between the two by a tapered lip and use of a threaded lock ring. All internal surfaces are machined as smooth and true as possible and brought to a high degree of polish, in order to maximize the cavity Q. Two magnetic coupling loops, mounted on retractable dumbbell-shaped teflon forms are used to couple power in and out of the cavity. The loops pass through small apertures in the top plate at points where the magnetic field is about 0.7 times the maximum value. The travel of the probes allows for a coupling factor variation from 0.01 to greater than critical coupling. Tight coupling is necessary to support oscillation in presence of the lossy samples. Additional variation in coupling is possible by orienting the loops with respect to the magnetic field. The bottom of the cavity is threaded

so as to screw into a shroud or vacuum chamber; thermal contact with the latter is improved by use of high-conductivity grease at the interface.

The nominal resonant frequency of the empty cavity at 300°K is 9.02 GHz for light coupling. The loaded cavity at 4.2°K resonates at a somewhat lower frequency. Typically, a 1/8" diameter 0.02" thick GaAs sample exhibits a G(filling) factor of 1.5×10^{-3}. With light coupling the principal TM_{020} mode dominates and it is separated by more than 100 MHz from adjacent interfering modes. However, at low temperature the loaded cavity requires the coupling loops to be inserted in deep enough to cause spurious (unidentified) modes to propagate. Extreme caution is required to ensure that the oscillator has not "latched-on" to a near-by spurious mode. The only manifestation of this effect is no photodielectric frequency shift on illumination; the electric field of the spurious mode is oriented differently but the frequency is close to the correct mode frequency.

The Q of the cavity is limited mainly by the sample losses and radiation through the central aperture. Although the top plate is made 1/4" thick to reduce aperture losses, they are still approximately equal to sample losses. The empty cavity, lightly loaded has a Q of 9000 at 300°K; without the aperture it is close to the theoretical value of 18000. The loaded resonator at 4.2°K has a Q of 3000 to 5000

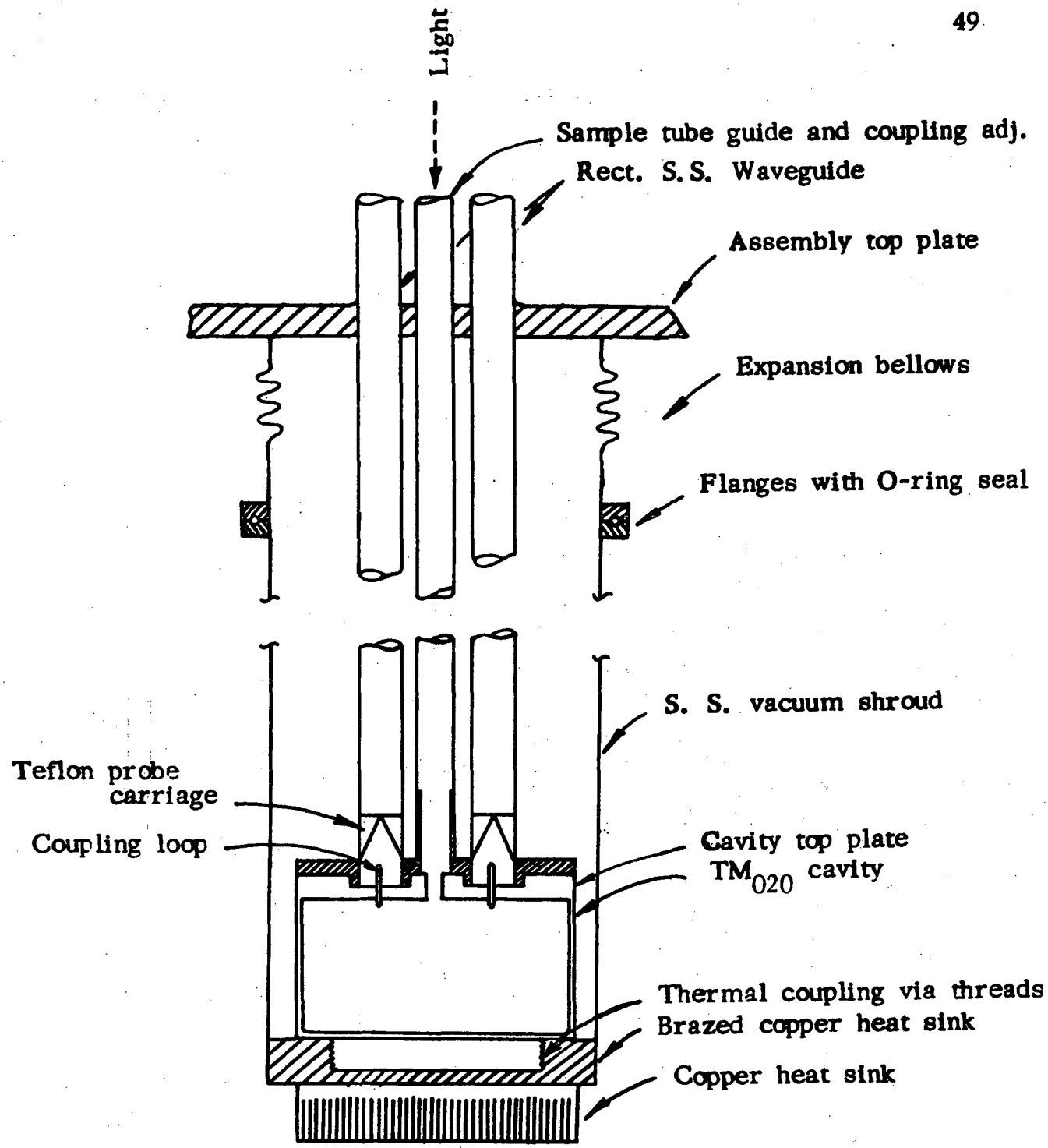

FIG. IV-2 Cryogenic Microwave Cavity Changer and Coupling System

depending on coupling. The high stability of the oscillator, resulting partly from tight coupling compensates for the low Q of the oscillator, since the "effective Q" of the system is $f/\Delta f$. Typically, the "effective Q" of the overall feed-back system is 9×10^6. Furthermore, the low Q of the cavity permits a response time or time constant ($\tau = Q/\pi f$) of approximately 0.2 microsecond. This low response time permits study of rapidly decaying phenomena in the semiconductor being studied. Since the cavity Q is already strongly limited by sample and aperture losses, and operation is desired at cavity temperatures up to 20°K or higher, no advantage exists in the use of a superconducting cavity.

In order to preclude non-linear effects due to carrier heating by the electric field, cavity input power was maintained less than lmW. The maximum electric field E_o in the cavity was computed from the relation[46]

$$P_{in} = \frac{\pi a}{\eta_1^2} E_o^2 R_s J_1^2 K_c a \, [h + a] \qquad (4.1)$$

where a is the cavity radius, η_1 is the intrinsic impedance of vacuum, h the cavity height, R_s the surface resistivity of copper, and J_1 the Bessel function of the zeroth order and first kind, and $(K_c a)$ is 5.5 for the TM_{020} mode.

Eq. (4.1) can be simplified to

$$E_o = 4.3 \times 10^{-5} \sqrt{Q P_{in}} \quad \text{volts/cm} \qquad (4.2)$$

The maximum field was maintained well below 0.01 volt/cm.

The cavity is fed by thin-walled stainless steel waveguides which minimize heat conduction and keep liquid Helium evaporation low. Teflon carriages, carrying the magnetic coupling probes slide in these guides; their position is controlled by rotating a central tube, which serves also as a light pipe. The assembly is placed in a vacuum chamber which is immersed in the Helium bath. Mylar-sealed microwave flanges make the assembly vacuum tight. The assembly is contained in a 6" I.D. stainless steel Helium dewar. A heater on the cavity is used to alter the cavity temperature. Cavity temperature is monitored by a calibrated carbon resistor and a Au-Co : Cu thermocouple. Fig. IV-2 shows the details of the cryogenic cavity assembly.

B. Microwave Oscillator

The variation of cavity susceptance with frequency forms the basis of the discriminator. The system, shown in Fig. IV-1, is essentially similar to that of Pound.[47] A good analysis of the system is done by Albanese.[24] A Varian X-13 klystron drives the cavity via an adjustable attenuator. This attenuator is needed to prevent "pulling" of klystron frequency by the cavity. The discriminator generates a

signal proportional to the instantaneous frequency error between the source and the resonator. This signal is amplified approximately 10^3 times by two low-noise hybrid operational amplifiers and the resultant signal modulates the repeller potential of the klystron, via an optically coupled isolator, to correct the frequency error. The bandwidth of the dc amplifiers limits the transient response to approximately 8 milliseconds. The amplified output of the discriminator is directly proportional to the desired frequency shift. Pound has shown that the discriminator output voltage V is given by

$$V = P_o D \frac{\alpha a}{(1+\alpha)^2+a^2} \qquad (4.3)$$

where α is the coupling coefficient, P_o is the power available from the matched generator connected to the discriminator, a is $2\Delta f Q_{Load}$, and D is the rectification efficiency of the detector crystals. The linear range of the system depends on α; it can be shown[47] that optimum system stability occurs at α near unity. When fast transients have to be studied, the output of the discriminator is viewed directly on an oscilloscope.

Several factors affect the attainable stability of the oscillator. The most important one is slow "flicker" (1/f) noise in the detector diodes. Use of Schottky-barrier (D5880B) diodes reduces this contribution by about 6dB. Other factors are: operating power level, amplifier

1/f noise, mechanical vibration of the components especially the dewar and cavity, and temperature variations of the cavity. Under good operating conditions a Δf of 1KC is achievable readily at 9GHz. This resolution is adequate for many experiments.

A PIN diode switch enables microwave power to be rapidly interrupted, for cavity Q measurements. He-Ne laser light, from a Spectra Physics 125 Laser is direct by a system of mirrors down through the cavity aperture on the sample. The intensity is varied by a variable analyser-polarizer assembly; approximately four orders of variation are obtainable in conjunction with added filters. A Spectra Physics light meter is used to calibrate optical power levels. For transient measurements, light can be interrupted by two means: a camera shutter for study of slow transients and an electro-optic shutter for rapid transients. The latter is biased to 10KV via limiting resistors; a mercury relay shorts-out the bias, when necessary, to generate a sharp light pulse edge with rise time of less than 10^{-7} secs.

HALL MEASUREMENTS

Carrier concentration and mobility as a function of temperature were determined by Hall measurements on clover-leaf shaped samples using the Van der Pauw technique.[48] Ohmic contacts were applied to the sample by alloying-in high purity tin spheres in an atmosphere of Hydrogen. This essentially renders the underlying

region N^+ by incorporating Sn on Ga sites. Fine wires were soldered onto the spheres. The electric field across the sample was maintained lower than 1 V/cm to prevent the impact ionization of impurities occuring at 3 to 5 V/cm at helium temperatures. The contacts were approximately linear at 4.2°K. A constant current source of 1μA facilitated measurements.

PHOTOCONDUCTIVITY MEASUREMENTS

PC and spectral response measurements were performed on the samples as prepared above. Care was excercized to minimize surface recombination by etching the surface lightly in a H_2SO_4:H_2O_2 etch for 15 secs prior to use. For low temperature measurements, the sample was mounted (on a copper heat sink) inside a brass 'thimble' located at the end of a thin-walled stainless steel tube. A fiber-optic light pipe illuminated the sample. A 1/8 watt carbon resistor was used as a thermometer. The arrangement is shown in Fig. IV-3. The assembly was inserted directly in the liquid He dewar and temperature adjusted by retracting the tube into the He vapor by suitable amounts. Sample heating by light was less than 0.25°K for light power up to 3mW. A low field was maintained across the sample both to preclude impact ionization[49] as well as to prevent minority carrier sweepout effects.[50] The use of a very low noise, high gain

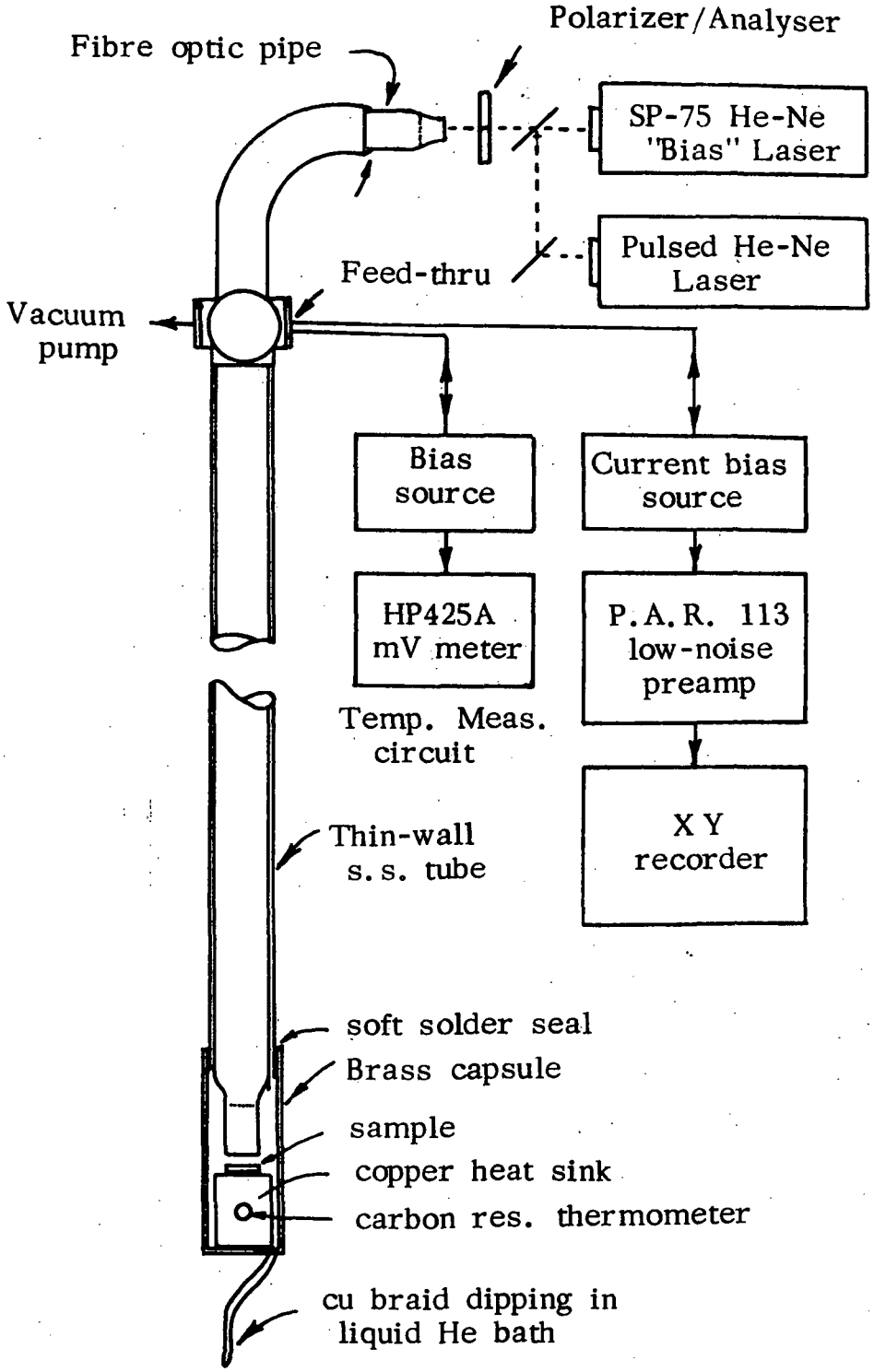

FIG. IV-3 Apparatus Used for Photoconductivity Measurements

PAR 113 preamplifier made low-level dc measurements possible. The optical system used was the same as for PD experiments; for spectral measurements a Jarrel-Ash grating monochromator was used. For light "bias" experiments, a smaller 0.8 mW Metrologic pulse-modulated laser was used as source, and the larger laser for setting the bias. Both light sources were directed onto the light pipe by a simple optical arrangement. For noise measurements, the scheme used was basically the same as for PC except for the use of a HP312A wave analyser, and a 4-sec time constant filter coupling its output to a wideband milivoltmeter.

PROPERTIES OF GaAs SAMPLES

Table IV-1 lists for reference the principal properties of the high purity GaAs under study. Room temperature properties were determined by Hall as well as differential-capacitance measurements.[51]

TABLE IV-1

CHARACTERISTICS OF SAMPLES USED

SUBSTRATE: Cr-doped Semi-Insulating GaAs
Resistivity $300^{o}K > 10^{8}$ Ω-cm

EPITAXIAL LAYER: 57-60 m thick, undoped; grown by vapor-phase from AsH_3-$GaCl_3$-H_2 reaction open-tube process

CARRIER CONCENTRATION: (C-V METHOD): $N_o(300^{o}K)$: 6×10^{13}

Hall Measurement: $300^{o}K$: 6×10^{13}

MOBILITY: $\mu_{300^{o}K}$: 7800 cm^2/V-S
$\mu_{77^{o}K}$: 100,000 to 130,000 cm^2/volt-sec.

SAMPLE SIZE: 1/8" diameter x 0.015" (typical)

CONTACTS: on clover-leaf geometry samples:

SURFACE TREATMENT: High polished as-grown, etched in 1:1 H_2SO_4:H_2O_2 15 sec.

CHAPTER V

EXPERIMENTAL RESULTS AND ANALYSES

INTRODUCTION

Experimental data on the two types of n-type GaAs samples, whose properties are listed in Table IV-1, are presented in this chapter. Hall effect data are discussed first, in order to lay the groundwork for interpretation of photo-conductive and photo-dielectric data to follow.

HALL EFFECT MEASUREMENTS

Hall effect measurements performed on the clover-leaf van der Pauw samples in the range of 4.2°K to 77°K are shown in Fig. V-1. The carrier concentration was derived from the Hall constant by using Blakemore's expression[52] for the case of a single donor species of density N_D, and partly compensated by acceptors of density N_A:

$$\frac{n(N_A+n)}{N_D-N_A-n} = \frac{N_c}{g} \exp\left(\frac{-E_D}{kT}\right) \qquad (5.1)$$

where n is the carrier concentration, E_D the donor ionization energy, g the degeneracy of the donor level, taken to be 2.0 and N_c the effective density of states at the temperature T. The solid curve is obtained by fitting the experimental data to Eq. (5.1) as discussed by Putley.[53] The material is seen to be quite closely compensated; the density of

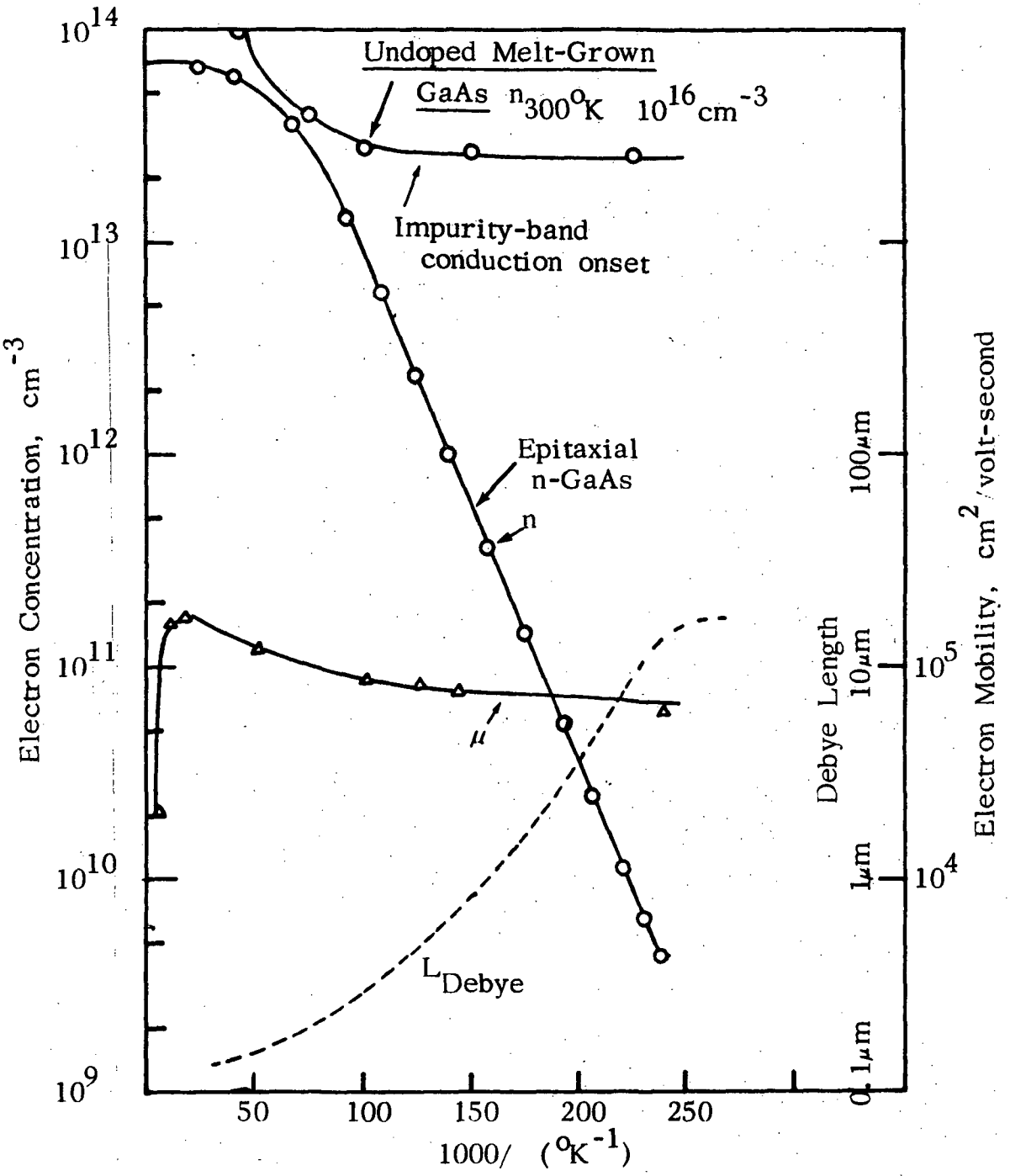

FIG. V-1 Hall Effect Measurements. Electron Concentration and Mobility as a Function of Temperature. The Calculated Debye Lengths are also Shown. Curve Fitting to Eq. (5.1) Shows $N_D = 2 \times 10^{14}$ cm^{-3} and $N_A = 1.4 \times 10^{14}$ cm^{-3} and $E_D = 4.95$ meV.

residual donors in the epitaxial layer is $N_D = 2 \times 10^{14}$ cm^{-3} and that of residual acceptors is 1.4×10^{14} cm^{-3}. This material is several orders of magnitude purer than undoped bulk GaAs, and represents the state-of-the-art of vapor-phase grown pure n-GaAs. One measure of the quality of the material, often used, is the electron mobility at 77°K. In this material, it is approximately 130,000 cm^2/vs, which compares favorably with about 150,000 cm^2/vs, the purest material reported by Lincoln Laboratories.[54]

The donor ionization energy, derived by curve-fitting, as mentioned above, is approximately 4.95×10^{-3}eV, which corresponds to a very shallow residual donor. This procedure of deriving the donor activation energy is liable to be quite inaccurate. A much more direct and accurate procedure, using a non-contact technique is discussed under Thermally Stimulated Susceptibility changes. The value of E_D obtained agrees reasonably well with the value 0.006 eV calculated on the basis of a hydrogenic model for the effective mass and dielectric constant of GaAs.[54] The nature of this donor will be commented upon later. Fig. V-1 shows clearly that up to temperatures as low as 20°K appreciable donor de-ionization does not occur, and the carrier concentration decreases rapidly with temperature only below about 20°K. This is a consequence of the very low ionization energy of the donor. The Hall constant increases monotonically with decreasing temperature,

and does not saturate or decrease. This indicates that impurity-band conduction[55] does not take place in this material. The onset of impurity band conduction at very low temperatures occurs when the donor density exceeds a certain critical value in compensated materials; the large electron orbitals of the light electrons, in materials such as GaAs, begin to overlap with each other if the density of donors is sufficiently high. In bulk-grown "undoped" GaAs (or the lesser purity epitaxial GaAs) onset of impurity-band conduction is clearly in evidence at a temperature of $20^{o}K$.

Mobility data, derived from Hall and electrical conductivity measurements are also presented in Fig. V-1. The general features of the mobility-temperature curve agree with theory.[56] On lowering the temperature below $300^{o}K$, the mobility increases due to reduction in polar-optical mode lattice scattering i.e. polar interaction of charge carriers with the optical lattice vibrations. At very low temperatures, ionized-impurity scattering limits the mobility. The latter mechanism is described[27] by $\mu \alpha T^{3/2}$ with the result that the mobility peaks in the vicinity of $50^{o}K$. The temperature dependence of electron mobility in GaAs has been discussed by Sze.[57] Lattice mobility varies as $(m^*)^{-5/2}T^{-3/2}$ and ionized-impurity-scattering as $(m^*)^{-1/2}N_I^{-1}T^{3/2}$ so that the overall mobility, which is a parallel combination, is given by $\mu \alpha (m^*)^{-3/2}T^{1/2}$. This relation is approximately borne out by the

curve in Fig. V-1.

In photodielectric experiments, the momentum relaxation time τ appears as an important variable, and determines the magnitude of frequency charges observed.

It is related to mobility by $\tau_{mom} = q\mu/m^*$ where μ is the mobility in meters^2/volt-second, m^* is the effective mass of free electrons ($m^* = .065$ m. for GaAs) and q the electron charge.

STEADY-STATE PHOTOCONDUCTIVITY

A. Spectral Response

Photoconductive (PC) as well as photodielectric measurements reflect both surface and bulk phenomena. In attempting to study the latter, surface effects must be suppressed as much as possible. Although careful surface-etch procedures were done in order to reduce surface recombination, it cannot be eliminated. It is desirable, at the outset, to estimate the relative extent of surface effects in the experiments. Spectral response of photoconductivity can be used for this purpose. Fig. V-2 shows the small-signal PC spectral response of epitaxial GaAs at 4.2°K. The sharp peak in PC at 8170 Å is close to the exciton absorption peak at 8190 Å reported by Sturge.[39] There is no other structure to the curve, indicating the absence of electronic transitions, other than the band-to-band transitions, in the range of measurement.

The ratio of the PC signal peak to the plateau height, designated F, can be related to the surface recombination velocity s, the lifetime of minority carriers and ambipolar diffusion length L. The analysis here is similar to that given by Goodwin.[59] Excess hole distribution in n-type GaAs by strongly absorbed light is described by

$$\frac{D d^2 \Delta p}{dx^2} - \frac{\Delta p}{\tau_p} = - \frac{G \alpha e^{-\alpha x}}{h \nu} \qquad (5.2)$$

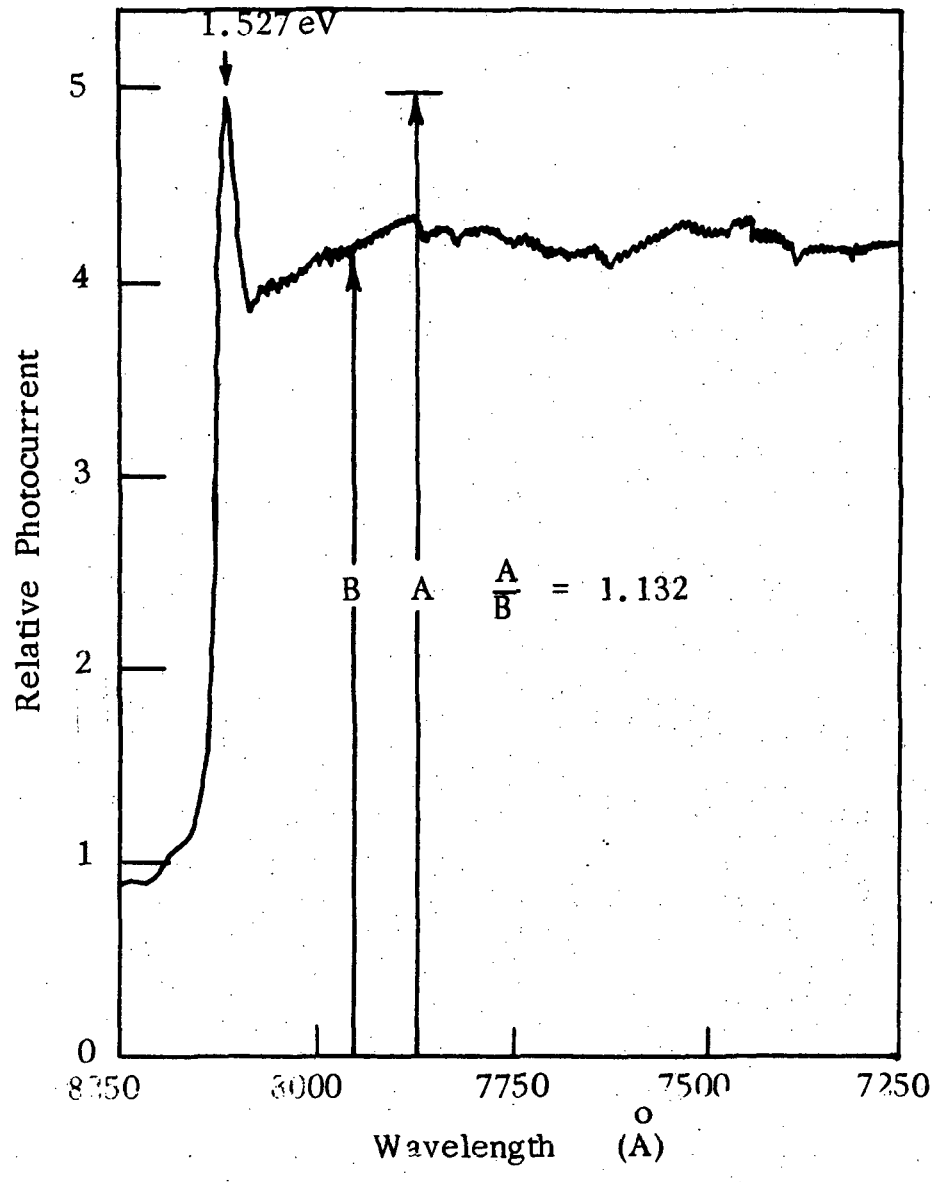

FIG. V-2 Spectral Response of Small-Signal Photoconductivity of Pure GaAs at 4.2°K. The Ratio A/B is a Measure of Bulk to Surface Recombination.

where D is the diffusion coefficient, α the optical absorption coefficient and G the optical pair-generation rate. Since $n \gg p$, D and L are simply the parameters of the minority carrier.

The solution of Eq. (5.2) is

$$\Delta p = Ae^{-x/L} - \frac{\tau \alpha I}{h\nu} \frac{1}{(\alpha^2 L^2 - 1)} \tag{5.3}$$

where A is a constant. Use of the boundary condition

$$D \frac{\partial \Delta p}{\partial x} = s\Delta p \quad \text{at} \quad x = o$$

leads to

$$\Delta p = \left[\frac{\alpha I}{h\nu(\alpha^2 L^2 - 1)}\right] \left\{\frac{\alpha L^2 + s\tau_p}{L + s\tau_p} e^{-x/L} - e^{-\alpha x}\right\} \tag{5.4}$$

The total photoconductance σ_{PH} is obtained by integrating Eq. (5.4) and results in

$$\sigma_{ph} = \frac{B \tau_p}{h\nu(L + s\tau_p)} \left[1 + \frac{S\tau_p}{L} \cdot \frac{1}{1 + \alpha L}\right] \tag{5.5}$$

where the constant B absorbs geometry and other factors.

When $S\tau_p \gg L$, σ_{ph} will depend upon wavelength; it will increase as decreases with $h\nu$. At short wavelengths $\alpha \gg 1/L$ and surface recombination will dominate, decreasing σ_{ph}. On the other hand, long wavelength radiation will pass through the epitaxial

layer without sufficient absorption, decreasing σ_{ph}. Thus a hump in the σ_{ph}-λ curve is expected, and this is seen in Fig. V-2. The ratio F, referred to earlier is given by the term in the square brackets of Eq. (5.5). In Fig. V-2, $F = 1.13\ D_p$ at 4.2°K can be calculated to be approximately 1 cm^2/sec; if τ_p is assumed to be 1 nanosecond, L becomes 0.3 μm, which is consistent with other measurements. Use of these values in Eq. (5.5) shows that S is about 7800 cm^2/sec, which is quite low; this can be expected, also, from the small hump in Fig. V-2. The composite lifetime τ_c is related to the bulk lifetime as follows:

$$\frac{1}{\tau_c} = \frac{1}{\tau} + \frac{2s}{d} \qquad (5.6)$$

Substitution of calculated values in Eq. (5.6) indicates that surface recombination rate is less than 10% of the bulk recombination rate for the etched GaAs sample.

B. Sub-linear Photoconductivity

The results of steady-state photoconductivity measurements are presented in Fig. V-3 and Fig. V-4. The latter figure is obtained by re-plotting Fig. V-3 for a constant light level, low enough to insure "small-signal injection" conditions in the sample. The differential photoconductance was separated from the overall sample conductance in a straight-forward manner.

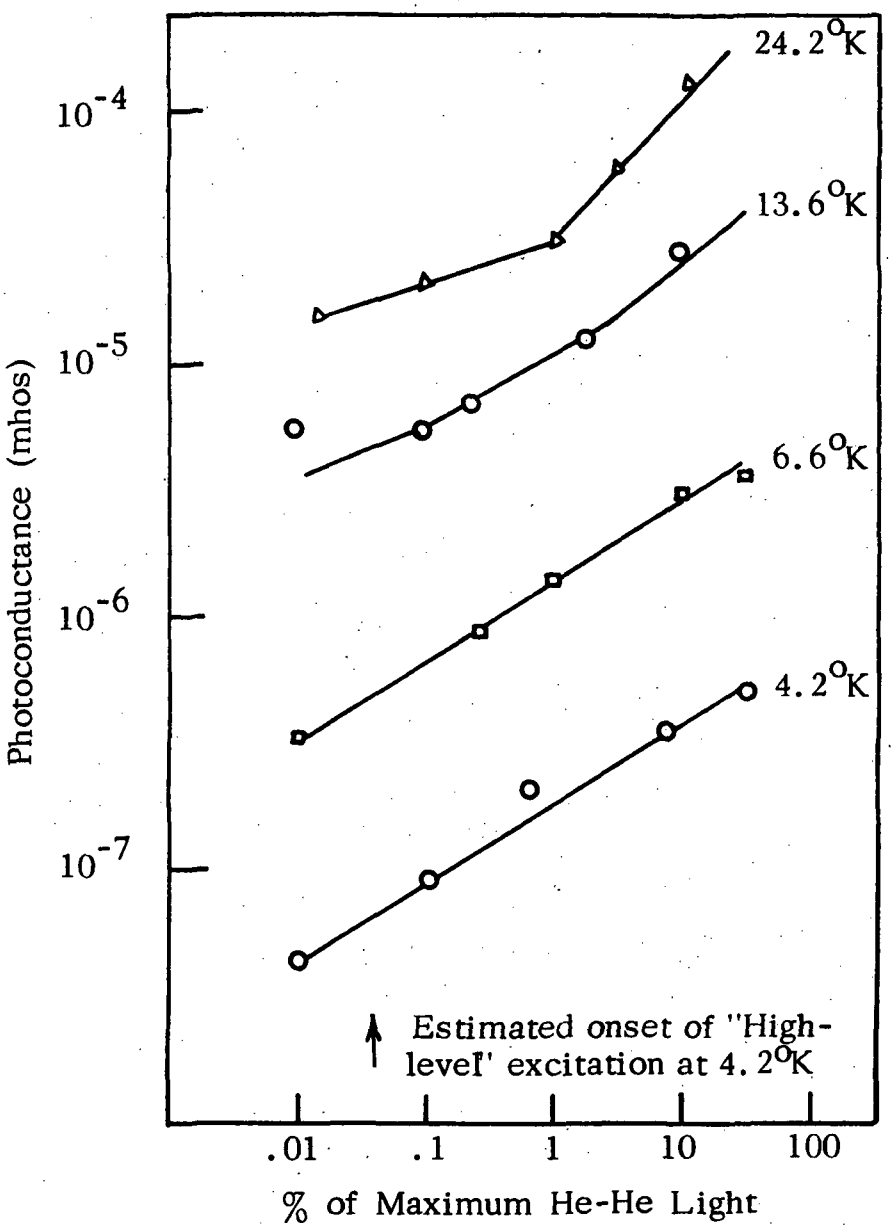

FIG. V-3 Steady-State Photo-Conductance as a Function of Light Level for Various Temperatures

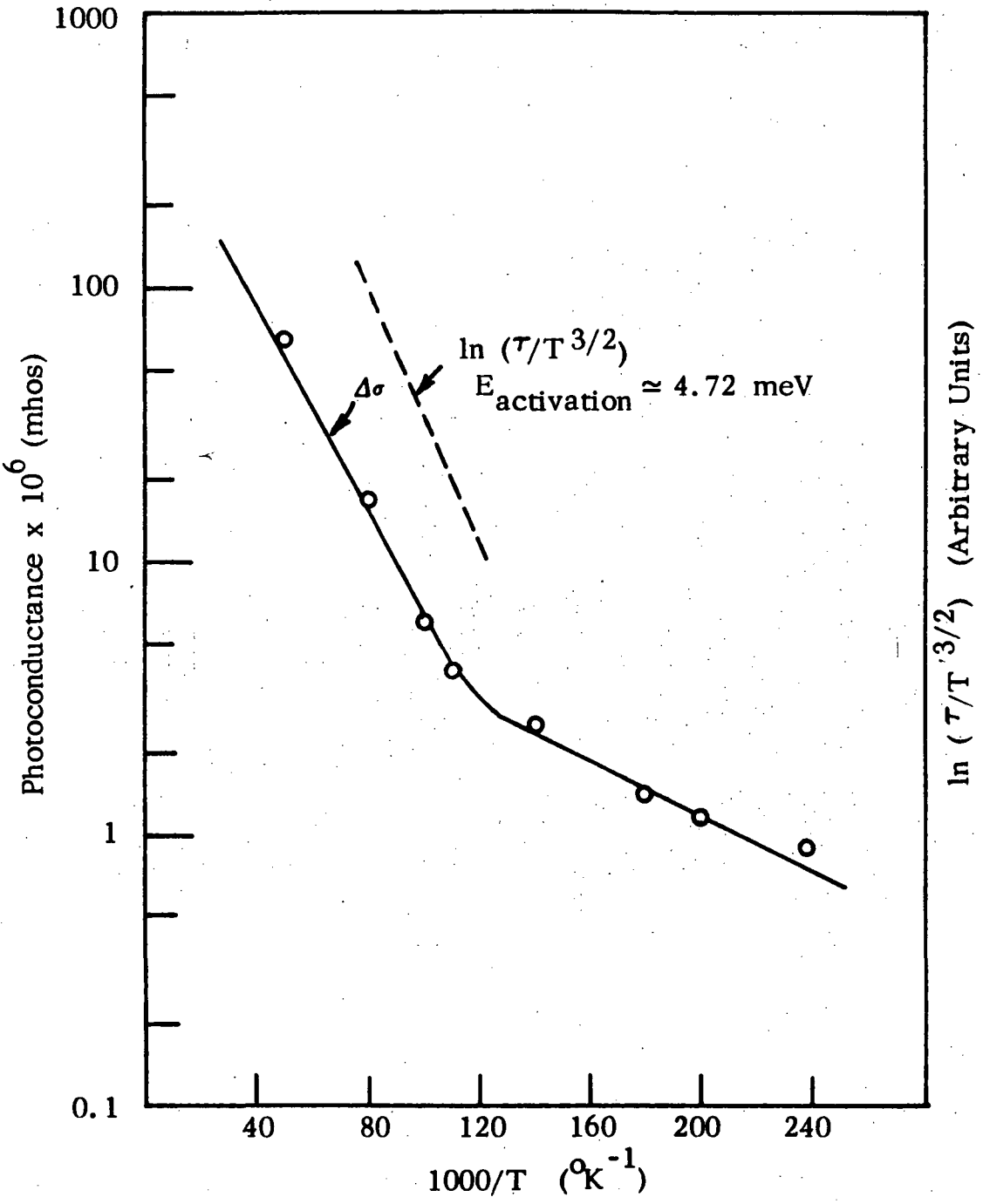

FIG. V-4 Photoconductance and ln $(\tau/T^{3/2})$ as a Function of Reciprocal Temperature. The Slope of the Latter Curve Yields the Activation Energy of the Centers Involved in Controlling the Lifetime.

Two features of the data are noteworthy. First, the lifetime of the dominant carrier increases rapidly as temperature rises from 4.2°K. This is a relatively unusual behavior. Between 4.2°K and 60°K the lifetime increases by nearly three orders of magnitude. Secondly, at a fixed temperature, the relationship between photoconductance and exciting light is highly sublinear. When this curve is corrected for mobility variation with electron temperature (the relationship between light power input and temperature of the excited electrons is discussed separately) and replotted as the $n - \psi$ curve of Fig. V-5, it is noted that n is proportional to $\psi^{0.34}$.

Such a strong degree of sub-linearity between photocarriers and the exciting light is difficult to explain on the basis of conventional photo-electronic models. Rose[20] discusses a wide variety of models of sub-linearity, all of which have in common the feature that certain trapping levels are converted into recombination centers as the Fermi level sweeps through them with increasing light. Such models, however, yield indices greater than 0.5 and are not applicable.

To explain the observed behavior we consider a model of surface-generated carrier pairs by strongly-absorbed light, and subsequent diffusion of carriers away from the surface. Since GaAs has an absorption co-efficient of 3.8×10^4 cm^{-1} at low temperatures, light is absorbed approximately at 0.25 μm surface layer, making the model

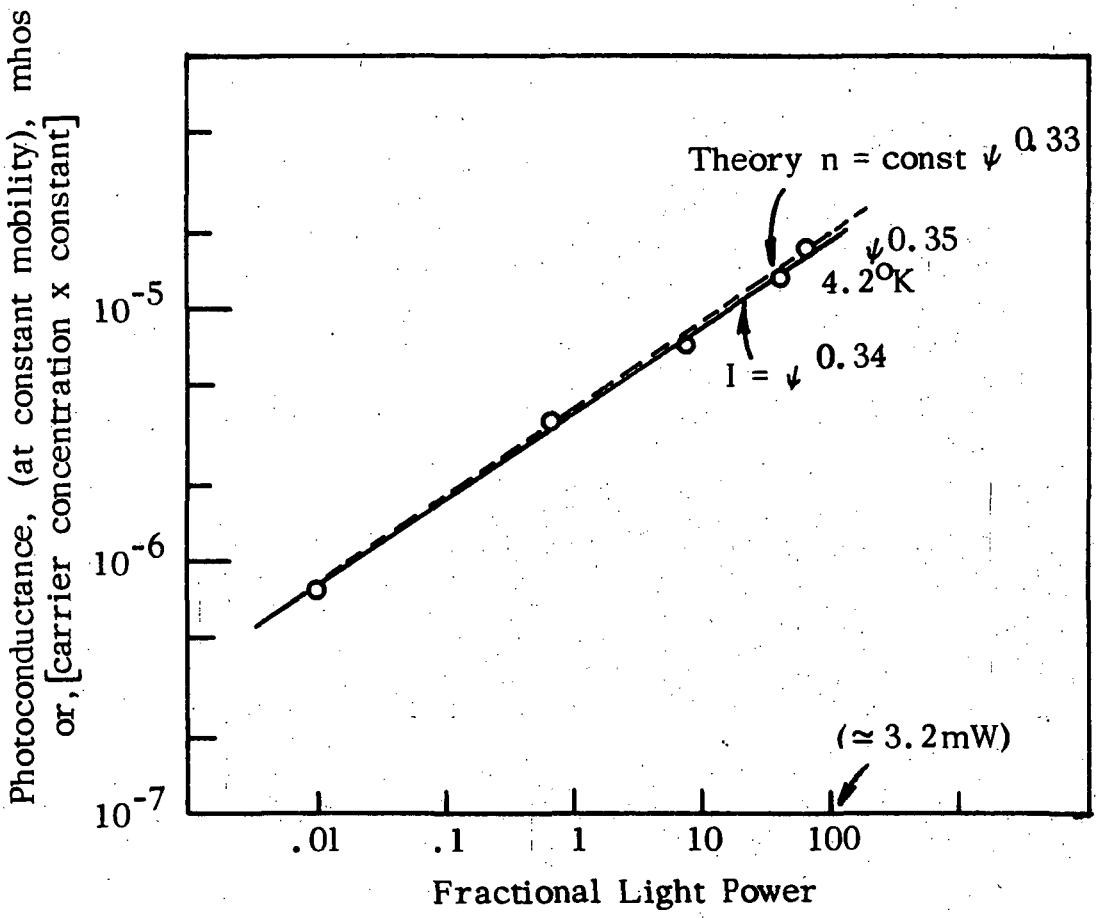

FIG. V-5 Comparison of Theoretical and Experimental "Lux-ampere" Curves ($n \sim \psi$) for High-Level Excitation (4.2°K)

applicable. Such a model is also consistent with photodielectric behavior, discussed later.

At low temperatures, thermal densities of electrons and holes are very small compared to optically-generated densities. The recombination of the carrier is then quadratic, i.e.

$$\left(\frac{dn}{dt}\right)_{recomb.} = \left(\frac{dp}{dt}\right) = r(n^2 - n_i^2) \qquad (5.7)$$

where n_i is the intrinsic density

The equation of continuity can be written

$$\frac{dn}{dZ} = D\,\frac{d^2n}{dZ^2} - r\,(n^2 - n_i^2) \qquad (5.8)$$

where Z is the direction of the diffusion gradient, D the diffusion coefficient of carriers, and r is given by

$$r = \frac{1}{2n_i\tau} \qquad \text{for intrinsic recombination.}$$

The first term in Eq. (5.8) accounts for the diffusion of carriers away from the surface and the second term represents bulk recombination of photo-excited pairs.

The above equations can be solved, subject to appropriate boundary conditions, to determine the desired n-ψ relationship. The solution is presented in Appendix I. The result is, for high light intensities,

$$n = (\text{const})\,\psi^{1/3} \qquad (5.9)$$

which agrees well with the experimental data. The conditions for validity of Eq. (5.9) are not obtained at low intensities or high values of lifetime, and the index departs from 1/3, as observed.

Physically, the cubic dependence of recombination rate of concentration stems from quadratic recombination coupled with a linear efflux of carriers away from point of generation.

This sublinearity prevents observation of photodielectric dispersion characteristics over a wide enough interval of carrier density for He-Ne light.

C. Temperature-dependence of Lifetime

The strong temperature dependence of free-carrier recombination lifetime as manifest in Fig. V-4, will now be discussed. It is more usual for lifetimes in solids to increase when the material is cooled. The observed behavior can be explained on the basis of the Shockley-Read model[44] for recombination via traps. It is shown that the active traps responsible are, in this situation, the shallow donor centers themselves. Alternative viewpoints are discussed later.

According to the Shockley-Read model, the lifetime of carriers under low-injection-level conditions can be expressed by the general equation[44]

$$\tau = \tau_{po} \frac{n_o + N_{cm}}{n_o + p_o} + \tau_{no} \frac{p_o + P_{vm}}{n_o + p_o} \qquad (5.10)$$

The symbols are defined as follows: n_o and p_o are the equilibrium densities of electrons and holes in their respective bands, N_{cm} is physically the density of electrons that would exist in the conduction band if the Fermi level coincided with the trap level:

$$N_{cm} = N_c e^{-\Delta E_m/kT} \qquad (5.11)$$

ΔE_m being the energetic location of the center below the conduction band. P_{vm} applies analogously to holes. τ_{no} is the low-injection-level lifetime in a heavily doped p-type material i.e. in a situation where centers are all occupied by holes and readily capture injected electrons;

$$\tau_{no} = \frac{1}{S_{nt} v_{th} N_t} \qquad (5.12)$$

where S_{nt} is the capture cross-section of empty centers for electrons, N_t the density of these centers and v_{th} the thermal velocity of electrons, τ_{po} is defined analogously.

The energy band scheme of pure epitaxial GaAs containing the proposed trap, active at very low temperatures, is shown in Fig. V-6. When the traps are located in the upper half of the band,

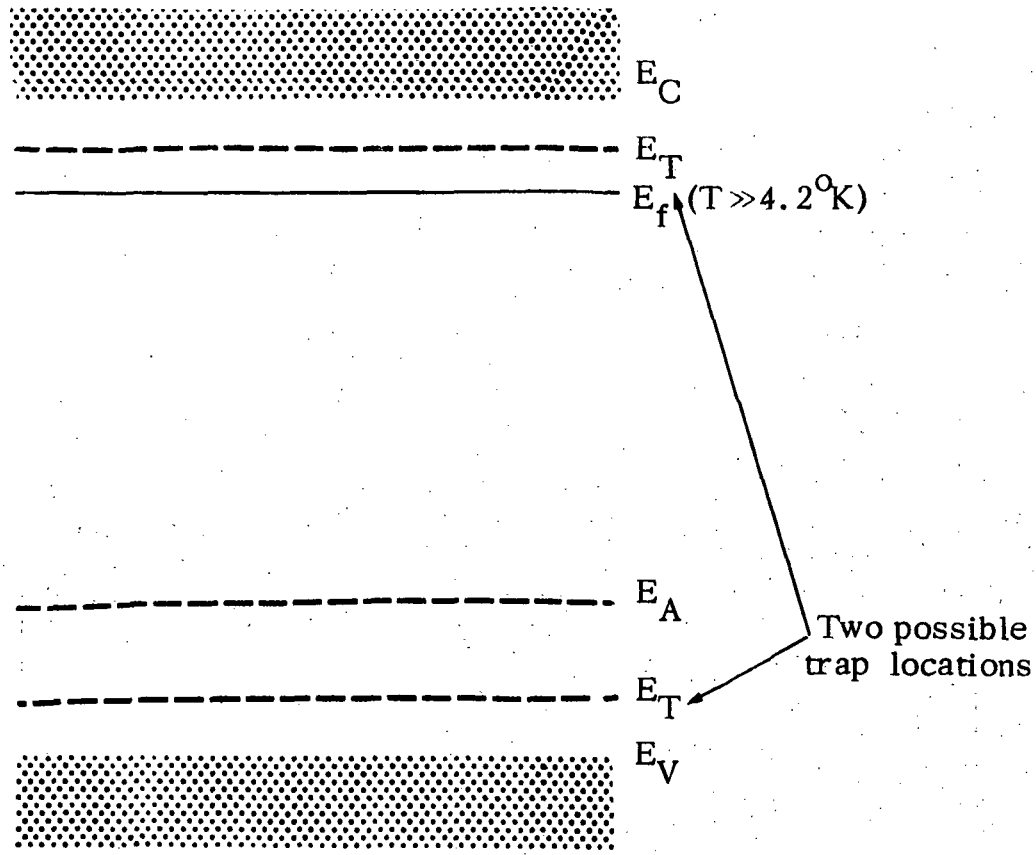

FIG. V-6 Showing Two Possible Energetic Locations of Shallow Traps Revealed by Shockley-Read-Model Analysis of Photoconductivity Data. Temperature is Assumed to be $>>4.2^oK$.

it can be seen with the help of Eq. (5.11) that

$$N_{cm} >> n_i >> p_{vm} \tag{5.9}$$

Using the above inequality, Eq. (5.10) reduces, for an n-type semi-conductor, to

$$\tau = \tau_{po} \left(1 + \frac{N_{cm}}{n_o} \right) \tag{5.13}$$

The temperature-dependence of τ can now be examined by tracing the effect of the moving Fermi level position as the temperature rises from absolute zero. Blakemore[52] has discussed the location of Fermi level for the case of a semiconductor containing N_D donors, partly compensated by N_A acceptors with $N_D > N_A$. The analysis is somewhat lengthy, but straightforward, and results in the following expression: $E_F - E_c =$ (5.14)

$$kT \ln \left\{ \frac{2\beta (N_D - N_A)}{\beta N_c + N_A \exp\left(\frac{E_D}{kT}\right) + \sqrt{\left\{\left[\beta N_c + N_A \exp\left(\frac{E_D}{kT}\right)\right]^2 + 4\beta N_c (N_D - N_A) \exp\frac{E_D}{kT}\right\}}} \right\}$$

where E_f is the Fermi Energy.

So long as $n_o << N_a$, i.e. for temperature insufficient to cause complete ionization of the donor atoms, Eq. (5.14) can be simplified considerably to

$$E_f = E_c - E_D + kT \ln \left[\frac{\beta (N_D - N_A)}{N_A}\right] \qquad (5.15)$$

For $N_D = 2 \times 10^{14} cm^{-3}$, $N_A = 1.4 \times 10^{14} cm^{-3}$, as determined from Hall measurements, and taking the spin degeneracy factor to be 0.5, Eq. (5.15) can be written

$$E_F = E_c - E_D - 0.54\ kT \qquad (5.16)$$

Thus, at absolute zero temperature, the Fermi level is fixed at the donor level. The presence of the compensating species does not permit E_f to cross the donor level and move closer to the conduction band, as happens in an uncompensated semiconductor.

Returning to Eq. (5.10) it is noted that at temperatures approaching absolute zero, $N_{cm} < n_o$ and $\tau = \tau_{po}$. As the temperature is further increased, and the Fermi level drops, n_o rises as donors get ionized. $N_{cm} = N_c e^{-\Delta E_m/kT}$ increases exponentially. When donor ionization is almost completed, N_{cm} exceeds n_o and it increases further as temperature rises. The unity in Eq. (5.13) can now be neglected, and

$$\tau = \frac{\tau_{po}}{n_o} \cdot N_{cm} \qquad (5.17)$$

Eq. (5.17) can be simplified to

$$\frac{\tau_{po}}{n_o} N_{cm} = \frac{\tau_{po}}{n_o} \cdot 2 \frac{(2\pi m^* kT)^{3/2}}{h^3} e^{-\Delta E_m/kT}$$

$$\therefore \quad \tau = \text{constant } T^{3/2} e^{-\Delta E_m/kT} \qquad (5.18)$$

Thus, the slope of $\ln (\tau/T^{3/2}) - \frac{1}{T}$ curve (Fig. V-4) or (photoconductance/$T^{3/2}$) - $\frac{1}{T}$ directly yields the principal trap energy.

This slope, derived from Fig. V-4 yields an activation energy of 0.0047 eV. This energy is very close to E_D, the ionization energy of the donor, and indicates that at low temperature the active recombination center is, in fact, the donor level itself. Such behavior has previously been observed in doped Germanium at very low temperatures.[58]

Physically, the donor "traps" communicate directly with the conduction band at higher temperatures: an electron captured by such centers is much more likely to be ejected back to the conduction band than to trap a hole. Thus, at higher temperatures, the donor centers simply act as "safe" traps and not as recombination centers. As the temperature is lowered, thermal transitions back to the nearest band become exponentially less likely since less energy is available to overcome the 0.005 eV barrier. Under the circumstances holes have a much higher probability of being captured. Thus, recombination traffic flows through additional (donor) centers and free carrier lifetime

decreases exponentially on cooling. Conceptual tools such as demarcation levels, etc., used by Rose[20] can also be used in this situation; they are merely alternative viewpoints of the Shockley-Read model discussed above.

Two implications of the above analysis must be considered. First, although it has been assumed so far that the active centers are located close to the conduction band, an equally plausible model can be created for active centers close to the valence band; in fact, the slope of Fig. V-3 does not identify the band close to which these centers lie.[44] An additional experiment is necessary to clear the ambiguity. Such experiments as quenching of photo-conductivity by infrared radiation can be used. In this case, however, far-IR radiation of several-hundred-micron wavelengths would be required in view of the low activation energy of the traps. This is precisely where the convenience and power of photodielectric measurements can be used to augment other data.

Secondly, if the model is correct, it predicts increased trapping as temperature rises from 4.2°K. Photodielectric measurements again provide a direct method to verify this, since trapped-carrier as well as free-carrier effects alter the dielectric constant. The next section is concerned with interpretations of such measurements.

STEADY-STATE PHOTODIELECTRIC BEHAVIOR

A. Thermally Stimulated Susceptibility Changes

Photodielectric measurements are best discussed by starting with thermally-stimulated dielectric constant changes, so that comparison may be made with Hall measurements discussed earlier. Thermally-stimulated susceptibility changes are conceptually analagous to the well-established technique of thermally-stimulated conductivity introduced by Garlick[19] et. al., and used extensively to study deep traps in materials. In that method, charge stored in traps is ejected out under thermal stimulation; the trap parameters are gleaned from knowledge of the temperature of peak conductivity as the temperature is swept. Thermally-stimulated changes in the dielectric susceptibility of semiconductors can be introduced in an analogous fashion; in this case, however, the total frequency change is the relevant quantity measured.

When applied to study the polarization due to electrons in shallow donor states, it is convenient to determine the overall change in dielectric constant as donors are fully ionized. In the experiments performed, the requisite temperature range was not covered. Instead, the sample was heated by radiation from a carbon-dioxide laser, and the temperature range 4.2°K to 14.8°K was traversed. In later experiments, a heater wound around the cavity served to heat the sample

and cavity. The results were identical, indicating that the sole effect of the 10.6 μm radiation from the CO_2 laser was thermal, and no other electronic transitions were involved.

The frequency decrease observed on heating the cavity and sample from 4.2°K to 14.8°K was 138kHz. Thermal expansion of the copper cavity contributes a frequency decrease $\Delta f = f \alpha \Delta T$ where α the mean linear expansion coefficient in the temperature range is 1.49×10^{-6}. This gives a frequency decrease of 13.5kHz and leaves 124kHz as the contribution of the sample.

The contributions to polarizability of thermally-generated free electrons and ionized traps can be determined using Eq. (2.12) and Eq. (2.16) respectively. The entire epitaxial layer, 50 μm thick is active in this experiment; the substrate contribution was found to be zero, in an independent experiment using a chromium-doped GaAs (semi-insulating substrate material) of identical geometry. The relevant filling factor, G, is then G^1 = G (experimentally determined for sample) x epi-layer thickness/overall sample thickness. G^1 was determined to be approximately 1.5×10^{-4}.

At 14.8°K the free-carrier concentration, from Fig. V-1 is $4 \times 10^{13} cm^{-3}$. For a shallow trap $(\omega/\tau)^2$ is much smaller than ω_o^2, and the cavity frequency ω is also several orders smaller. Hence Eq. (2.16) simplifies to

$$(\Delta\epsilon)_{\text{detrapping}} = \frac{-ne^2}{m^*\epsilon_o} \cdot \frac{1}{\omega_o^2} = \frac{-1.69 \times 10^{25}}{\omega_o^2} \qquad (5.19)$$

The negative sign arises because of detrapping, i.e. loss of polarization of previously bound electrons. The free-carrier contribution to susceptibility change can be calculated using Fig. V-1 to determine ω_p and τ. The result is $\Delta\epsilon$ (free carriers) $\simeq$ -17.

The initial dielectric constant, at 4.2°K is the sum of the lattice contribution and that due to $(N_D - N_A)$ trapped electrons, since the thermal free-carrier component is negligible. This gives $(\epsilon)'_{4.2^oK} \simeq 20$. Now using Eqs. (5.19) and (2.16) yields

$$\frac{-1.69 \times 10^{25}}{\omega_o^2} = -5.6$$

which, with Eq. (2.15) yields E_t = 0.0049eV. This is almost exactly the value obtained by a least-squares-fit analysis of the slope of the Hall Coefficient-temperature curve. Thus, we have a non-contact technique that can accurately determine shallow trap locations, or active impurity ionization energies. In practice it would be sufficient to stimulate the material thermally until full donor ionization occurs and use the room-temperature carrier concentration in calculations. This technique is particularly apt for strongly compensated materials where the material turns insulating even above 77°K. A good case in point

is the "Gunn quality" Te + O_2 doped material which becomes insulating about -55°C, even though very shallow (Te) donors are involved.

It is interesting to note the strong changes induced in the dielectric constant in this simple experiment; also, under optical stimulation, the free-and trapped-carrier photo-dielectric effects are generally of opposite sign. In the situation described above, both effects are of comparable magnitude and like sign.

B. Photodielectric Changes as a Function of Temperature

If strongly absorbed He-Ne laser light is incident on the surface of the sample, a gradient of photo-generated carriers is superposed on the thermal free carriers. In order to study changes in the dielectric constant caused by this gradient, it is first necessary to discuss the distribution of photo-carriers.

As discussed earlier, photo-excitation of GaAs at low temperature results in generation of excess electrons, since the non-equilibrium holes have a very short lifetime due to preferential trapping. The strongly asymetric photoconductivity can be treated essentially as being unipolar, much the same as for impurity photoconductivity. In this case, the distribution of excess electrons is very different from the ambipolar case, where a lifetime dependent diffusion length characterizes the diffusion.

The unipolar-photoconductivity case has been treated by Ryvkin[26], who has shown that the density gradient of excess electrons is described by

$$\frac{d^2\Delta n}{dx^2} - \frac{\Delta n}{L_e^2} = \frac{1}{L_e^2}\,\frac{\kappa I}{2n_o\gamma} \qquad (5.20)$$

where γ is the recombination coefficient, Δn is the excess electron concentration, along the direction normal to the surface, in a thick sample illuminated by surface-absorbed light of intensity I, and κ the optical absorption coefficient. For GaAs at low temperature, (6328Å light) κ is approximately $3.8 \times 10^4\ cm^{-1}$ i.e. He-Ne light is absorbed in about a 0.25 μm surface skin. For samples with active epitaxial layers exceeding a few tens of microns, Eq. (5.20) is, therefore, an excellent approximation. The important parameter governing the diffusion is the Debye length of electrons, L_e given by

$$L_e = \left(\frac{\epsilon kT}{8\pi q^2 n_o}\right)^{\frac{1}{2}} \qquad (5.21)$$

where k is Boltzmann's constant and ϵ the permittivity of the semiconductor. L_e is the counterpart of the diffusion length, $L_D = (D_{ambipolar} \cdot \tau_n)^{\frac{1}{2}}$ which occurs in the ambipolar photoconductivity case. Equations (5.20) and (5.21) are based on a model of weak photo-excitation, viz. $\Delta n \ll n_o$. In the experiments with laser-

light excitation this condition does not obtain. The diffusion for strong excitation is difficult to analyze, since it is non-linear, being characterized by a Debye length which increases as the excess density falls off. Nevertheless, as Ryvkin points out, Eq. (5.21) still can be used to estimate the diffusion profile for strong excitation.

Solution of Eq. (5.20) subject to the boundary conditions $\Delta n \to 0$ as $x \to \infty$ yields

$$\Delta n = (\Delta n)_{surf} e^{-x/L_e} \tag{5.22}$$

Using the above expression, we can write for the plasma frequency at depth x from the surface:

$$\omega_{p\psi}^2(x) = \omega_{p\psi_o}^2 e^{-x/L_e} \tag{5.23}$$

where the subscripts ψ and o refer to optically generated and surface charges, respectively.

This allows us to extend the previously derived expression (2.12) for dielectric constant of a uniformly excited material to the case of surface-excitation, obtained experimentally:

$$\epsilon_{\psi}(\omega) = \epsilon_{\infty} \left[1 - \frac{1}{L_e} \int_0^{L_e} \frac{\omega_{p\psi_o}^2 e^{-x/L_e}}{1 + \omega^2 \tau^2} dx \right] + \epsilon_T' \tag{5.24}$$

i.e.

$$\epsilon_{\psi}(\omega) = \epsilon_{\infty}\left[1 - \frac{0.63\,\omega_{p\psi_o}^{2}}{1+\omega^{2}\tau^{2}}\right] + \epsilon'_{T} \qquad (5.25)$$

Eq. (5.25) represents the dielectric constant averaged over the penetration depth, L_e of the photo-excited carriers. For clarity, the thermal-electron contribution has been neglected in this expression. It must be included when computing frequency shift on illumination. ϵ'_T is now the average, over this same distance, of the contribution of electrons trapped in shallow trapping states, i.e. donor-like centers. $\epsilon'_{T\psi}$ will, in general, differ from ϵ'_T the dielectric constant contribution of these same species under dark-equilibrium conditions.

The averaging performed in Eq. (5.25) requires some justification. Since photodielectric frequency shifts experimentally observed depend on reciprocals of the dielectric constants, it is strictly correct only to determine the frequency shifts due to each elemental layer, illuminated and un-illuminated, using Eq. (2.11) and (2.25). However, such an analysis becomes quite difficult to perform. Furthermore, since the frequency shift is physically caused by the difference in the electrostatic energy stored per cycle in the sample, the averaging process appears to be justified.

Combining Eq. (5.25) with Eq. (2.24) yields the desired

relation between observed frequency change Δf_{ψ} on illumination, and other parameters:

$$\frac{\Delta f_{\psi}}{f} = G \frac{L_e}{t} \left\{ \frac{1}{\epsilon_\infty \left[1 - \frac{0.63\omega_{p\psi_o}^2 + \omega_{pth}^2}{1+\omega^2\tau_{hot}^2} \right] + \epsilon'_{T\psi}} - \frac{1}{\epsilon_\infty \left[1 - \frac{\omega_{pth}^2}{1+\omega^2\tau^2} \right] + \epsilon'_T} \right\} \quad (5.26)$$

In the foregoing expression G is the experimentally determined "filling-factor" (0.0015 in the X-band measurements), t, the thickness of the sample, ω_{pth} the plasma frequency for the thermal-equilibrium electron density. τ_{hot} represents the momentum relaxation time for hot carriers, as previously discussed. τ is the corresponding value for "thermal" electrons.

The photo-dielectric data obtained on steady-state frequency shift under illumination, Fig. V-7, can now be combined with conventional photoconductive data to glean additional information.

Values for $\omega_{p\psi_o}^2$, the surface plasma frequency due to photocarriers, can be calculated quite readily, as follows. For a "thick" sample, i.e. whose thickness greatly exceeds absorption length of light, the photoconductance can be shown,[44] by simple integration, to be independent of the optical absorption coefficient and given by

$$\Delta\sigma = \text{geometry factor} \times q\mu \times n_{\psi o} \quad (5.27)$$

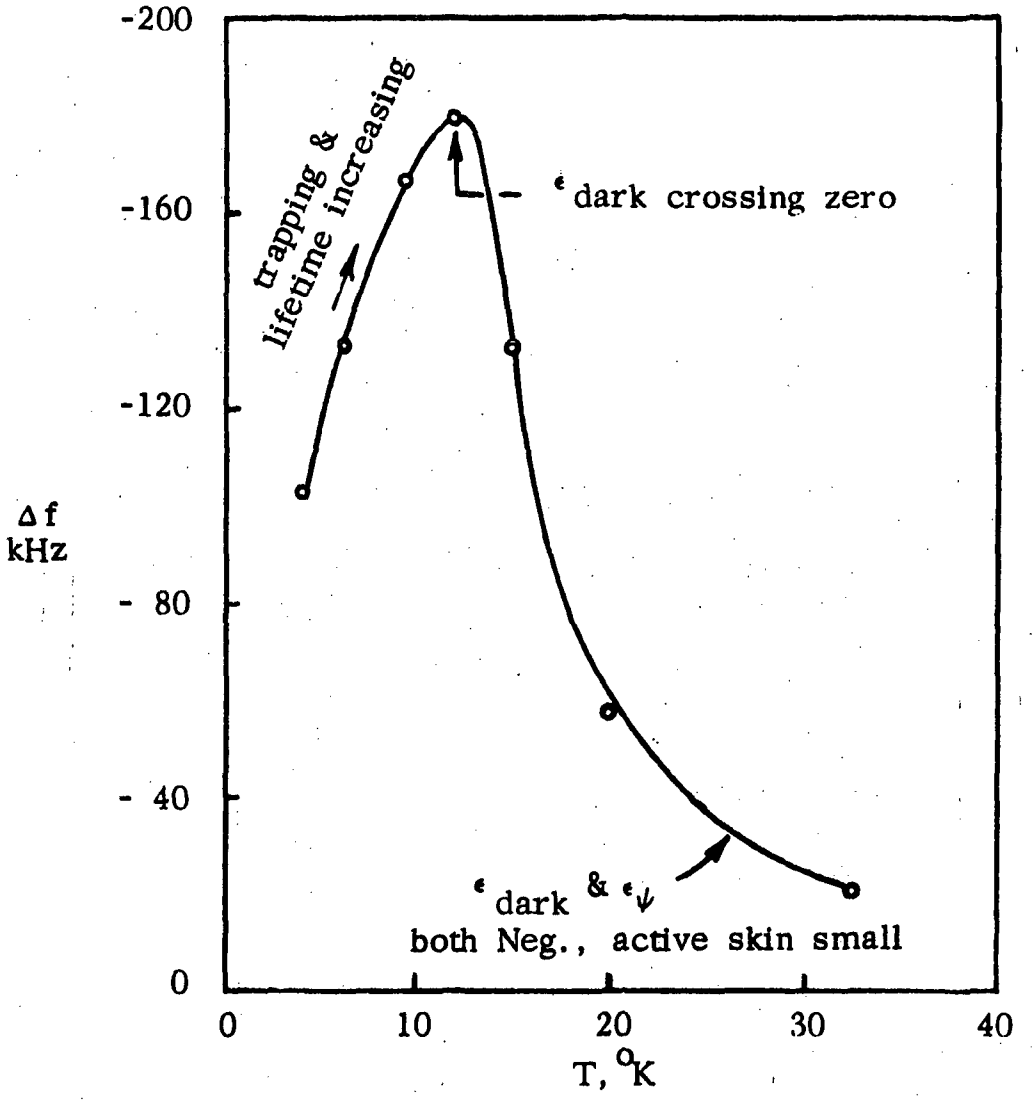

FIG V-7 Frequency Shift on Illumination As a Function of Temperature. Strong (≃20mW) He-Ne Light Excitation

Using Eq. (5.27) and the photoconductance data from Fig. V-2, $\omega^2_{p\psi_o}$ is readily determined, since $n_{\psi o}$ and $\omega^2_{p\psi_o}$ are related by Eq. (2.21) ω^2_{pth} can likewise be calculated from the thermal equilibrium concentration n_o, derived from Fig. V-1 for a given temperature. τ is obtained from Fig. V-1 and the relation $\tau = \mu q/m^*$. It varies from 2.4×10^{-12} sec at 4.2°K to approximately 8.4×10^{-12} sec. at 55°K. ω is 5.5×10^{10} rad sec^{-1} for the X-Band cavity frequency of 9.02 GHz. The lattice dielectric constant varies but little over the low temperature range of interest and its value can be taken as 10.5.

In discussing the thermally stimulated polarizability changes, it was noted that for a partially compensated material containing N_D donors and N_A acceptors per unit volume, $N_D > N_A$, the donor atoms compensate the acceptors even at temperatures near absolute zero. Thus, at 4.2°K the density of neutral donors is approximately $(N_D - N_A)$ i.e. $\sim 6 \times 10^{13}$ cm^{-3} for the pure epitaxial material under study. The number of free carriers at 4.2°K is several orders of magnitude smaller. Hence, the number of electrons trapped by shallow states of 0.005 eV binding energy is 6×10^{13} cm^{-3} at 4.2°K. The real part of the dielectric constant contributed by these trapped electrons, ϵ'_T can be calculated from Eq. (2.14) and (2.15).

This contribution is plotted as a function of temperature in Fig. V-8 which also shows the overall dielectric constant change derived from Eq. (2.25) and the experimental data of Fig. V-7.

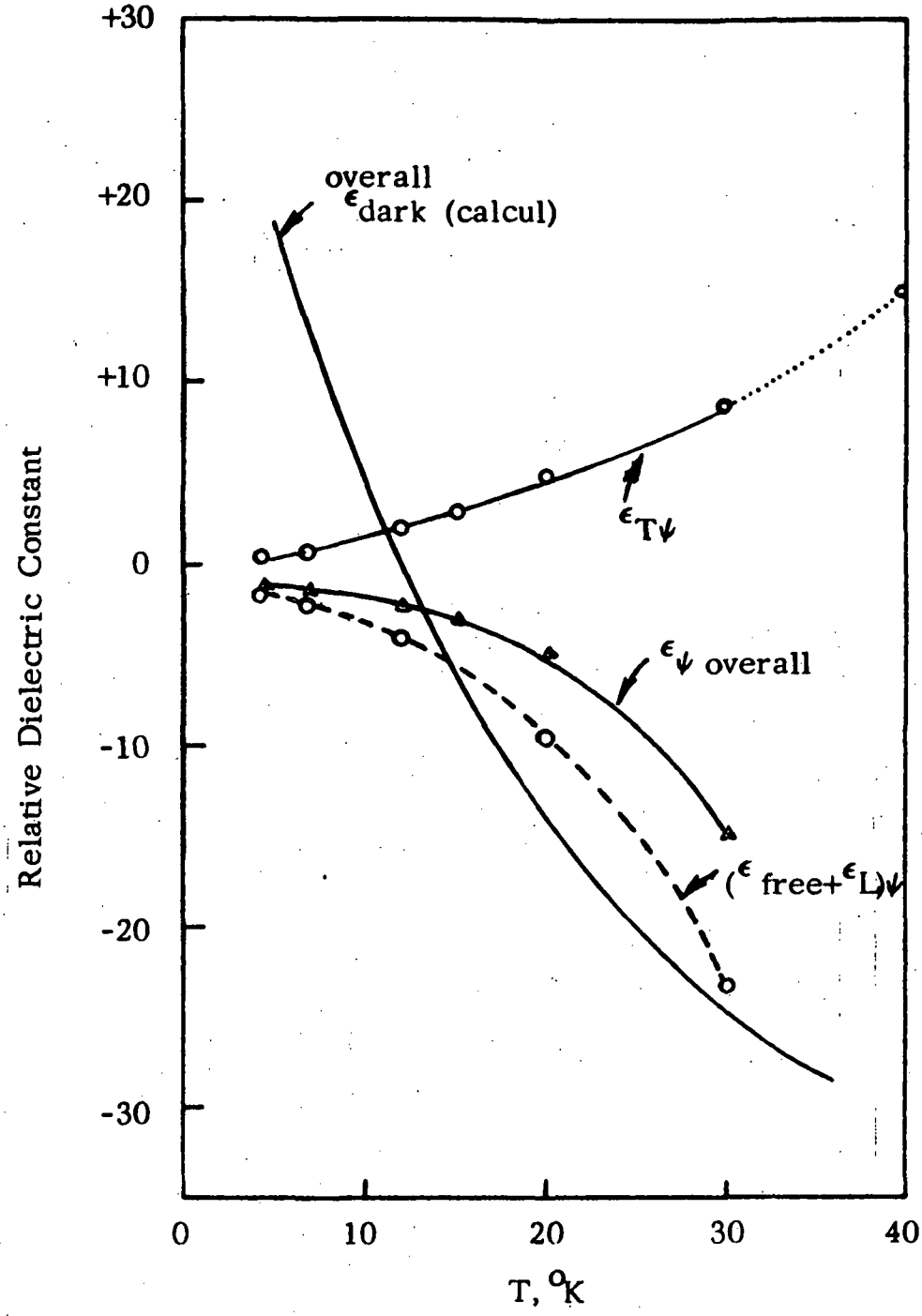

FIG. V-8 Temperature Dependence of Contributions to Overall Dielectric Constant

The calculated contributions of the core electrons (lattice dielectric constant) and free carriers is superposed on the same figure. The desired data, viz. $\epsilon'_{T\Psi}$, can be extracted from the difference in the experimental and calculated curves.

The implications of the resulting curve will be discussed in some detail. The increase of $\epsilon'_{T\Psi}$ i.e. the optically-induced trapped-electron dielectric constant change, as temperature rises clearly reflects the availability of an increasing density of shallow electron traps. The activation energy for this process is, of course, the ionization energy of the shallow donor-like traps, since the same physics governs the rate of free-electron lifetime increase. Alternatively stated, as temperature rises, the dark Fermi-level sweeps through the shallow centers, and changes their role from recombination to trapping. This process increases the dielectric constant, as opposed to the decrease that takes place due to thermal ionization of donors, discussed earlier. The two processes take place simultaneously.

Frequency changes caused by hole trapping can be neglected, for three reasons. First, the shallowest centers, near the valence band, in GaAs are approximately several times as deep as shallow donors, viz. about 20 meV. This occurs because the ionization energy E_a is related to the effective mass of the hole, m_p^* as follows:

$$E_a = \left(\frac{\epsilon_o}{\epsilon_s}\right)^2 \left(\frac{m_p^*}{m_o}\right) E_H \qquad (5.28)$$

where E_s is the static dielectric constant and E_H the ionization energy of hydrogen atom. Since the hole mass is approximately seven times higher than electron effective mass, the acceptor levels are correspondingly deeper. Secondly, Eq. (5.29) and Eq. (2.14) indicate that the frequency change due to trapped holes will be about 20% of the changes expected if the same density of electrons were trapped in shallow electron states. Hence, dielectric constant changes due to hole trapping can be neglected. Furthermore, as mentioned earlier, at low temperatures hole recombination lifetime is extremely short---at least two orders shorter than electron lifetime. This renders the free hole photodielectric effect negligible. Hence, frequency changes cannot be ascribed to a shallow trap near the valence band.

Thus, the increased rate of electron trapping, manifest in the frequency changes discussed above is further confirming evidence for the model of lifetime-temperature behavior presented earlier. It allows an unambiguous assignment of the location of the trapping levels i.e. the active centers are located close to the conduction, and not the valence, band.

The above analysis illustrates how non-contact photodielectric data may be combined with conventional analytical techniques to provide enhanced insight into recombination and trapping in materials. Additional,

more direct data is provided by transient measurements. These will be discussed in the next section. Before leaving the subject of steady state photodielectric effects, it is interesting to note some facts. In the case of strongly absorbed light, the "active" volume of the material is a very thin surface skin, especially at higher temperatures where the Debye length is only a few microns thick. This effect causes the excess carriers to be localized and strong modulation of the dielectric constant results. Thus at 4.2°K, 6328 Å light of only a few milliwatts can cause the entire lattice dielectric constant to be masked out by the free carriers, resulting in a negative overall dielectric constant at X-Band. At higher temperature the surface skin becomes metal-like in its dielectric behavior.

This, and the rapidly decreasing "active" volume of the sample constitute the main reason for the rapid decrease in photodielectric frequency-changes observed as temperature rises.

TRANSIENT ANALYSES--PHOTOCONDUCTIVITY & PHOTODIELECTRIC

Lifetimes derived from steady-state PC measurements are of the order of 0.1 microsecond at 4.2°K, whereas the decay times of PC and PD signals are several milliseconds. This great disparity implies strong minority-carrier trapping. As shown earlier, the response time τ_r is related to τ_n the majority-carrier lifetime as follows:

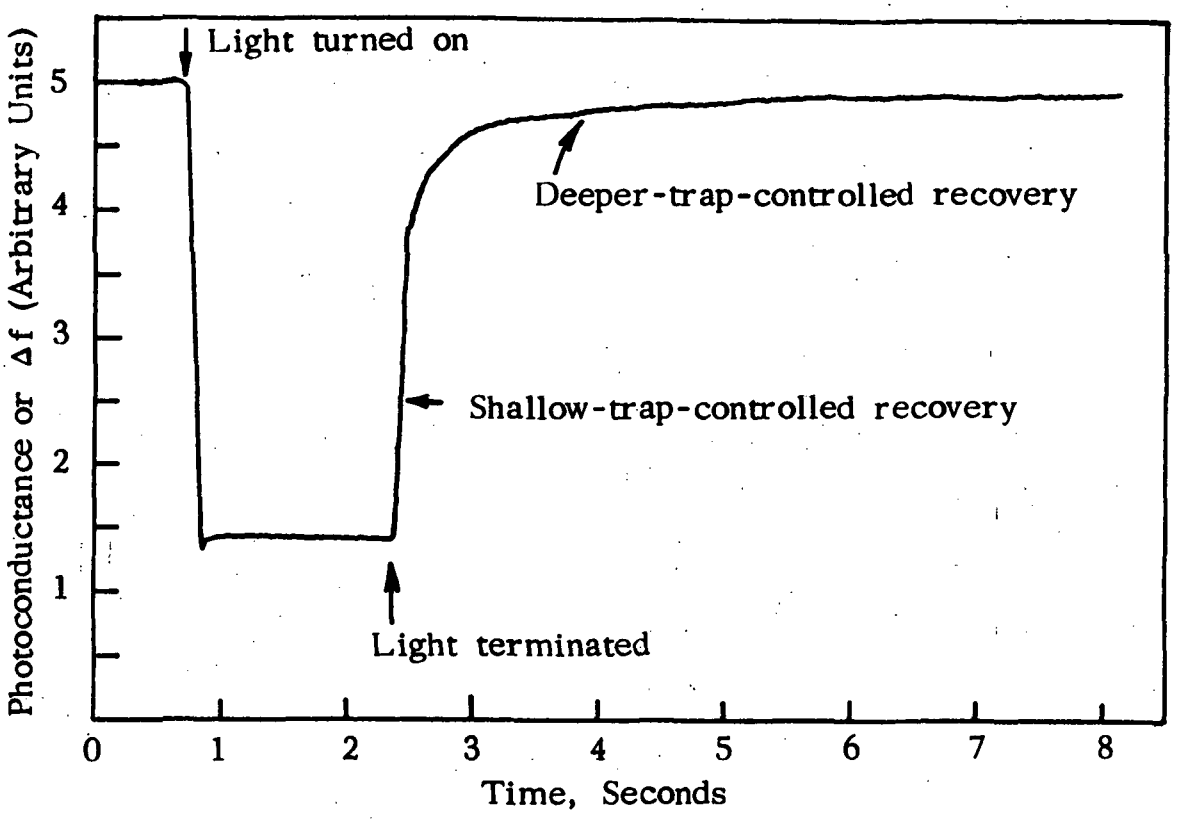

FIG. V-9 Typical Photoconductive or Photo-Dielectric Decay Curve ($10^{o}K$)

$$\tau_r = \left(1 + \frac{n_t}{n_o}\right) \tau_n \qquad (5.29)$$

which shows that the ratio of trapped-to-free carriers, is greater than 10^3. Fig. V-9 shows a recorder plot of a typical PC decay curve taken at $10^{\circ}K$. The fast drop at termination of the light, (when observed directly off the microwave discriminator with an oscilloscope) actually has a time constant of several milliseconds. The slow decay following on represents discharge of deeper traps. These features will be discussed in detail. Numerous curves such as shown in this figure have been recorded for a wide variety of conditions--e.g. varying temperature, optical excitation intensity, "bias" light, etc. Rather than present all of such basically similar curves, the data will be discussed more succinctly in text, in terms of the features of a few representative curves.

At $4.2^{\circ}K$, there is no evidence of the slow decay (region BC of curve in Fig. V-9) at any level of optical excitation, and there is only a single-step recovery. This agrees with the fact that the shallow (0.005 ev) centers are primarily acting as recombination centers. Deeper hole traps have an activation energy of approximately 9kT at this temperature, and therefore there is no slow-recovery segment in the decay curve. As the temperature rises to about $10^{\circ}K$, a large fraction of the shallow centers assume the role of traps and the PC

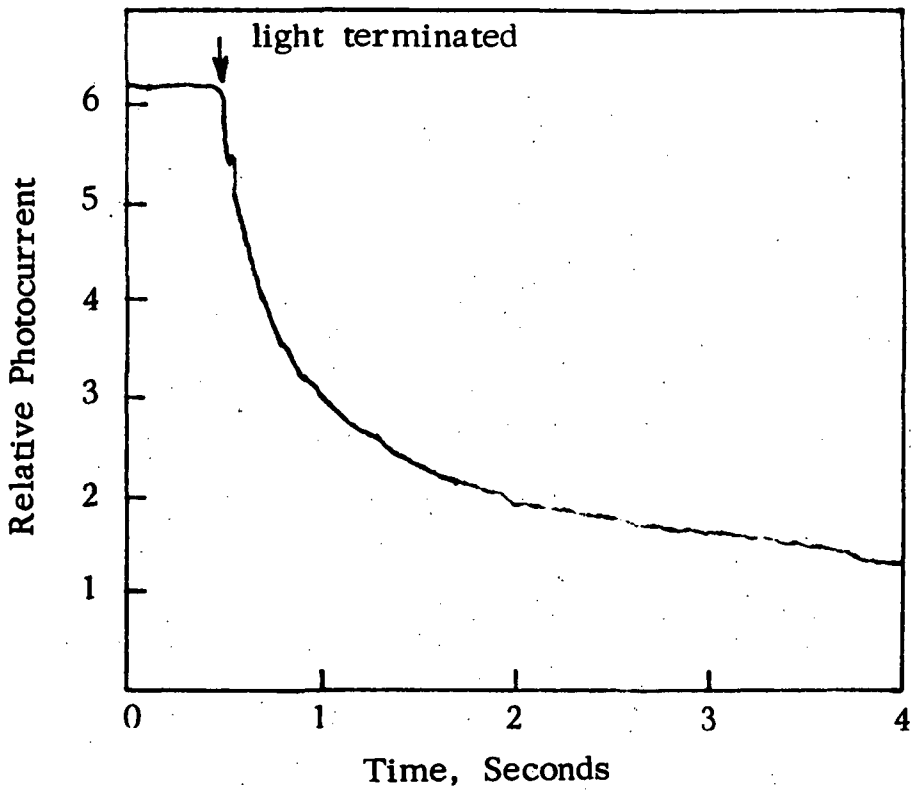

FIG. V-10 Typical Photoconductivity Decay Curve for Small-Signal Excitation at 48°K. The Curve is Non-Exponential After First Few Seconds

signal increases. Simultaneously, the deeper acceptor traps begin to discharge because of the increased thermal energy available, and the onset of the two-step recovery, with two characteristic "time-constants," takes place.

The parameters of the deeper trap are first determined, using decay curves exhibiting slow exponential recovery, such as shown in Fig. V-10. The recovery is exponential because the number of filled traps is small compared to their total number, so that the response time remains approximately constant, as mentioned in Chapter III. At T = 62°K, and 48°K the time constants are 0.45 and 0.61 secs. respectively, the thermal velocities are approximately 2×10^7 cm sec.$^{-1}$ and 1.27×10^7 cm sec.$^{-1}$. Assuming that the capture cross-section follows a 1/T dependence, the parameters can be substituted to solve a set of Eq. (3.26) simultaneously, to yield a trap energy Et of 0.033 eV. This trap position is quite close to the 30 meV acceptor-like trap observed by several workers, in their high purity epitaxial GaAs by low-temperature photoluminescence. Silicon on Arsenic sites gives rise to a $\approx$ 0.03eV acceptor level.

Reverting to Eq. (5.12) and taking N_t to be 1.4×10^{14}cm^{-3} section, S_{nt} at 62°K is approximately 2×10^{-20}cm^2. This is a very small cross-section, and presumably is a coulomb-repulsive center for holes, as similar to a center found in n-silicon. Such a center is

likely to constitute a terminal state for subsequent radiative capture of electrons from the conduction band. The residual acceptor density, $N_A = 1.4 \times 10^{14} cm^{-3}$, obtained from Hall measurements can be associated with this level. If other residual acceptors N_A' were present they would be manifest in Hall measurements as well as in photoconductive and photodielectric decay transients of different time constants. Other centers, if present, do not have a sufficiently high density-capture cross-section product to affect the sensitive transient measurements.

The shallow 4.9 meV donors which were influential in determining the steady-state photoconductive lifetime must also affect transient measurements. Examination of the photodielectric decay curves, (such as Fig. V-11) directly off the microwave discriminator in the PD experiments, as well as photoconductive decay curves confirms this. In Fig. V-11, the decay at $4.2^{o}K$ is not quite exponential, very probably due to the large number of traps optically saturated. However, an approximate time constant of 25 milliseconds, estimated from the storage-oscilloscope display, can be taken as a representative value. Eq. (3.26) gives

$$N_c \times S_{nt} \times v_{th} e^{-\Delta E/kT} = \frac{1}{\tau}$$

or

$$6.7 \times 10^{14} S_{nt} \times 10^{7} e^{-\Delta E/kT} = 160 \qquad (5.30)$$

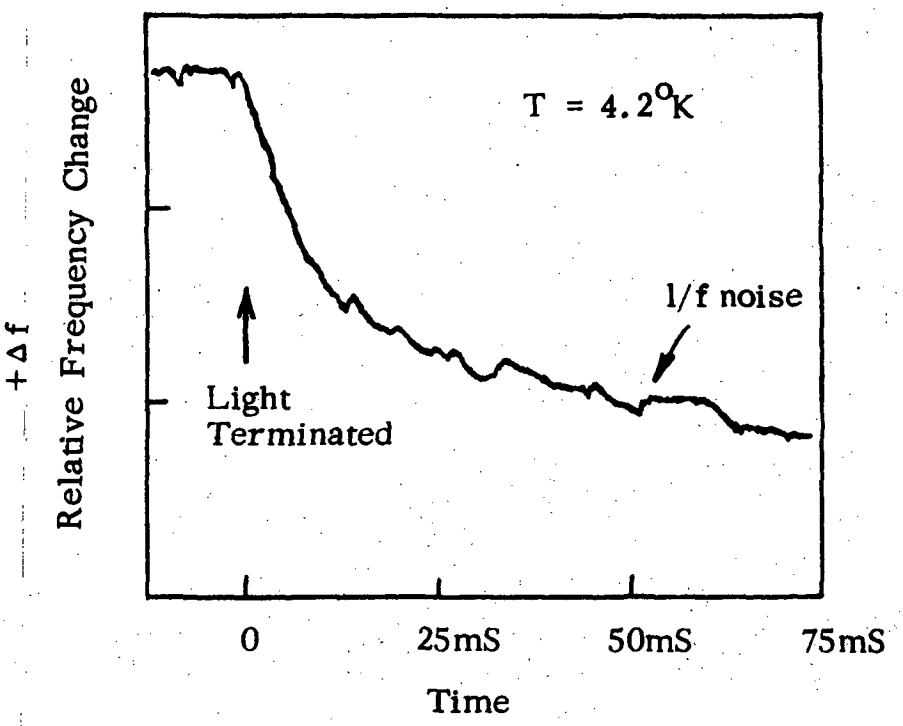

FIG. V-11 Typical Photodielectric Decay Curve, Observed at Output of Discriminator Using a Differential Storage Oscilloscope. Both 1/f Noise and Higher Frequency Components Influence Resolution

To find the cross-section of capture, S_{nt}, use can be made of steady-state photoconductive data. From Fig. V-2 lifetime τ is 1.25×10^{-7} sec. for low-level injection at 4.2°K. Use of Eq. (5.12) and $N_t = N_D$ (shallow) = $2 \times 10^{14}\,cm^{-3}$ yields S(shallow) of $4 \times 10^{-15}\,cm^2$. This value, used in Eq. (5.30) results in a trapping energy level of 0.0047 eV below the conduction band, in fair agreement with all previous data. Given a knowledge of the capture cross-section of a center, or its temperature behavior, the most direct and sensitive method to determine its energetic location is PC or PD transient measurements, and use of Eq. (5.30). The cross-section of the shallow donor, $4 \times 10^{-15}cm^2$ is rather small compared to values for shallow centers in Si and Ge, where values greater than $10^{-14}cm^2$ have been measured.[61] This center is therefore probably not in the class of "giant" capture centers discussed by Lax.[62] In such centers, capture takes place in a higher excited state of the center (and one whose geometric extent is therefore several unit cells), with subsequent cascading down to the ground state via emission of phonons. More important from the viewpoint of recombination dynamics is the fact that the shallow donor in GaAs is likely to be ineffective at room temperature. As discussed by Rose[20] the capture cross-section of many centers varies as T^{-2}, especially if they are coulomb attractive. If such a temperature dependence holds, at 300°K the capture cross-section shrinks to approximately $10^{-18}cm^2$.

Under these circumstances, some other center or mechanism is likely to dominate the recombination kinetics.

TEMPERATURE DEPENDENCE OF RESPONSE TIMES

At the lowest temperatures, the recovery transient at the termination of a light pulse is characterized by three distinct regions, when a curve such as given in Fig. V-9 is resolved further, using a storage oscilloscope. Fig. V-12 shows this transient. The initial rapid drop "A" corresponds to direct recombination of free electrons with free holes, and partly with holes trapped at deep acceptors. The next region, "B" corresponds to thermal excitation of electrons trapped at shallow donors being re-emitted to the parent band, and subsequent recombination via either route mentioned above. The third phase corresponds to discharge of holes from slower acceptor traps, and recombination, mostly with electrons ejected from donor traps. If the above explanation is correct, the resulting implications for the general behavior would be as follows: Starting at approximately 3.6^{o}K, the magnitude of electron trapping is expected to be low, as discussed earlier. See Fig. V-13. Hence component A is expected to be dominant, B very small, and C undiscernible at that temperature. As temperature rose, to 5.3^{o}K, the onset of majority carrier trapping would increase the size of B relative to component A, and C would

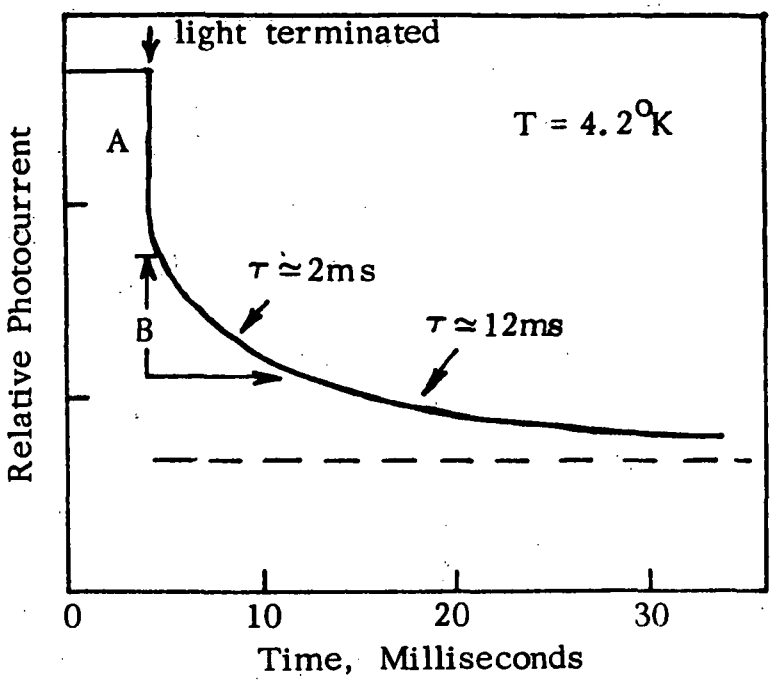

FIG. V-12 Expanded Decay Curve Showing Three Discernible Portions: Rapid Recovery, Shallow-Trap Controlled Recovery and Deeper-Trap Controlled Recovery. Excitation Level: 1 milliwatt

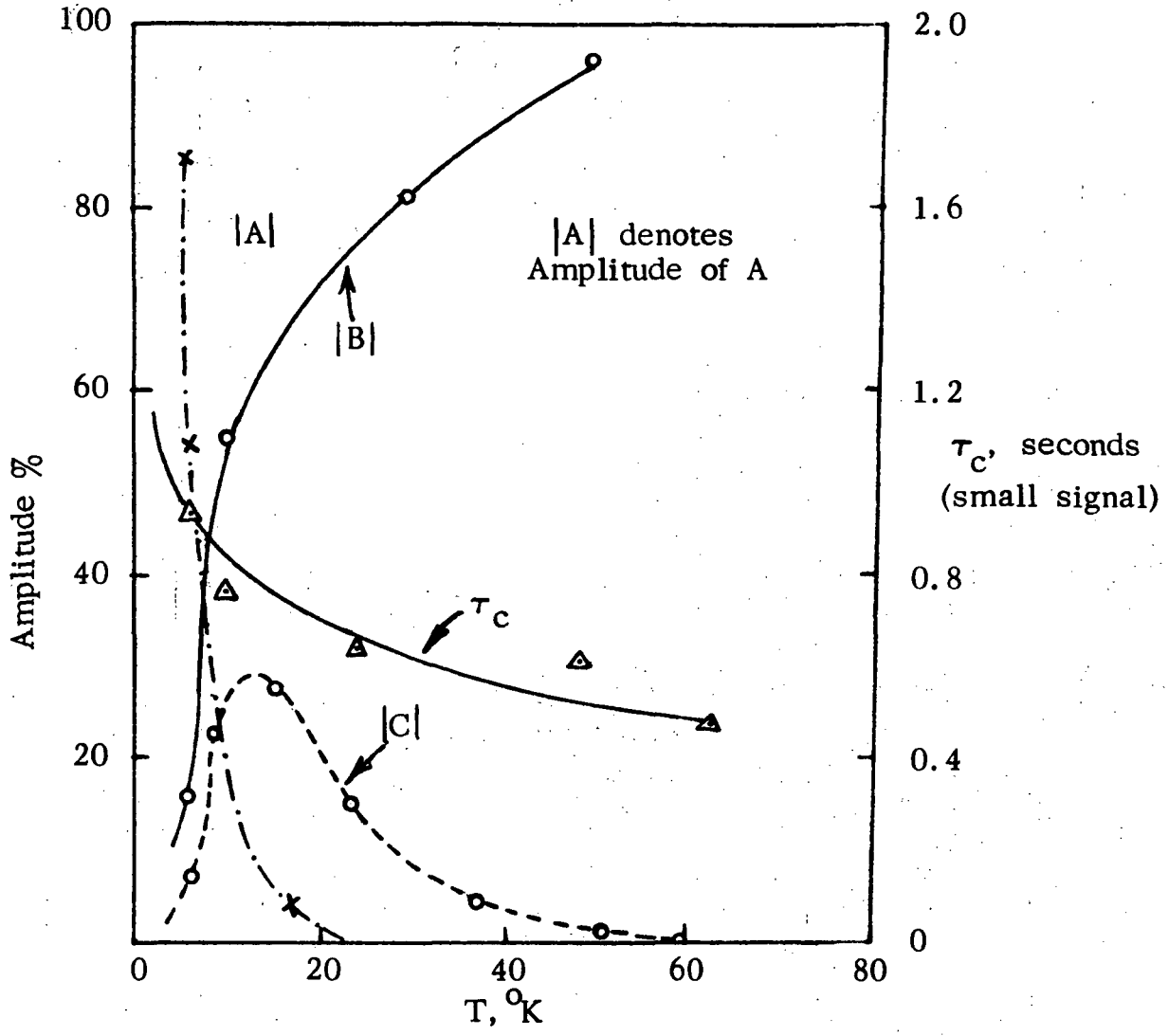

FIG. V-13 Relative Amplitude and Time-Constants of Decay-Curve Components as a Function of Temperature

A: Very Rapid Recombination
B: Shallow-Trap Controlled Recombination
C: Deeper-Trap Controlled Recombination

(Average Trend)

become noticeable as thermal activation increased. This general trend would continue as temperature rose. At a temperature such that kT becomes significant compared to E_t (i.e. 17°K) the rapid discharge of shallow traps would be expected to be counteracted by strong re-trapping from the conduction band, since the Fermi level location now is well below the trap. Thus component A would be expected to be very small compared to B, or be totally absent. The overall response time, would, however, be faster than that at say 12°K, because the slower component C (present at both temperatures) would, from Eq. (3.26) become more rapid (approximately) exponentially. Thus at a temperature of 55°K, a single-step recovery such as seen in Fig. V-12 is expected. All of the features qualitatively discussed above are confirmed in Fig. V-13 which presents the significant data extracted from a group of transient measurements.

OPTICAL BLEACHING OF TRAPS: RESPONSE TIME VARIATION

Another feature to be studied is the influence of a steady-state excitation superimposed on the low-level transients. It can be inferred from the discussion in Chapter III that progressive filling of traps by a steady excitation can reduce the "effective" number of traps. This phenomenon of "optical bleaching" of traps, can be seen in Fig. V-14. Steady He-Ne light, of different intensities, from a "bias" laser was shone on the sample in addition to pulse light excitation for

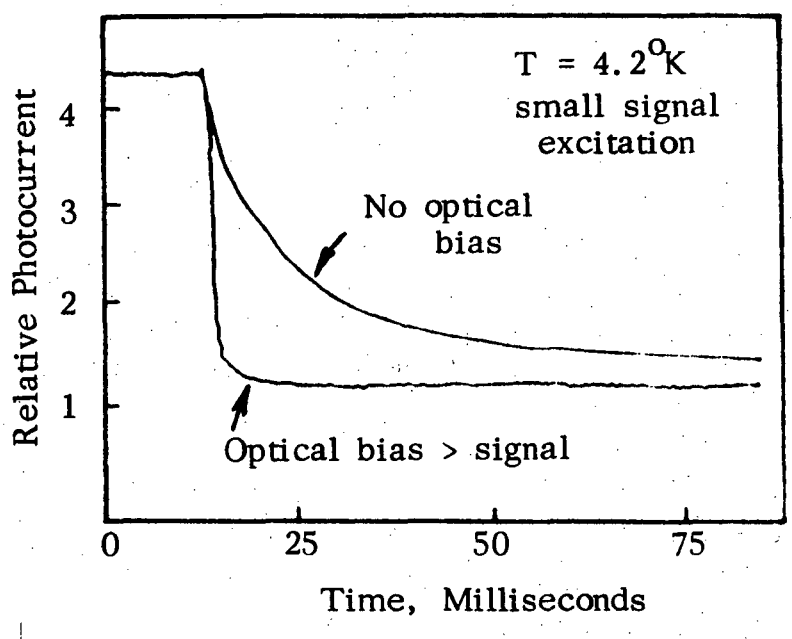

FIG. V-14 Showing Sharp Reduction in Photoconductivity Response Time Due to "Trap-Bleaching" By Optical Bias.

this experiment. The time constant of the 'B' component reduced from approximately 0.33 sec to 15 milliseconds when one mW of band gap light was superimposed.

OPTICAL QUENCHING OF TRAP NOISE

A striking demonstration of optical bleaching of traps was also found in the study of low-frequency noise due to trapping. (Fig. V-15) The current (shot) noise due to thermal emission of electrons trapped at shallow donor-like centers, and their subsequent re-capture by the same centers constitutes a source of thermal noise. In the present case, the noise was observed in a photodielectric experiment, and manifested itself in random frequency deviations about the mean frequency. The characteristic low frequency noise was found to have a power spectrum which was approximately flat, up to the corner frequency of 1 KHz. Inadequate noise data does not permit a quantitative analysis but the process is obviously one of bleaching of shallow traps and thus, removal of the noise due to trapping and detrapping.

RECOMBINATION MECHANISMS AT LOW TEMPERATURE

Thus far, the details of the recombination mechanisms ultimately limiting the lifetime of excess carriers at low temperature have not been discussed. The foregoing PC and PD analyses can now be used to synthesize a suitable model. The only states that have

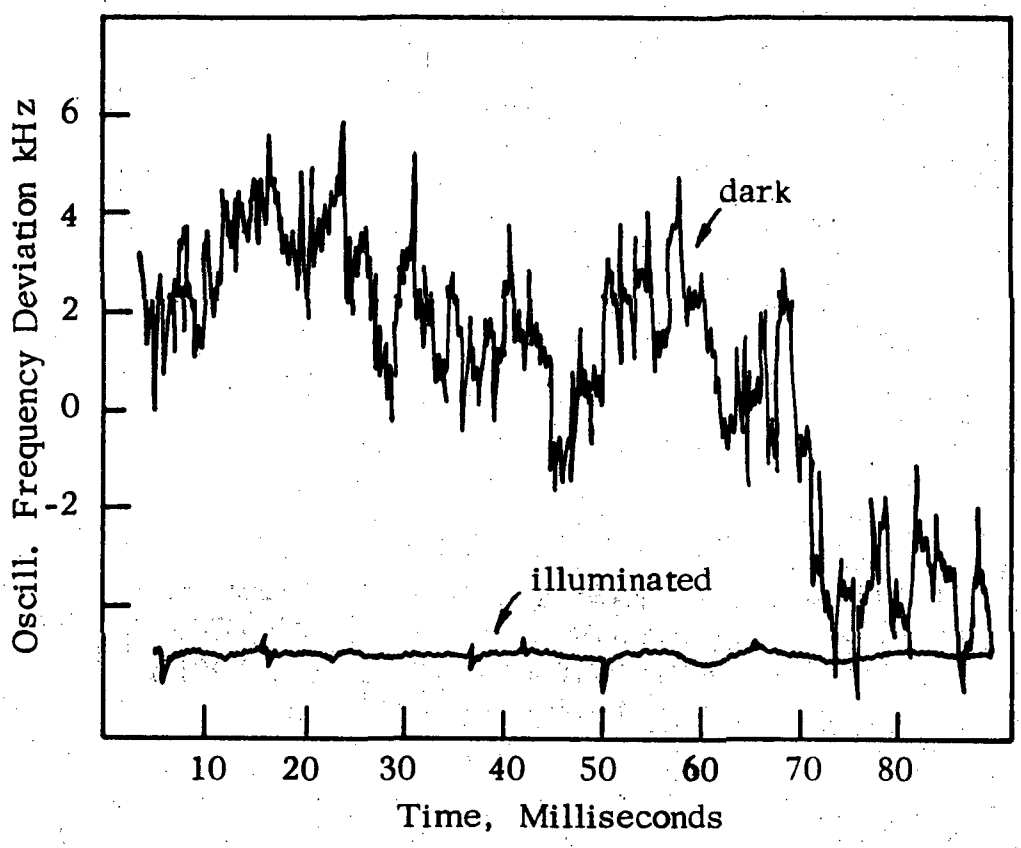

FIG. V-15 Optical "Bleaching" of Trap Noise - Upper Trace: Random Frequency Fluctuations With Dark Sample. Lower Trace: Frequency Noise With Illuminated Sample.

been revealed in the data thus far are the residual donor and acceptor states. As discussed earlier, these are evidently the active trapping states for high purity n-GaAs at low temperatures. A variety of modes of recombination are possible, viz. (i) band-to-band radiative free carrier recombination (ii) donor-acceptor pair recombination (iii) radiative recombination of excitation at an impurity site (iv) conduction band to acceptor center radiative recombination (v) radiative or non-radiative recombination via some other deep impurity (vi) Auger recombination, especially under higher level optical excitation. Other modes also can exist. All of the above modes have been discussed since 1966 by a large number of investigators.[16-18] The most comprehensive review article to date is by Bebb and Williams[63] who discuss in detail recent photoluminescence and related measurements by various workers. The present work supports model (iv) viz. radiative recombination of free electrons from the conduction band edge with holes trapped at residual acceptor sites. This mechanism will now be elaborated on, and compared with the viewpoints presented in the literature.

The temperature dependence of PC lifetime suggests that at very low temperatures the shallow donor acts as a recombination center. The photoexcited electron is first captured at this center, and the complementary transition of a hole bound at the acceptor center completes the recombination process. (Fig. V-16) This latter transition

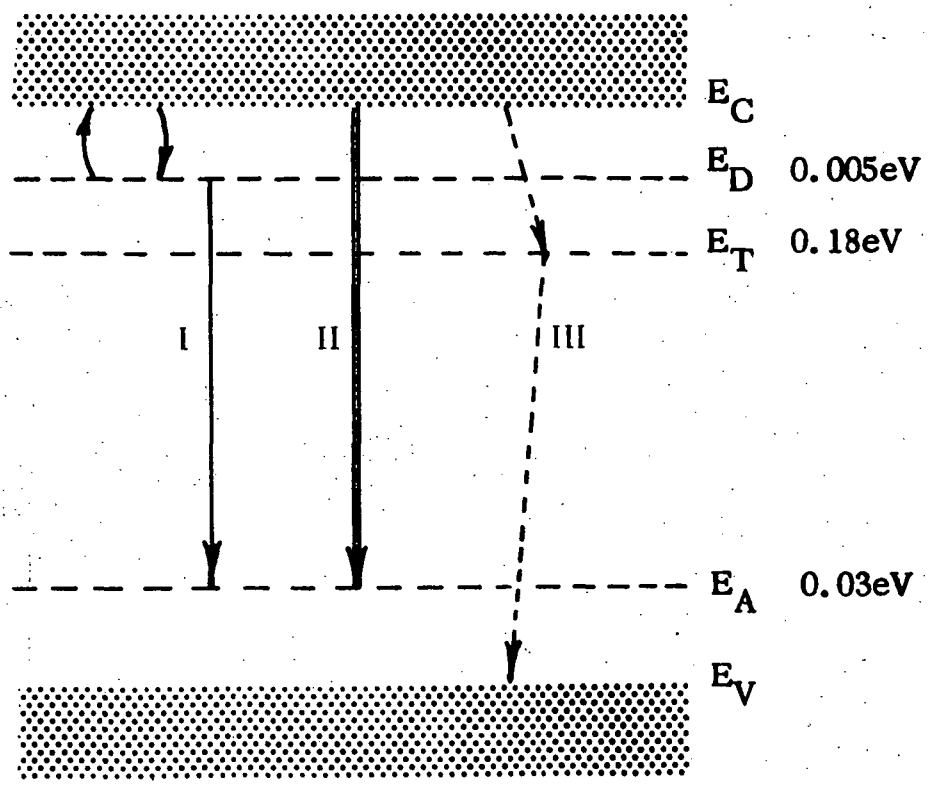

FIG. V-16 Proposed Recombination Model for Pure Epitaxial GaAs. The Donor-Acceptor Pair Recombination (labeled I) Operates at the Lowest-Temperatures. The Dominant Transition Above a few ^{o}K is the Radiative Recombination of Free Electrons With Holes Bound at Acceptors (II). At Room Temperature, a Deeper Level (perhaps the 0.18 eV trap) Takes Over the Recombination Traffic.

could, in principle, be either radiative or non-radiative. The theory of donor-acceptor pair recombination indicates that such transitions are generally radiative, because a bound (localized) electron has, by the Uncertainty Principle, a large spread in momentum, allowing the momentum conservation requirement to be easily fulfilled.[64]

For donor-acceptor pair recombination the emitted photon energy expected is given by[64]

$$h\nu = E_G - (E_A + E_D) + \frac{q^2}{Kr} \qquad (5.31)$$

where E_A and E_D are energies corresponding to the terminal acceptor and donor levels, and r is the radial distance between the pairs, and K the lattice dielectric constant. A series of sharp lines corresponding to $E_A = 0.03eV$, $E_D = 0.005eV$ and for various values of separation are expected. Photoluminescence (PL) studies or high purity epitaxial GaAs of very similar properties to those used in this work, performed by Dingle[65] and Bogardus and Bebb,[66] amongst others confirm the presence of a series of PL lines at 1.490eV and adjacent energies.

As the temperature is raised above approximately 7^oK or 8^oK, the dropping Fermi level would be expected to alter the role of the E_D level, as discussed earlier, and reduce the donor-acceptor recombination. This has also been observed in PL studies. At the same time, the more probable process, that of direct recombination of a free

electron with a bound hole, is expected to dominate. This is shown by the transitions in Fig. V-16 The work on acceptor luminescence in high purity n-GaAs of Rossi[67] et. al. strongly indicates that the dominant recombination process involved at low temperature is a free-electron-to-neutral acceptor (e, A^o) radiative transition. Fig. V-17 shows the PL lines they observed. Using the correlation of magnetic field, temperature, and light intensity data they conclude that the above transition is the correct assignment, in contrast to exciton-ionized-acceptor and other mechanisms. Rossi et. al. also observe that the intensity of the above PL line increases as temperature is raised while that of the donor-acceptor pair lines decreases. All of these findings are quite consistent with the results of PC, PD and other measurements in the present work. The precise PL measurements of Rossi et. al. reveal two acceptors at 27 meV and 31 meV; this difference is unresolvable in the present work.

It is worthwhile to estimate the transition probabilities (or lifetimes) associated with band-to-acceptor trap transitions. Dumke[68] has performed the quantum-mechanical calculations for direct gap materials, and assuming that the bands are parabolic, the impurities shallow, discrete and non-overlapping. His results for the transition probabilities are as follows.

For conduction band-to-acceptor, the transition probability at

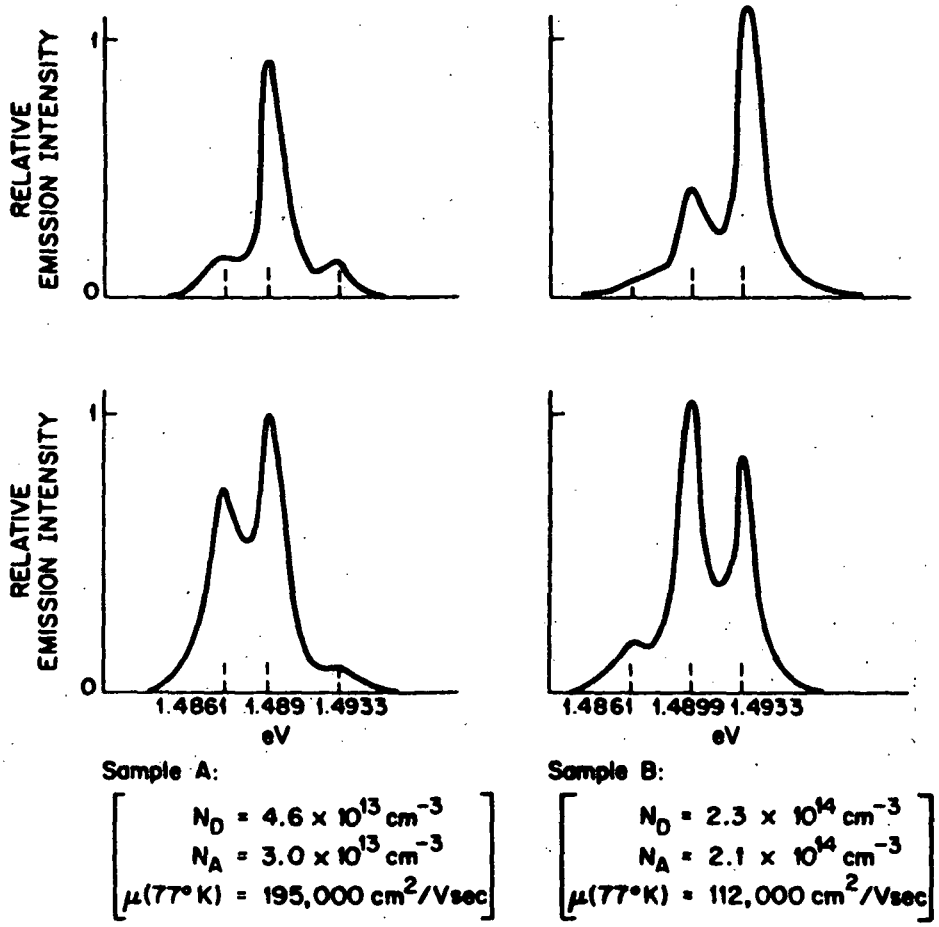

FIG. V-17 Pertinent Photoluminescence Spectra From Two GaAs Epitaxial Layers. The Bottom Two Traces Were Taken With Each Sample at 4.2°K, the Upper Two at 10°K.
(After Rossi et, al, Ref. 67)

$k = 0$ is

$$\frac{1}{\tau_{no}} = \frac{64\sqrt{2}\,\pi\, n\, q^2\, \hbar^2\, \omega \left|\overline{P_{vc}}\right|^2 p_A}{c^3 m^2 (m_p E_A)^{3/2}} \qquad (5.32)$$

where $\left|\overline{P_{vc}}\right|$ is the averaged inter-band matrix element of the momentum operator; n_D and p_A are concentration of electrons in donors and of holes in acceptors, respectively. m_p is the equivalent effective mass for holes and n the refractive index. Higher energy carriers (at $k \neq 0$) have a lower transition probability.

For GaAs, Eq. (5.32) simplifies to

$$\frac{1}{\tau_{no}} = 0.43 \times 10^{-9}\ p_A\ \text{cm}^3/\text{sec} \qquad (5.33)$$

At low temperatures $p_A = 2 \times 10^{14}\ \text{cm}^{-3}$ and Eq. (5.33) gives the radiative lifetime of 10 microseconds. The overall (PC) lifetime, from Fig. V-2 at 4.2°K and low-level excitation is 1.25×10^{-7} sec. This stresses the fact that even a liquid Helium temperatures the competitive recombination via shallow donor-like defect states manifests itself in limiting lifetime of excess carriers.

Direct band-to-band radiative recombination has not been mentioned in the present work. This mode has also not been observed in the luminescence work of other investigators at liquid Helium

temperatures. Reports by Gilleo[69] et. al. of free-carrier recombination have recently been shown to be due to grating ghosts. Much higher material purity than is presently obtainable is required for free carrier recombination to be observable.

Fig. V-3 shows that the lifetime of excess carrier rises exponentially up to 55°K, and this trend will be retained to perhaps 77°K or 100°K, yielding millisecond lifetimes. At 300°K, on the other hand, a simple PC measurement yields a lifetime of 2 to 5 microseconds. Obviously, as the temperature rises above the liquid Nitrogen range some other rate-limiting process takes over from the low-temperature processes discussed. The center responsible for this recombination traffic has not been investigated in detail in the present work. However, some noise-spectra measurements carried out at room temperature suggest that a recombination level located about 0.15 to 0.2 eV from the conduction band may be responsible for lifetime limitation at 300°K. The above range encompasses a level at 0.19 eV observed in pure material by Copeland[70] and 0.18 eV observed by the present author in compensated Gunn-quality melt-grown material. Thus this level may be a native defect. The evidence is, however, insufficient.

CHAPTER VI

SUMMARY AND CONCLUSIONS

In the preceding chapters some physical theories pertinent to the measurement properties of GaAs have been presented, and experimental data has been analyzed. In this chapter, the main features of the theory are summarized. A model for explaining recombination and trapping in high purity GaAs, valid below 77°K is next assembled from points made at various places, and some additional comments made on this model. In conclusion, an appraisal is given of photodielectric techniques for material property studies.

PHOTODIELECTRIC THEORY

A detailed discussion between the internal field seen by free and bound charges in a solid and the external driving fields has permitted revision of earlier description of photodielectric dispersion characteristics of a semiconductor. In particular, when the momentum relaxation time is taken to be energy-independent, the free-carrier susceptibility monotonically diminishes the total susceptibility as the carrier density is increased. At the plasma frequency the overall dielectric constant is zero, and it becomes negative as the plasma frequency exceeds the cavity or driving frequency. This behavior is a smooth transition from insulating to metallic conditions, as expected.

When the energy-dependence of the relaxation time is considered, the behavior becomes non-linear and complex. It is possible to then obtain a free-carrier susceptibility of the same sign as the lattice susceptibility, as observed, for instance, in Germanium by Gibson[41] et. al. for field-excited hot electrons. This non-linear behavior is particularly likely under high cavity-field conditions and perhaps may explain some anomalous results in earlier work. This cannot be verified since the working field-strength was unknown. In the present work, electric field strengths were maintained below 0.01 V/cm to obviate such and other non-linear effects, e.g. impact ionization of impurities.

The change in dielectric constant of GaAs on illumination is very large, especially since the 6328 $\mathring{A}$ light is surface absorbed. In most semiconductors, the change can easily be several-fold for light powers in the submilliwatt levels. This makes possible very sensitive instrumentation of material properties. The momentum relaxation time, τ_m must be as high as possible in order to make the dominant parameter ($\omega_p \tau$) large. The factor ($\omega \tau$), however, need not be large to cause a large PD effect.

PHOTOELECTRONIC PROPERTIES OF GaAs

Most earlier work on GaAs has either been based on relatively impure material or has been at temperatures above 77^{o}K.

The present work shows that the majority carrier lifetime in high purity n-GaAs, epitaxially grown on semi-insulating Cr-doped bulk GaAs, is approximately 0.5 millisecond in the $60^{o}K$-$70^{o}K$ range. This is an extremely long lifetime and occurs because of potent minority carrier trapping. On cooling to $4.2^{o}K$ the lifetime decreases by more than three orders of magnitude. The dominant mechanism for this effect is Shockley-Read recombination via shallow donors at low temperatures. As the temperature rises, the centers assume the role of trapping rather than recombination, and do not limit the lifetime. Photodielectric data clearly identify these shallow centers as being located near the conduction band and not the valence band. Additionally, thermally stimulated susceptibility measurements indicate the presence of donor-like traps, approximately 4.8 meV away from the conduction band. Hall effect measurements conducted over the temperature range between liquid nitrogen and liquid Helium confirm these results. The residual donor density is 2×10^{14} cm^{-3} and that of residual acceptors is 1.4×10^{14} cm^{-3}. Thus, high purity epitaxial GaAs is actually n-type, although compensated quite closely. These densities are very similar to high quality material grown in Lincoln Laboratories, and several other laboratories recently.[54,67] Electron mobility ranges from 6×10^{4} cm^{2}/vs to about 1.4×10^{5} cm^{2}/vs at $50^{o}K$. This is at least one order higher than previous "undoped" bulk GaAs. The

mobility peak is determined by the overlap of ionized impurity and lattice-scattering regimes.[1]

Other features noteworthy in the photoconductivity excited by strongly absorbed 6328 Å Helium-Neon light in GaAs are the creation of hot carriers and the sub-linear photoconductivity. The competition between polar optical-mode lattice scattering and carrier-carrier scattering determines the equilibrium "temperature" of hot electrons. Temperatures as high as 40°K occur when about 10 milliwatts of light is absorbed by the material. Thus when the sample is at 4.2°K the electron mobility is actually characteristic of a 40°K sample temperature under strong illumination conditions. For other materials such as InSb the disparity between sample temperature may be even greater, depending on the exact conditions. The sublinear nature of the photoconductivity is a result of strong surface-absorption of the light, followed by quadratic recombination of carrier pairs as well as diffusion away from the surface skin. This manifests itself in an overall characteristic of the form $n \alpha \Psi^{0.33}$ where Ψ is the light intensity. This sublinear photoconductivity limits the range of carrier concentration over which photodielectric phenomena can be experimentally determined.

RECOMBINATION MODEL

Fig. V-16 shows the simple energy level scheme proposed to explain the observed recombination and trapping at low temperatures in

pure GaAs. The role of the shallow donors in the mechanism of lifetime control has already been mentioned. Shallow donors at approximately 0.004 to 0.0052 eV have been observed by Naseldov,[5] Eddols[15] and Wolfe[54] et. al. The lower donor ionization energy seen in the first reference is a consequence of the onset of impurity-banding that occurs above about 10^{15} cm^{-3}. The earlier material was less pure. With higher concentrations of residual impurities there is a dual effect: the impurity wave-functions begin to overlap, and an independent band forms. Simultaneously, the lattice strain caused by impurities and the inevitable precipitates results in local deformations of the energy band, as discussed by Pankove.[71] Thus, a tail of conduction band states is formed into the forbidden gap: these states can merge with the impurity band. Such material is characterized by temperature-independent carrier-concentration down to the lowest temperatures. "Undoped" melt-grown GaAs (obtained from Monsanto) with a carrier concentration of approximately 10^{16} cm^{-3} at room temperature did in fact exhibit such impurity-banding effects (Fig. V-2) and no photodielectric effect was observed in that material. A monotonic increase of the Hall Coefficient as a sample of GaAs is cooled through the Helium temperature range is thus a clear indication of low total impurity content, since virtually any specific net carrier concentration can be established by suitable compensation. Commercially

available vapor or liquid epitaxial GaAs samples do not fulfill this criterion of purity.

The donor-ionization energy of ≈ 5 meV agrees with the values of 4.51 meV and 5.09 meV obtained by Stillman[54] et. al. for n_{300^oK} of 3.68×10^{14} cm^{-3} and 1.62×10^{14} cm^{-3} respectively. The calculated value, on the basis of a hydrogenic model[54] with effective mass of 0.066 m_o is 5.8 meV.

The compensating acceptor, also presumably acts as the deep acceptor-trap since no other level could be determined from transient data. This level is located approximately 0.033 eV from the valence band, and is responsible both for the high majority carrier lifetimes and slow decay transients at intermediate temperatures. This level acts as a terminal level in radiative recombination at helium temperatures. The mechanisms of recombination have been discussed in detail in Chapter V. It is significant that in most photoluminescence studies at low temperatures the same terminal state appears for roughly similar quality material.[16-18] There is little evidence of direct band-to-band recombination, and in view of the very short (10^{-9} sec. or less) lifetime of free holes, this is not surprising.

The trend of close compensation and an energy level scheme characterized by a simple set of two dominant levels--at least so far as behavior below 77^oK is concerned--for GaAs made in different

laboratories suggests that there may be some auto-compensation arising from one and the same contaminant. Silicon on Gallium sites gives rise to a shallow donor level.[71] Its ionization energy has been reported as 0.005 eV to 0.003 eV. Silicon can also give rise to an acceptor level in Gallium Arsenide by occupying the Arsenic site.[73] Thus amphoteric doping by silicon, arising by contamination from the quartzware in the epitaxial growth process is a distinct possibility. The relative amounts of silicon incorporated on the two sites has been a function of temperature, etc., has been studied in connection with amphoterically doped liquid epitaxial light emitting diodes. The results of that work may serve to confirm the auto-compensation idea. Native structural defects such as crystal defects, vacancy complexes, etc., can also give rise to levels observed, as suggested by Williams.[72] However, it is not obvious how in such a case close compensation can be achieved every time.

APPRAISAL OF THE PHOTODIELECTRIC TECHNIQUE

Although photodielectric measurements, like conventional techniques, are by themselves insufficient to permit complete analysis of recombination, trapping and other transport properties of semiconductors, they provide a very useful adjunct to conventional techniques, and take their place along with photoconductivity, Hall effect, optical quenching, thermally stimulated conductivity, etc., as a standard tool

of measurements and analysis. Thus, the fact that no ohmic contacts are required is of great practical significance, since in general the technique of alloying ohmic contacts on a material necessarily contaminates it; for high-purity materials this is especially undesirable. PD measurements also obviate the non-linear thermoelectric and photovoltaic effects often observed at contacts, and give confidence to interpretations of PC and PD transient phenomena. Furthermore, whereas defect states do not manifest themselves directly on photoconductive experiments unless the charge accumulated at them significantly alters the recombination dynamics, they show up directly in photodielectric measurements.

Although the experiments for this work were limited to temperatures below about 55°K, there is no reason why photodielectric measurements cannot be performed at liquid nitrogen temperatures for many materials. Shallow 5 meV states require that <u>any</u> conventional experiment be carried out at very low temperatures, as indeed they have been for pure GaAs. However, so long as the $\omega_p \tau$ product can be made comparable to unity, PD measurements can be performed at higher temperatures. A suitable material for such measurements would have sufficiently deep impurity levels to ensure at least partial de-ionization at 77°K and also a high mobility so that the $\omega_p \tau$ product is high. Materials such as InAs could conveniently be

studied by photodielectric methods at liquid nitrogen temperatures.

The sensitivity of the technique can be increased by two methods:

i) by increasing the filling-factor of the cavity. Since cavity dimensions are much smaller at 24GHz and 35GHz, measurements at these wavelengths (for the same sample size) would greatly enhance the sensitivity of measurements in addition to resulting in more compact equipment, and

ii) the stability of the feedback oscillator can be improved by avoiding 1/f noise effects through the use of an ac modulation technique, and with improved mechanical and thermal stabilization of the system.

APPENDIX I

Mechanism of Sub-linear Photoconductivity

In the steady state the left-hand side of Eq. (5.7) $\frac{dn}{dt}$ is zero, and the solution of Eq. (5.8) can be written as

$$n^3 - 3n_i^2 n = \frac{3}{2}\frac{D}{r}\left(\frac{dn}{dz}\right)^2 - A \qquad \text{(AI.1)}$$

At the surface, the diffusion current is

$$J_z^+ = -eD\frac{dn}{dz} \qquad \text{(AI.2)}$$

as $z \to \infty$, $n \to n_i$ and $J_z+ \to 0$ $\quad \frac{dn}{dz} \to 0$

which, with (AI.1) yields $\quad A = 2n_i^3$

Using this value in Eq. (AI.2)

$$n^3 - 3n_i^2 n + 2n_i^3 = \frac{3}{2}\frac{D}{r}\left(\frac{dn}{dz}\right)^2 = 3n_i L^2\left(\frac{dn}{dz}\right)^2$$

where $L = \sqrt{D\tau}$ is the diffusion length.

The above equation can be solved to yield

$$\frac{dn}{dz} = -\frac{12n_i C}{L}\, e^{-z/L}\,(C+e^{-z/L})\,(c-e^{-z/L})^{-3}$$

at $z = 0$, $J_z = qG - qS(n - n_i) = -qD\frac{dn}{dz}$

The term qG represents the photogenerated current and $qS(n - n_i)$ represents surface recombination component. S is the surface recombination velocity.

Thus,

$$G - 12 n_i cs (c - 1)^{-2} = 12 n_i \frac{D}{L} c(c+1) (c-1)^{-3}$$

or $$G\tau = 12 n_i Lc (c + 1 + \alpha c - \alpha) (c - 1)^{-3}$$

where $$= \frac{S\tau}{L} = S\left(\frac{\tau}{D}\right)^{1/2}$$

Now the total excess electrons per unit area

$$N = \int_o^\infty (n - n_i)\, dz = - 3 n_i \left[\frac{4cL}{c - e^{-z/L}}\right]_o^\infty = \frac{12 n_i L}{c-1}$$

or

$$G\tau = N \left(1 + \frac{N}{12 n_i L}\right) \left(1 + \alpha + \frac{2N}{12 n_i L}\right)$$

The photo current is directly proportional to N. At low intensity i.e. when $N << 12 n_i L$ we get the linear photoconductivity relation, $N = G\tau$. At higher intensities, such that $N >> 12 n_i (1+\alpha)$ the relation becomes $\frac{N^3}{72 n_i^3 L^2} = G\tau$ or $N = (G)^{1/3}$ which corresponds to the experimentally observed relationship.

APPENDIX II

Hot-Electron Photodielectric Effect

In Chapter II, it was assumed that τ_{mom}, was independent of carrier energy, i.e. of the driving field. Likewise, a constant energy-relaxation time was implied, equal to τ_{mom}. These assumptions are, in general, not valid. For instance, when the cavity field is high, or one is dealing with a photo-diode with depletion-region fields of several kilovolts/cm, the momentum relaxation time becomes field dependant. Modulation of the relaxation times gives rise to additional in-phase and quadrature terms, and it is then quite possible for the free carrier susceptibility to be of the same sign as the lattice contribution. A simplified theory, based on Conwell's[43] work, follows.

Consider a situation where τ_{mom} is given by

$$\tau_m = a\mathcal{E}^{-n_1} \qquad \text{(AII. 1)}$$

where n_1 is non-zero and $\mathcal{E}$ is the carrier energy. A similar relation, with index n_2 characterizes the energy-dependance of τ_{en}. The equation of motion is now

$$\frac{d^2r}{dt^2} + \frac{1}{a\mathcal{E}^{-n}} \frac{dr}{dt} = \frac{q}{m^*} E_o e^{j\omega t} \qquad \text{(AII. 2)}$$

This non-linear equation is difficult to solve for the general case. If a small ac field is superposed on a system already heated by a

steady field to energy $\mathcal{E}_o$, the analysis can be linearized by writing

$$\tau_m^{-1} = \tau_{m_o}^{-1} \left(1 + n_1 \frac{\Delta\mathcal{E}}{\mathcal{E}_o}\right) \qquad \text{(AII.3)}$$

A similar equation can be written for τ_{en}:

$$\tau_{en}^{-1} = \tau_{eno}^{-1} \left(1 + n_2 \frac{\Delta\mathcal{E}}{\mathcal{E}_o}\right) \qquad \text{(AII.4)}$$

The two exponents n_1 and n_2 are, in general, different. Thus, in GaAs, at low temperatures, τ_m is determined by ionized-impurity scattering and n_2 by polar optical lattice scattering.

Substituting (AII.3) and (AII.4) in (AII.2) and making the simplifying assumptions that $(\omega\tau_m)^2 \ll 1$ and $\tau_{en} \gg \tau_m$, the resulting expression for $\epsilon'(\omega)$ becomes[43]

$$\epsilon'(\omega) = \epsilon_L - \frac{4\pi N q^2 \tau_m}{m^*}\left(\tau_m - \frac{\Omega\pi^2}{1+\omega^2\pi^2}\right) \qquad \text{(AII.5)}$$

where N is the free carrier concentration, and Ω is given by

$$\Omega \equiv 2n_1 \frac{(\mathcal{E}_o - \mathcal{E}_{th})}{\tau_{en}\,\mathcal{E}_o} \qquad \text{(AII.6)}$$

τ_{th} being the energy of thermal-equilibrium electrons, also,

$$\pi \equiv \tau_{eno}\left[1 + (n_1 + n_2)\frac{(\mathcal{E}_o - \mathcal{E}_{th})}{\mathcal{E}_o}\right]^{-1} \qquad \text{(AII.7)}$$

An equation for $\epsilon''(\omega)$ can also be written, containing these constants.

Eq. (AII.5) is similar in form to Eq. (2.12) and the two become identical when $n_1 = n_2 = 0$. The composite factor π now plays the role of the relaxation time τ.

When $n_1 > 0$ the sign of the second term of (AII.5) is positive, i.e. the free-carrier and lattice susceptibilities have the same sign. For ionized impurity scattering $n_1 = 3/2$ so that the necessary mechanism for this effect exists, especially at low temperature. The experimental results of Conwell et. al. (Fig. AII.1) show that a normally negative dielectric constant of Germanium can be rendered positive, and made to exceed the lattice contribution substantially, when carriers are heated by a superimposed dc field. A large-amplitude ac field will cause stronger modulation of the τ's and the non-linear effects are then expected to be pronounced.

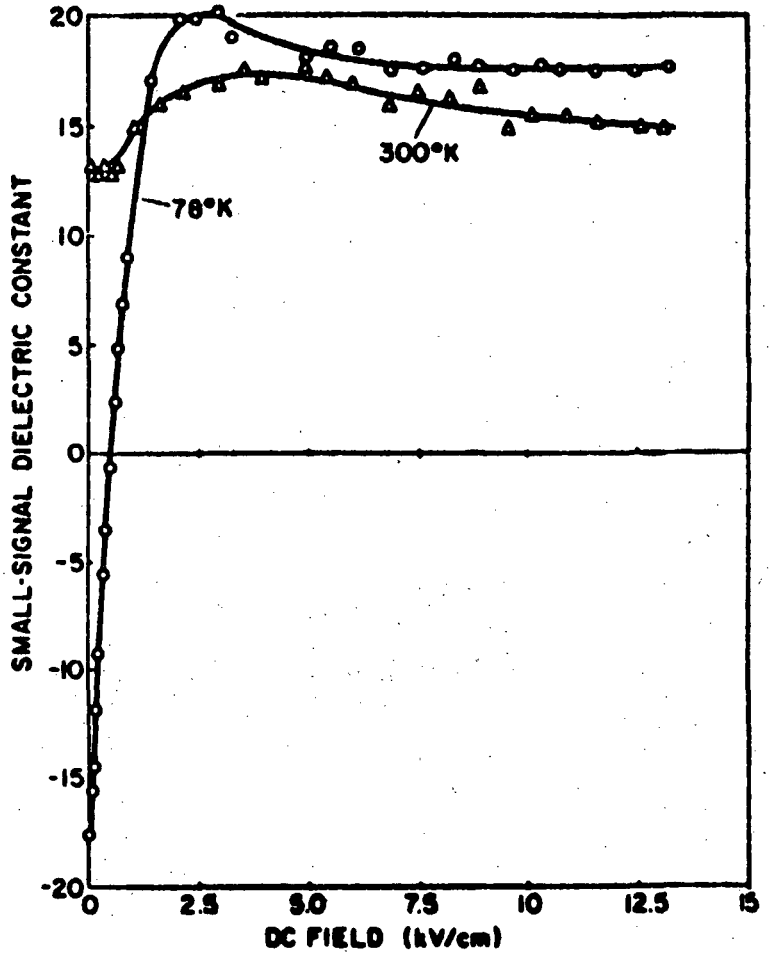

FIG. AII-1 Dielectric Constant of Germanium at 35GHz as a Function of Carrier Energy, Using DC Bias to Raise Mean Carrier Energy. (After Conwell Ref. 43)

BIBLIOGRAPHY

1. Stillman, G. E., et. al, "Far-Infrared Photoconductivity in High-Purity Epitaxial Gallium Arsenide," Applied Physics Letters, 13, 3, (1968).
2. Emelyanenko, O.V., et. al., "Hall Effect in Slightly Doped n-Type GaAs at Low Temperatures," 32, K175, (1969).
3. Sugiyama, K., "Recombination and Trapping Processes at Deep Centers in N-Type GaAs," Jap. J. Appl. Phys 6, 601, (1967).
4. Van Der Does De Bye, J. A. W., "The Role of Acceptors in the Luminescence of n-Type Gallium Arsenide," J. Phys. Cham. Solids, 28, 1485, 1967.
5. Voronkova, N. M. and D. N. Nasledov, "Concerning the Role of Trapping Levels in the Photoconductivity of Gallium Arsenide," Soviet Physics - Solid State, 7, 2050, (1966).
6. Shirafuji, J., "Temperature Dependance of the Photoconductive Lifetime in N-Type GaAs Diffused with Copper," Japan J. Appl. Phys. 7, 1974, (1968).
7. Blanc, J., R. H. Bube, and H. E. McDonald, "Properties of High-Resistivity GaAs Compensated with Diffused Copper," J. Appl. Phys. 32, 1666, 1961.
8. Kalashnikov, S. G., Soviet Physics - Solid State 2, 2505, (1962).
9. Kolchanova, N. M. and D. N. Nasledov, "Temperature Dependance of the Carrier Lifetime in n-Type Gallium Arsenide," Soviet Physics - Solid State 8, 876, (1966).
10. Hilsum, C. and H. Holeman, Proceedings of International Conference on Physics of Semiconductors, Prague, 1960, p963.
11. Hilsum, C., "Gallium Arsenide," in Progress in Semiconductors, Ed. A. F. Gibson and R. Burgess, London, Heywood, Vol. 9, 1965.
12. Willardson, R. K., and A. C. Beer, "Semiconductors and Semi Elements," vols. 1 to 7, New York, Academic Press, 1966 to 1971.

13. "Gunn-Quality," Te-O_2 Doped Bulk GaAs, made by Monsanto Chemical Company, St. Louis, Mo.

14. Knight, J. R., D. Effer, and P. R. Evans, "The Preparation of High Purity Gallium Arsenide by Vapour-phase Epitaxial Growth," Solid State Electronics 8, 178, (1965).

15. Eddolls, D. V., "Electrical Properties of n-Type Epitaxial Gallium Arsenide," Physica Status Solidi 17, 67, 1966.

16. Kressel, H. et. al., "Luminescence in Silicon-Doped GaAs Grown by Liquid-Phase Epitaxy," J. Appl. Physics 39, 2006, (1968).

17. Shah, J., R. C. C. Leite, and J. P. Gordon, Phys. Rev. 176, 938, (1968).

18. Stillman, G. E., C. M. Wolfe, and J. O. Dimmock, "Hall Coefficient Facts for Polar Mode Scattering in n-Type GaAs," J. Phys. Chem. Solids 31, 1199, (1970).

19. Bube, R. H., "Photoconductivity of Solids," New York, John Wiley and Sons, 1960.

20. Rose, A., "Concepts in Photoconductivity and Allied Problems," Interscience Publishers, New York, 1963

21. Hartwig, W. H., and J. J. Hinds, "Use of Superconducting Cavities to Resolve Carrier Trapping Effects in CdS," J. Appl. Phys. 4, 2020, (1969).

22. Arndt, G. D., W. H. Hartwig, and J. L. Stone, "Photodielectric Detector Using a Superconducting Cavity," J. Appl. Phys. 39, 2653 (1968).

23. Baker, G. L. and N. H. Hartwig, "Calculation of Free Carrier Photodielectric Parameters," NASA Tech. Rep., Electronics Res. Ctr., Univ. of Texas at Austin, 1969.

24. Albanese - Tarchi, A., "Analysis of the Photodielectric Effect as a Photodetector," Master of Science Thesis, Department of Electrical Engineering, University of Texas, Austin, May, (1972).

25. Hinds, J. J., and W. H. Hartwig, "Characteristics of Photodielectric Optical Detectors Using Superconducting Cavities," J. Appl. Phys. 42, 137, (1971).

26. Ryvkin, S. M., "Photoelectronic Effects in Semiconductors," New York, Consultants Bureau, (1964).

27. Wang, S., "Solid State Electronics," New York, McGraw Hill, (1966), p293.

28. Ratcliffe, A., "Magneto-Ionic Theory and It's Applications," Cambridge University Press, (1959).

29. Slater, J., "Insulators, Semiconductors and Metals," New York, McGraw Hill, (1967), p99.

30. Nozieres, P. and D. Pines, "Electron Interaction in Solids: Collective Approach to the Dielectric Constant," Phys. Rev. 109, 762, (1958).

31. Wilson, A., "Theory of Metals," Oxford University Press, (1949) p251.

32. Dresselhaus, G., A. F. Kip, and C. Kittel, "Plasma Resonance in Crystals: Observations and Theory," Phys. Rev. 100, 618, (1955).

33. Stern, F., "Elementary Theory of Optical Properties of Solids," Solid State Physics, Ed. F. Seitz and D. Turnbull, Vol. 15, (1960).

34. Slater, J. C. "Microwave Electronics," New York, Van Nostrand, (1950), p81.

35. Slagsvold, B., "Cavity Measurements in GaAs," Rev. Sci. Inst. 43, 154, (1972).

36. Sucher, M. and J. Fox, "Handbook of Microwave Measurements," New York, Interscience, (1963)

37. Hall, H., "The Theory of Photoelectric Absorption for X-Rays and -Rays," Rev. Mod. Phys. 8, 358, (1936).

38. Fan, H. Y., "Infra-Red Absorption in Semiconductors," Progress in Semiconductors, J. Phys. Chem. Solids 19, 271, (1961).

39. Sturge, M. D., "Optical Absorption in Gallium Arsenide," Phys. Rev. 127, 768, (1962).

40. Stratton, R., Proc. Roy Soc. A242, 335, (1957); also A246, 406, (1958).

41. Gibson, A. F., J. W. Granville and E. G. S. Paige, "A Study of Energy Loss Processes in Germanium at High Electric Fields Using Microwave Techniques," Phys. Chem. Solids 19, 198, (1961).

42. Frohlich, H. and B. V. Paranjape, Proc. Phys. Soc., (London) B69, 21, (1956).

43. Conwell, E. M., 'High Field Transport in Semiconductors,"' Solid State Physics, Ed. F. Seitz and D. Turnbull, Supplement 9, (1970).

44. Rose, A., "Concepts in Photoconductivity and Allied Problems," Interscience Publishers, New York, (1963), p26.

45. Stone, J. L., W. H. Hartwig and G. L. Baker, "Automatic Tuning of a Superconducting Cavity Using Optical Feedback," J. App. Phys. 40, 2015 (1969).

46. Ramo, S., J. Whimmery and T. Van Duzer, Fields and Waves in Communication Electronics, New York, John Wiley and Sons, (1966), p549.

47. Pound, R. V., "Frequency Stabilization of Microwave Oscillators," Proc. I.R.E. 35, 1405, (1947).

48. Van der Pauw, L. J., "A Method of Measurement of Specific Resistivity and Hall Effect of Discs of Arbitrary Shape," Phillips Res. Rept. 13, 1, (1958).

49. Hughes, F. D., and R. J. Tree, "Warm Electron Effects in GaAs at Low Temperatures," J. Phys. C: Solid State 3, 1943, (1970).

50. Williams, R. L., et. al., "Sweepout of Minority Carriers in Hg_{1-x} Cd_x Te," Proc. Int'l. Conf. on Photoconductivity, Stanford, (1969) (Pergamon Press).

51. Goodman, A. M., "Metal Semiconductor Barrier Height Measurement by the Differential Capacitance Method - One Carrier System," J. Appl. Phys. 34, 329, (1963).

52. Blakemore, J. S., "Semiconductor Statistics," New York, Pergamon Press, (1962), sec. 3.2.2.

53. Putley, E. H., "The Hall Effect and Semiconductor Physics," New York, Dover, (1968), p127.

54. Stillman, G. E., et. al., "Donor Magneto-Spectroscopy in High Purity Epitaxial GaAs," Proc. Int'l Conf. on Photoconductivity, Stanford, California, (1969), p265.

55. Emelyanenko, O. V., et. al., "Formation and Properties of an Impurity Band in n-Type Gallium Arsenide," Soviet Physics - Solid State 7, 1063, (1965).

56. Smith, R. A., "Semiconductors," Cambridge University Press, (1961).

57. Sze, S., "Physics of Semiconductors," New York, Wiley-Interscience, (1969), p38.

58. Smith, R. A., "Semiconductors," Cambridge University Press, (1961), p296.

59. Goodwin, D. W., "Report on Meeting on Semiconductors," April (1956), p137, (Physical Society, London), See also ref. 56, p310.

60. Garlick, G. F. J., and A. F. Gibson, "Electron Trap Mechanism of Luminescence in Sulphide and Silicate Phosphors," Proc. Phys. Soc. London 60A, 574, (1948).

61. Ascarelli, G., and Rodriguez, "Recombination of Electrons and Donors in n-Type Germanium," Phys. Rev. 124, 1325, (1961).

62. Lax, M., J. Phys. Chem. Solids 8, 66, (1959).

63. Bebb, H. B., and E. W. Williams, "Photoluminescence," Parts I and II, "Transport and Optical Phenomena," Ref. 12, vol. 8, (1972).

64. Bergh, A., "Light Emitting Diodes," Proc. IEEE 60, 155, (1972).

65. Dingle, R. and K. F. Rodgers, Jr., "Radiative Lifetimes in n-Type Gallium Arsenide," Appl. Phys. Lett. 14, 183, (1969).

66. Bogardus, E. H., and H. B. Bebb, Phys. Rev. 176, 993, (1968).

67. Rossi, J. A., et. al., "Acceptor Luminescence in High Purity Gallium Arsenide," Phys. Rev. Lett 25, 1614, (1970).

68. Dumke, W. P., "Interband Transitions and Maser Action," Phys. Rev. 127, 1559, (1962).

69. Gilleo, M. A., et. al., "Free-Carrier and Exciton Recombination Radiation in GaAs," Phys. Rev. 174, 898, (1968).

70. Copeland, J. A., "Semiconductor Impurity Analysis From Low-Frequency Noise Spectra," Trans. I. E. E. ED-18, (Jan. 1971).

71. Pankove, J. M., "Optical Phenomena in Semiconductors," New York, John Wiley and Sons, (1971), p11.

72. Williams, E. W., and D. M. Blacknall, "The Observations of Defects in GaAs Using Photoluminescence at 20°K," AIME Metall. Soc., Trans. 239, 387, (1967).